Diblock Copolymer - Nanocrystal Hybrids for Optoelectronic Applications

Dissertation

zur Erlangung des Grades

„Doktor der Naturwissenschaften“

im Promotionsfach Chemie am Fachbereich Chemie, Pharmazie und Geowissenschaften der Johannes Gutenberg-Universität Mainz

Lisa zur Borg

geboren in Seeheim-Jugenheim

Mainz, 2012

Die vorliegende Arbeit wurde unter Betreuung von [redacted] in der Zeit von Januar 2010 bis Dezember 2012 am Institut für Organische Chemie der Johannes Gutenberg-Universität Mainz angefertigt.

Dekan:	[redacted]
1. Berichtserstatter:	[redacted]
2. Berichtserstatter:	[redacted]
Tag der mündlichen Prüfung:	31.01.2013

D77: Dissertation Universität Mainz

CONTENTS

Abbreviations

A	acceptor
AFM	atomic force microscopy
AIBN	azobisisobutyronitrile
ATR	attenuated total reflection
ATRP	atom transfer radical polymerization
BCP	block copolymer
BHJ	bulk heterojunction
C	chromophore
CPD	contact potential difference
CPI	continuous precursor injection
CTA	chain transfer agent
CTAB	cetyltrimethylammonium bromide
D	donor
DDT	1-dodecanethiol
DMF	N,N‘-dimethyl formamide
DSSC	dye-sensitized solar cell
E.Q.E.	external quantum efficiency
GPC	gel permeation chromatography
HOMO	highest occupied molecular orbital
HTL	hole transporting layer
I-L	current-luminescence
IR	infrared spectroscopy
ITO	indium tin oxide
I-V	current-voltage
KPFM	Kelvin probe force microscopy
LC	liquid crystal
LED	light emitting diode
LUMO	lowest unoccupied molecular orbital
MLCT	metal to ligand charge transfer
M_n	molecular weight, number average
M_w	molecular weight, weight average
My	myristic acid
NC	nanocrystal
NMP	nitroxide mediated polymerization
NMR	nuclear magnetic resonance
OA	oleic acid
o-DCB	*ortho*-dichloro benzene
1-ODE	1-octadecanone

OLED	organic light emitting diode
OPV	organic photovoltaic
OSC	organic solar cell
P3HT	poly(3-hexylthiophene)
PCBM	[6,6]-phenyl-C_{61}-butyric acid methyl ester
PCPDTBT	poly[2,6-(4,4-bis-(2-ethylhexyl)-4H-cyclopenta[2,1-b;3,4-b′]dithiophene)-alt-4,7-(2,1,3-benzothiadiazole)]
PDDTT	poly(5,7-bis(4-decanyl-2-thienyl)-thieno(3,4-b)diathiazolethiophene-2,5)
PDI	polydispersity index
PFPA	pentafluorophenyl acrylate
PL	photoluminescence
PPV	poly(*para*-phenylene vinylene)
PTPA	poly(vinyltriphenylamine)
PTPD	poly(vinyltriphenylamine dimer)
QD	quantum dot
QLED	quantum dot light emitting diode
Q.Y.	quantum yield
RAFT	revesible addition-fragmentation chain transfer
RI	refractive index
SC	solar cell
SEM	scanning electron microscopy
SPPS	solid phase peptide synthesis
ssDSSC	solid state dye-sensitized solar cell
TCTA	4,4',4"-Tris(carbazol-9-yl)-triphenylamine
TEM	transmission electron microscopy
TFT	thin film transistor
TGA	thermal gravimetric analysis
THF	tetrahydrofuran
TLC	thin layer chromatography
TOP	n-trioctylphosphine
TOPS	n- trioctylphosphine sulfide
TOPSe	n- trioctylphosphine selenide
TPA	triphenylamine
TPD	triphenylamine dimer
UV-Vis	ultraviolet-visible
V	volt
wt%	weight per cent

Abstract

Small, smaller, nano - it is a milestone in the development of new materials and technologies. Nanoscience is now present in our daily lives: in the car industry with self-cleaning surfaces, in medicine with cancer therapies, even our clothes and cosmetics utilize nanoparticles. The number and variety of applications has been growing fast in recent years, and the possibilities seem almost infinite. Nanoparticles made of inorganic materials have found applications in new electronic technologies, and organic nanomaterials have been added to resins to produce very strong but light weight materials.

This work deals with the combination of organic and inorganic materials for the fabrication of new, functional hybrid systems. For that purpose, block copolymers were made with a long, solubility-enhancing and semiconducting block, and a short anchor block. They were synthesized by either RAFT polymerization or Siegrist polycondensation. For the second block, an active ester was grafted on and subsequently reacted with the anchor molecules in a polymer analogue reaction. The resulting block copolymers had different properties; poly(*para*-phenylene vinylene) showed self-assembly in organic solvents, which resulted in gelling of the solution. The fibers from a diluted solution were visible through microscopy. When polymer chains were attached to TiO_2 nanorods, the hybrids could be integrated into polymer fibers. A light-induced charge separation was demonstrated through KPFM. The polymer charged positively and the charge could travel along the fibers for several hundred nanometers. Polymers made via RAFT polymerization were based on poly(vinyltriphenylamine). Ruthenium chromophores which carried anchor groups were attached to the second block. These novel block copolymers were then attached to ZnO nanorods. A light-induced charge separation was also demonstrated in this system. The ability to disperse inorganic nanoparticles within the film is another advantage of these block copolymers. This was shown with the example of CdSe tetrapods. Poly(vinyltriphenylamine dimer) with disulfide anchor groups was attached to CdSe tetrapods. These four-armed nanoparticles are supposed to show very high charge transport. A polymer without anchor groups was also mixed with the tetrapods in order to investigate the influence of the anchor groups. It was shown that without them no good films were formed and the tetrapods aggregated heavily in the samples. Additionally, a large difference in the film qualities and the aggregation of the tetrapods was found in the sample of the polymer with anchor groups, dependent on the tetrapod arm length and the polymer loading. These systems are very interesting for hybrid solar cells. This work also illustrates similar systems with quantum dots. The influence of the energy level of the polymer on the hole transport from the polymer to the quantum dots, as well as on the efficiency of QLEDs was studied. For this purpose two different polymers were synthesized with different HOMO levels. It was clearly shown that the polymer with the adjusted

lower HOMO level had a better hole injection to the quantum dots, which resulted in more efficient light emitting diodes.

These systems all have in common the fact that novel, and specially designed polymers, were attached to inorganic nanocrystals. All of these hybrid materials show fascinating properties, and are helpful in the research of new materials for optoelectronic applications.

Zusammenfassung

Klein, kleiner, nano – ein Meilenstein in der Entwicklung neuer Materialien und Technologien. Die Nanowissenschaft ist in unserem Leben alltäglich geworden: in der Autoindustrie mit selbstreinigenden Oberflächen, in der Medizin zur Krebstherapie, und sogar unsere Kleidung und Kosmetik beinhaltet Nanopartikel. Die Anzahl und Vielfalt der Anwendungen ist in den letzten Jahren rasant gestiegen, und die Möglichkeiten scheinen fast endlos. Nanopartikel aus anorganischen Materialien wurden in neuen elektronischen Technologien eingebaut, und organische Nanomaterialien wurden zum Beispiel zu Harzen gegeben, um belastbare aber dennoch leichte Materialien herzustellen.

Diese Arbeit befasst sich mit der Verbindung organischer und anorganischer Materialien um neue funktionelle Hybridsysteme herzustellen. Dazu wurden Blockcopolymere mit einem langen, löslichkeitsvermittelnden und halbleitenden Block, und einem kurzen Ankerblock synthetisiert. Diese wurden entweder durch RAFT Polymerisation oder Siegrist Polykondensation hergestellt. Für den zweiten Block wurde zunächst ein Aktivester mit RAFT Polymerisation aufpolymerisiert und anschließend mit den Ankermolekülen polymeranalog umgesetzt. Die Blockcopolymere hatten verschiedene Eigenschaften. Poly(*para*-phenylenvinylen) zeigte Selbstorganisation in organischen Lösungsmitteln, was zu einer Gelbildung führte. Die Fasern konnten im Mikroskop aus einer verdünnten Lösung visualisiert werden. Bei Anbringen des Blockcopolymers auf anorganische TiO_2 Nanostäbchen konnten diese in die Fasern des Polymers integriert werden. Eine licht-induzierte Ladungstrennung konnte durch KPFM gezeigt werden. Das Polymer lud sich positiv auf, und die Ladung konnte entlang der Faser für einige hundert Nanometer wandern. Polymere, die durch RAFT hergestellt wurden, basierten auf Poly(vinyltriphenylamin). Als zweiten Block wurden Ruthenium-Komplexe angehängt, die selbst Ankergruppen trugen. Diese neuartigen Blockcopolymere wurden auf ZnO Nanostäbchen aufgebracht. Auch in diesem System konnte eine lichtinduzierte Ladungstrennung gefunden werden. Die Fähigkeit, anorganische Nanopartikel im Film gut zu dispergieren, ist ein weiterer Vorteil dieser Blockcopolymere. Am Beispiel von CdSe Tetrapods wurde dies gezeigt. Poly(vinyltriphenylamindimer) Blockcopolymere mit Disulfid Ankergruppen wurde auf CdSe Tetrapods aufgebracht. Dies sind Nanokristalle mit vier Armen, von denen ein exzellenter Ladungstransport erwartet wird. Ein Polymer ohne Ankergruppen wurde im gleichen Verhältnis mit den Tetrapods versetzt, um den Einfluss der Ankergruppen zu untersuchen. Ein starker Unterschied in der Filmqualität und der Aggregation der Tetrapods konnte gefunden werden, in Abhängigkeit der Tetrapodarmlänge und der Polymerbeladung. Zudem konnte gezeigt werden, dass ohne Ankergruppen meist keine guten Filme erhalten werden konnten, und die Tetrapods stark aggregierten. Diese Systeme sind sehr interessant für Hybridsolarzellen. Ähnliche Systeme,

aber mit Quantenpunkten, wurden auch in dieser Arbeit behandelt. Der Einfluss der Energielevel des Polymers auf die Lochübertragung zwischen Polymer und Quantenpunkten, sowie auf die Effizienz von QLEDs wurde untersucht. Hierzu wurden zwei Polymere synthetisiert, die verschiedene HOMO Levels hatten. Es zeigte sich deutlich, dass das Polymer mit dem angepassten niedrigeren HOMO Level eine deutlich bessere Lochübertragung auf die Quantenpunkte aufwies, was sich in einer Erhöhung der Effizienz der Leuchtdiode auswirkte.

Diese Systeme haben gemeinsam, dass neuartige und eigens für den Anwendungszweck entworfene Polymere an anorganische Nanokristalle aufgebracht wurden. All diese Hybridmaterialien zeigen faszinierende Eigenschaften und sind hilfreich in der Erforschung neuer Materialien für optoelektronische Anwendungen.

초 록

나노과학은 새로운 소재 및 기술의 개발을 위한 새로운 이정표를 제시하고 있다. 자가 세척능력을 지닌 자동차의 표면, 암 치유를 위한 새로운 신약 개발, 또는 의복 및 화장품에 이르기까지 나노과학은 우리의 일상 생활에 이미 널리 적용되고 있으며, 현재까지의 다양한 응용사례를 넘어 향후에도 무한한 응용가능성을 지닌 것으로 전망된다. 그 중에서 무기나노입자의 경우 신개념의 전자기술을 구현함에 있어 이미 널리 적용되고 있으며, 특히 기능성 유기나노물질을 무기나노입자와 융합함으로써 더욱 강하고, 가벼우며, 독특한 광전기적 특성을 지닌 신소재를 개발할 수 있으리라 기대된다.

본 연구는 유기 및 무기물의 조합을 통해 새로운 기능성 하이브리드 소재를 구현하는 것을 다루고 있다. 두 가지 물질의 융합을 위하여, 나노물질의 분산을 돕는 기능기와 더불어 반도체성 블록을 지닌 블록공중합체를 RAFT 중합 또는 Siegrist 중축합을 이용하여 합성하였다. 결합기능기 블록의 경우, 활성에스터기 우선적으로 중합한 이후 결합기능기를 블록공중합체에 도입하였다. 이상의 방법을 통해 합성된 블록공중합체는 고분자의 구조에 따라 상이한 특성을 보였다. Poly(*para*-phenylene vinylene) 블록공중합체의 경우 유기용매 상에서 섬유상으로의 자기조립을 통해 젤 화가 이루어지는 특성을 광학현미경을 통해 확인하였다. 이상의 고분자를 이산화티타늄 나노입자에 결합시킨 결과, 나노입자가 고분자 섬유상 내부에 자기조립된 나노구조를 관측할 수 있었으며, 계면에서 광유도 전하가 분리되어 홀이 고분자를 섬유상을 통해 수백나노미터 이동하는 현상을 켈빈 탐침 원자힘 현미경을 통해 확인할 수 있었다. Poly(vinyltriphenylamine) 기반의 전도성 고분자를 RAFT 중합을 이용해 합성하고, 루테늄 광흡수체를 지닌 결합기능기를 고분자 블록으로 도입하여 산화아연 나노막대에 결합시킨 결과, 광유도전하의 분리현상이 동일하게 일어남을 확인하였다. 한편, 이상의 블록공중합체와 나노입자를 화학결합으로 하이브리드하여 박막 내부에서 나타나는 나노입자의 분산성을 제어하는 연구를 수행하였다. Poly(vinyltriphenylamine dimer) 계열의 전도성 블록공중합체에 다이설파이드 결합기능기의 존재 유무에 따라 나타나는 사지상형 나노입자의 분산 및 응집 거동을 확인한 결과, 결합기능기를 지니지 않은 블록공중합체와 사지상형 나노입자의 혼합물 박막은 나노입자의 불균일한 응집이 유발되어 박막균일도가 저하되었으나, 결합기능기가 존재할 경우 사지상형 나노입자가 박막 내부에 고르게 분산됨을 확인하였으며 사지상형 나노입자의 가지 길이 및 고분자/나노입자의 질량비 조절을 통해 분산정도를 제어할 수 있음을 보였다. 이상의 결과는 향후 유기-무기 하이브리드 태양전지를 구현함에 있어 활용될 수 있을 것으로 보인다. 한편, 블록공중합체와 양자점을 하이브리드화 하여 양자점 발광소자에 적용하는 연구를 수행하였다. 균일한 나노구조를 보이는 양자점-전도성고분자 하이브리드 시스템을 기반으로, 두 가지의 상이한 HOMO 에너지준위를 지닌 전도성 고분자로부터 양자점으로의 홀 주입특성 및 외부양자효율 변화를 확인하였다. 그 결과, 양자점의 전자가 띠 근방의 HOMO 에너지준위를 지닌 전도성 고분자가 향상된 홀 주입 특성 및 개선된 외부양자효율을 보였다.

이상의 기능성 고분자-무기나노입자 하이브리드는 기존 소재 대비 독특한 전기적·광학적 특성을 나타냄을 확인하였으며, 나노소재 기반의 광전자소자에 대한 연구에 기여할 수 있으리라 생각된다.

1. Introduction

Small, smaller, nano - it is a milestone in the development of new materials and technologies. Nanoscience is now present in our daily lives: in the car industry with self-cleaning surfaces, in medicine with cancer therapies, even our clothes and cosmetics utilize nanoparticles. The number and variety of applications has been growing fast in recent years, and the possibilities seem almost infinite. Nanoparticles made of inorganic materials have found applications in new electronic technologies, and organic nanomaterials have been added to resins to produce very strong but light weight materials.

Organic and inorganic materials can be classified by their electrical conductivity: as conductors, semiconductors or insulators. Semiconductors are particularly interesting with regards to electronic devices. This work deals with the combination of polymeric semiconducting materials with inorganic semiconducting nanocrystals (NCs). The polymers offer high functionality and excellent film forming properties, which allow the design of flexible devices. The inorganic semiconducting NCs offer excellent charge conductivity and a large surface to volume ratio. The combined materials are called hybrids and show enhanced properties. In this dissertation the synthesis of new hybrid materials, their characterization, and application in optoelectronic devices is described. The focus will be on the control of the self-assembled morphology at nanoscale, and the light-induced charge generation.

1.1 Semiconducting Polymers

Alan J. Heeger, Alan G. MacDiarmid and Hideki Shirakawa received the Nobel Prize for chemistry in the year 2000 for the discovery of semiconducting polymers.[1] Considerable investigation has been devoted to improving the properties of the polymers, like their band gap or charge-carrier mobility. Most semiconducting polymers are fully conjugated systems, but polymers with aromatic side groups also show semiconducting behavior. In the latter case, π-π stacking of the aromatic rings provides the pathway for intramolecular charge migration via the polymer side groups. In the case of conjugated backbone polymers, the delocalized π orbitals provide the charge transport along the backbone on a local scale (Figure 1).[2, 3]

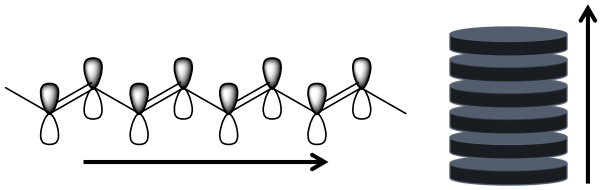

Figure 1. Schematic of the charge transport in conjugated polymers (left) and π-π stacked semiconductors.

The charge-carrier mobility along the polymer backbone was investigated and found to be higher compared to the intermolecular hopping.[4] Thus, either very long polymer chains or a high degree of order is required to build efficient devices with high charge carrier mobility. The liquid crystalline behavior of certain molecules can be used to increase the order and thereby the charge-carrier mobility.[5] The next paragraph will introduce the most important semiconducting polymers, first the main class, conjugated backbone polymers, and then side-chain semiconducting polymers.

1.1.1 Main-Chain Conjugated Polymers

Alan J. Heeger and Alan G. MacDiarmid's idea of the conducting behavior of a chain of π-bonded CH-units was realized with polyacetylene films by Hideki Shirakawa.[6] Since then, many different conjugated polymers have been synthesized (Scheme 1). The introduction of hetero nuclei, in particular nitrogen and sulfur, led to many new polymers with improved electrical and optical properties. Among them, poly-*para*-phenylene vinylene is famous for its electroluminescent behavior and was applied in organic light emitting diodes (OLEDs).[7] Another prominent polymer is polythiophene. A derivative, poly-3-hexylthiophene (P3HT) is the most commonly used polymer for organic solar cells (OSCs), in combination with an electron accepting material.

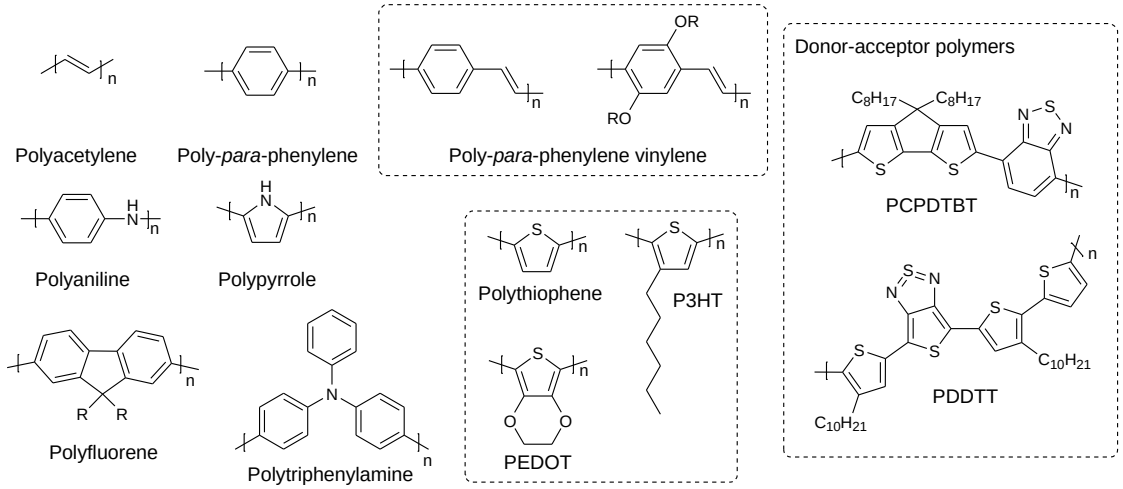

Scheme 1. Examples of conjugated polymers.

There are a large variety of synthetic strategies for conducting polymers, depending on their application. Precursor routes often give insoluble but high molecular weight semiconducting polymer films.[8] In contrast, polymers synthesized by solution based methods are often very well defined but the molecular weight is low. New applications in the fields of light emitting diodes (LEDs) and solar cells (SCs) require new and improved materials. Considerable research has been devoted in the last few years to find new materials suitable to absorb light and show high charge-carrier mobility. For the use in SCs, the band gaps of the polymer need to be carefully aligned in order to harvest more light. For that, D-A alternating polymers were found to be suitable. By performing small variations in the chemical structure, the band gap can be changed. The most famous D-A polymer is poly[2,6-(4,4-bis-(2-ethylhexyl)-4H-cyclopenta[2,1-b;3,4-b′]dithiophene)-alt-4,7-(2,1,3-benzothiadiazole)] (PCPDTBT). Recently poly(5,7-bis(4-decanyl-2-thienyl)-thieno(3,4-b)diathiazolethiophene-2,5) (PDDTT) found popularity because of the high charge transfer and crystallinity.[9]

1.1.1.1 Siegrist Polycondensation

Siegrist polycondensation is a method to synthesize well defined end group PPV and was applied in this work.[10, 11] *N*-[[2,5-bis(alkyloxy)-4-methylphenyl]methylene] derivatives are used as monomers. Potassium *tert*-butoxide deprotonates the methyl group and the monomer anion attacks another monomer at the imine functionality. A dimer with negative nitrogen is formed, which is protonated by *tert*-butanol, followed by subsequent anilide elimination. The thermodynamically stable *trans* product is formed. Several condensation steps give the polymer, and the polymerization is quenched by water. The major advantage of this reaction is the defined

end group (imine) which can easily undergo different reactions and thereby provide various functionalizations to the polymer.

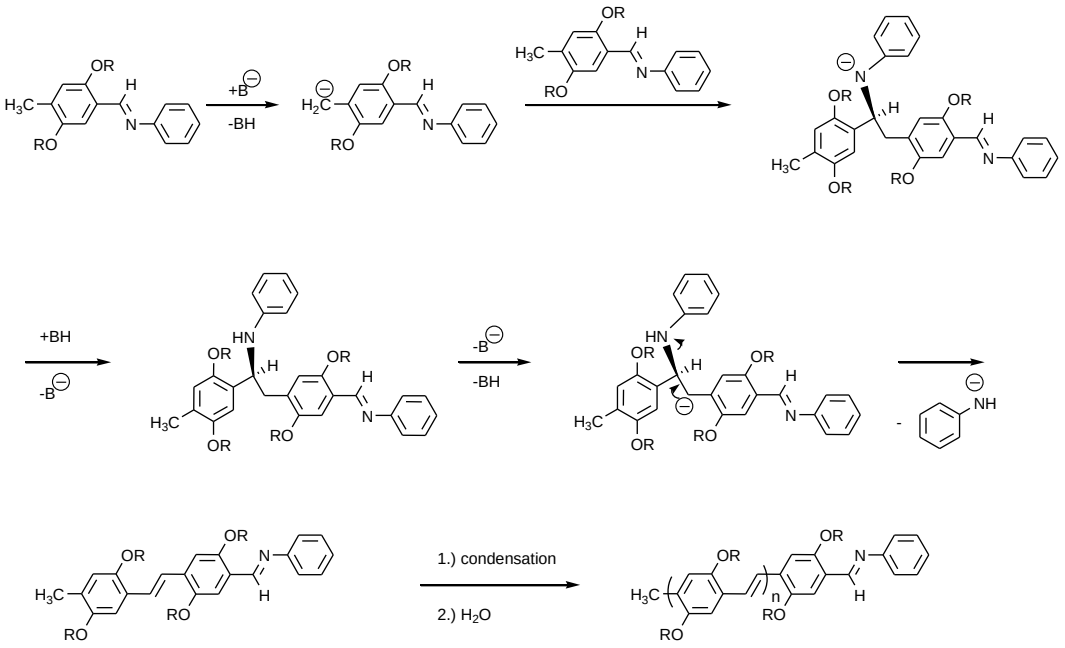

Scheme 2. Mechanism of the Siegrist polycondensation

1.1.2 Side-Chain Semiconducting Polymers

The variety of side chain semiconducting polymers is lower compared to the main-chain conjugated polymers. As an example, polytriphenylamines show semiconducting behavior and can therefore be used in optoelectronic devices such as LEDs or solar cells. Further examples are shown in Scheme 3. The monomers typically have a vinyl group which can be polymerized by radical polymerization.[12-14] Controlled radical polymerizations were investigated thoroughly in the last few years and applied to many systems of this type. Reversible addition fragmentation chain transfer (RAFT) polymerization[15-17] is one of the three main living radical polymerization methods along with atom transfer radical polymerization (ATRP)[18-20] and nitroxide mediated polymerization (NMP).[21, 22] Living radical polymerizations provide good control of the polydispersity and molecular weight, and the defined end groups offer the synthesis of block copolymers. In addition, RAFT polymerization tolerates a broad variety of functional groups and can be easily adapted to new systems. For these reasons it was used in this work.[23] The mechanism is as follows.

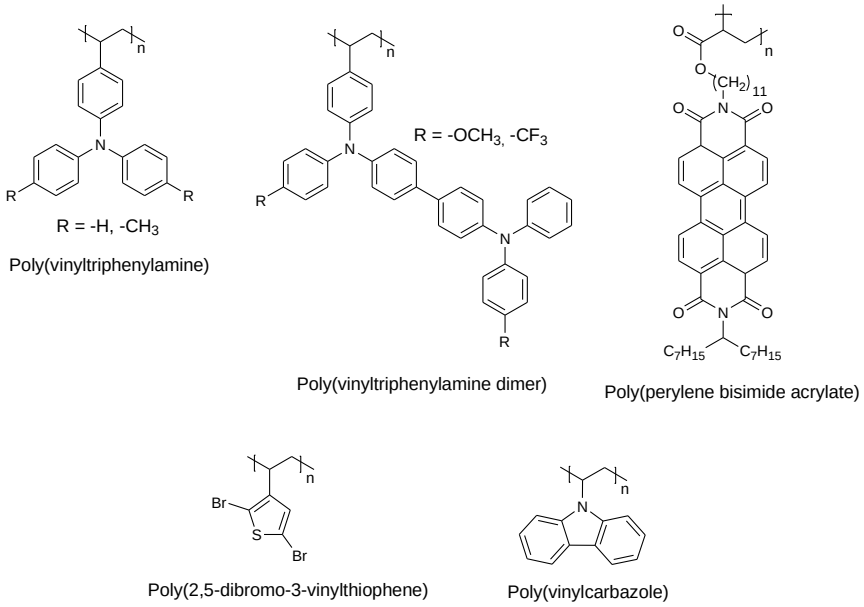

Scheme 3. Functional side-chain semiconducting polymers.

The initiator disproportionates homolytically (mostly thermal disproportionation of an azobis- derivative) and reacts with the vinyl group of a monomer. The activated monomer can subsequently react with a chain transfer agent (CTA). The CTA usually consists of a group that activates the C=S bond towards radical addition (Z), a reactive double bond and a good free-radical leaving group (R).[15] It is designed to transfer radicals by regenerative transfer, which is important for a well controlled mechanism. A fast transfer is also desired, to achieve good control of the molecular weight and thereby obtain a narrow molecular weight distribution. Polydispersities of less than 1.1 can be achieved with optimized systems.

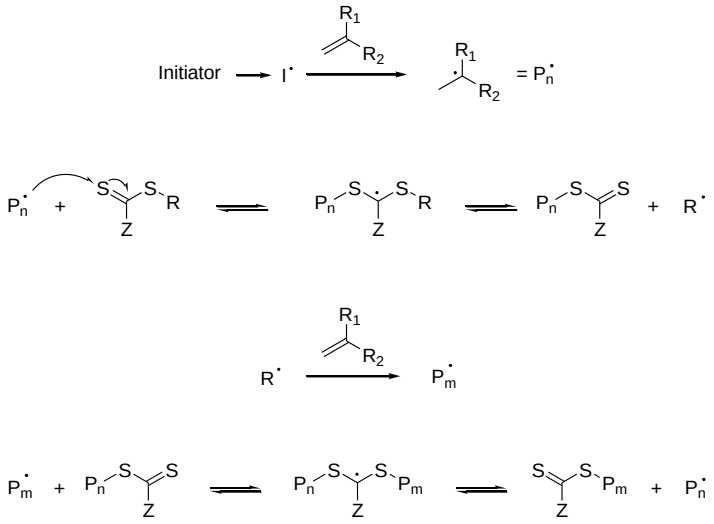

Scheme 4. Mechanism of RAFT polymerization

1.2 Inorganic Nanocrystals

Nanocrystals (NCs) are crystalline particles in the size range of 1-100 nm. They show very interesting size-dependent optical, electrical, chemical and physical properties and are therefore interesting for various applications.[24] Metals, metal oxides or semiconductors can be used for the synthesis. Considerable research in the synthesis of NCs made different morphologies possible (Figure 2). Spherical particles made of semiconductors or semiconductor chalcogenids (e.g. CdSe, CdTe,…) are called quantum dots (QDs) and are found to be suitable in light emitting diodes (LEDs).[25] They will be discussed in detail in paragraph 1.2.2) One dimensional nanostructures like rod-shaped particles, tubes or wires provide a higher anisotropy and long pathways for charge transport as well as a linearly polarized emission.[26-28] They are used in solar cells[29] or lasers[30] due to their interesting photoluminescent properties. Additionally, the high surface to volume ratio makes their electrical properties very sensitive to adsorbed species and therefore very useful in chemical or biological sensor applications.[31, 32] Higher anisotropic systems are achieved in tetrapods. Well-connected networks can provide excellent pathways for a fast charge transport.[33]

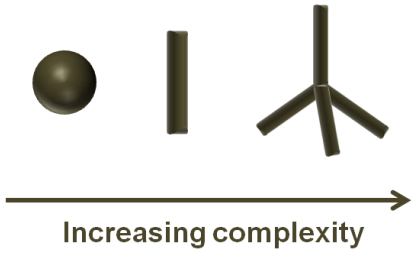

Figure 2. Schematic of different morphologies of nanocrystals.

Another very important class of nanomaterials shall be briefly mentioned here. Carbon based nanomaterials have drawn significant attention due to their unique optical, electronic, chemical and mechanical properties. Examples are fullerenes (0-dimensional), carbon nanotubes (1-dimensional) and graphene (2-dimensional). These materials find various applications in electronic and optoelectronic devices as well as in sensors or photovoltaics. [34]

1.2.1 Oxidic Nanocrystals

The most prominent material for oxidic nanoparticles is titanium dioxide. TiO_2 nanoparticles were found to be non-toxic and therefore have various applications in the chemical industry, like sunscreens, toothpaste or white pigments as well as in technologies like photo-catalysts and solar cells.[35, 36] It was shown that TiO_2 nanoparticles can split water photolytically under UV irradiation.[37-39] They are mostly synthesized by the sol-gel method in various shapes and sizes (e.g. spheres, rods, wires).[40] Further methods are micelle or inverse micelle, sol, hydrothermal,

solvothermal, direct oxidation or chemical vapor deposition.[36] Nanoporous TiO_2 is used in dye-sensitized solar cells, in which it acts as electron acceptor material (paragraph 1.5.2). When used in solar cells, power conversion efficiencies of >10% can be achieved.[41] TiO_2 can occur in three different crystal structures: rutile, anatase and brookite.[39, 42] The differences between the three forms cause different mass densities and electronic band structures.[36] The crystal structure depends on the preparation method. It was found that for small nanoparticles <14 nm, anatase was more stable, but for larger particles, rutile was found to be more stable. The reason lies in the different surface energies of the particles.[43] Zinc oxide (ZnO) is another very important oxidic material to synthesize nanoparticles and shows interesting optical and electrical properties.[44] It can be synthesized in various shapes like spheres, rods, tetrapods, comb structures and as nanoribbons.[33] Hexagonal patterned ZnO nanorod arrays can be used for nano-optoelectronics and nanosensors.[45] Thin films of ZnO nanoparticles are found to be good electron injection/transporting layer in inverted structure light emitting diodes.[46] As well as TiO_2 nanoparticles, ZnO nanocrystals show an increased sensitivity for gases (e.g. C_2H_2, H_2, CO) with decreasing grain sizes.[47] Other commonly used materials for oxidic nanoparticles are SnO_2, which is used in solar cells and gas sensing[48] and iron oxide (Fe_2O_3 or Fe_3O_4), which finds applications in biological detection because of its magnetic behavior.[49] Nanosized coupled ZnO/SnO_2 systems were found to split water[50] in similarity to TiO_2 nanocrystals.[35]

1.2.2 Semiconductor Nanocrystals

Quantum dots (QD) are nanocrystals which consist of hundreds to several thousands of atoms. They can be synthesized from many semiconducting materials, such as CdS, CdSe (II-VI), InP, InS (III-V) or PbSe (IV-VI).[51-53] There have been two main application fields developed in recent years: i) Biological (in vivo) imaging and detection in cells because of the long fluorescence lifetime of QDs,[53-55] and ii) optical applications like quantum dot based light emitting diodes (QLEDs)[25] (paragraph 1.4), lasers,[30] photovoltaic devices[56] (paragraph 1.5.3.3) or displays.[57] The most attractive property is the size-dependent band gap change of the QDs, through which the continuous fluorescent emission can be tuned over the entire visible spectrum (Figure 3).[58]

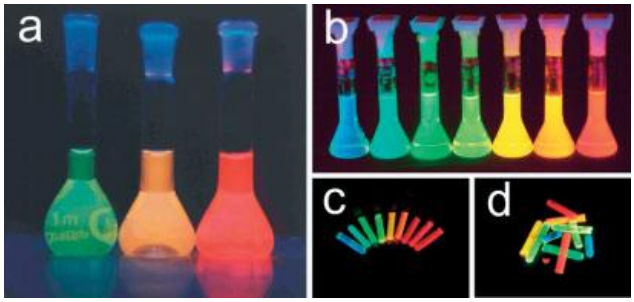

Figure 3. Photograph of different luminous nanoparticles. **a)** CdTe nanocrystals in aqueous solution, **b)** CdSe/ZnS core-shell nanocrystals in non-polar organic solvent, **c)** and **d)** CdSe/ZnS nanocrystals embedded in a polylaurylmethacrylate matrix.[58]

For example, CdS QDs can have a deep red (diameter 20 nm) or green (diameter 2 nm) emission. This fascinating property is a quantum size effect. Semiconductors have, in contrast to metals, two electronic bands: a filled valence band and an empty conducting band.[59] Figure 4 illustrates the energy levels in metal and semiconductor bulk, nanocrystal and atomar material. The NCs are between the bulk and the atoms because they have confined energy levels. Pure QDs have an highly imperfect surface. Electrons or holes can be trapped and thereby change the electrical and optical properties. To overcome this, the surface can be passivated with a material that has a larger band gap. A series of CdSe@ZnS core shell QDs was synthesized[60] and by carefully designing the shell and using ZnSe instead of ZnS, the quantum yield was largely preserved (up to 85%).[61]

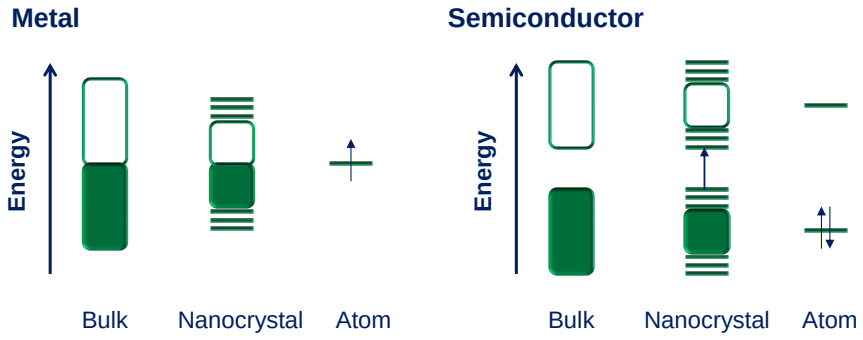

Figure 4. Energy levels in metals and semiconductors at different densities of states[59, 62]

In order to increase the charge carrier separation at the surface and to allow an efficient carrier transport along interconnected branches, tetrapods of semiconducting material like CdS, CdSe or CdTe have been synthesized.[63-67] A high morphological uniformity and crystallinity are required for various applications. A suitable synthesis was found with the continuous precursor injection (CPI) method. In this method arm constituting precursors (e.g. organic cadmium salts) are injected successively into the seed solution (CdSe NCs) at a controlled rate so that the reaction

condition remains in the kinetic growth regime.[68] The seeds have a zinc blende structure and the arms a wurtzite-phase. Using this approach, well defined CdSe tetrapods could be synthesized and variations in the arm lengths as well as arm diameters were possible.

1.3 Semiconducting Polymer – Inorganic Nanocrystal Hybrids

As described in the introduction, semiconducting polymer-inorganic semiconducting hybrids are promising materials for future technological devices. There are several ways to create hybrid materials.[69] The most straight forward way is by physically mixing the two materials. But for the design of highly efficient devices the morphology at nanoscale is important, especially for hybrid solar cells.[70-73] By simple blending, severe aggregations and phase separations occur which result in poor film morphologies and low device performances.[74] The reason for this is that nanoparticles which are capped with small organic molecules like oleates or staearates tend to aggregate and even form highly ordered supercrystals upon solvent removal.[24] On the other hand, the stiff conjugated polymers can also build regions with a high crystalline order, prohibiting the nanocrystals from penetrating.[75] By using different solvents and annealing at high temperatures, or exposing the materials to a strong electric field, the quality of the morphology can be improved.[76, 77]

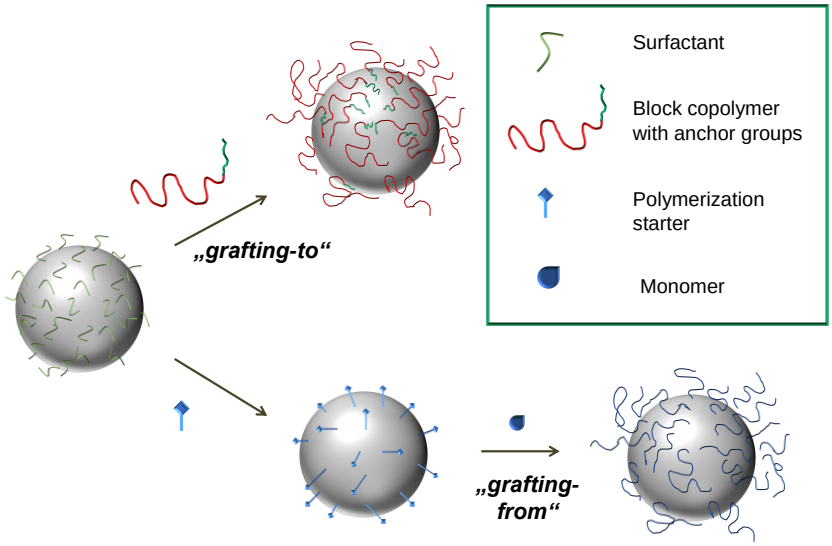

Figure 5. Schematic of the grafting-to and grafting-from approaches.

An approach to prevent demixing is chemical binding the polymers to the surface of the NCs.[78] Thus, phase separation at microscale is impossible and the morphology of the nanocomposites is well defined. There are three main strategies to synthesize the hybrid nanocomposites: namely, i) grafting-to,[79-81] ii) grafting-from,[82-84] and iii) direct nanocrystal growth in the presence of functional polymers.[85-87] In order to synthesize well defined nanocomposites, the first two strategies are more favorable because both the polymer and the NC can be characterized thoroughly before the hybridization. The third strategy has the advantage of being more straight forward and needing less synthetic steps, but the quality of the nanocrystals and the variety of shapes is poorer. The first two strategies are discussed in the following text. The

NCs usually carry short surfactants with carboxylic acid or phosphonic acid head groups in order to avoid aggregation during synthesis. In the grafting-to approach, a block copolymer which consists of a long solubility enhancing and a short anchor block is mixed with the NC (Figure 5). The bonding occurs by sonification or stirring in a diluted dispersion to avoid interparticle crosslinking. Purification is done through several washing/centrifugation steps. In the grafting-from approach the NC are decorated by ligand exchange with a polymerization starter e.g. an ATRP initiator or a CTA which is chemically tethered to the surface. The polymerization is performed on the surface of the NCs in the next step. The advantage of this approach is that no polymer needs to be synthesized beforehand. However, control of the polymerization is limited and not easy. In the grafting-to approach the polymer needs to be synthesized before but it can be characterized thoroughly. For these reasons we chose the grafting-to approach as the preferred strategy for the work in hand.

Figure 6. Picture of the solubility change of the hybrids: 1) pure polymer in toluene, 2) hybrid in toluene, 3) hybrid in hexanes, 4) QDs in hexane (from left to right, respectively).

The resulting semiconducting polymer-inorganic nanocrystal hybrids show the solution behavior of the polymers, as shown in Figure 6. In the left vial, pure polymer is dissolved in toluene. The second vial contains the hybrid, also showing a clear dispersion in toluene. In the third vial, the hybrid is dispersed in hexanes, where it forms aggregates, whereas the pristine QDs form a clear dispersion in hexanes, as shown in the right vial. This solubility change clearly proves the attachment of the polymers to the QDs. Another method to investigate the morphology is microscopy. The morphology at nanoscale is especially interesting. TEM images give a lot of information about whether the particles are aggregated or well dispersed. Figure 7 gives an example of pristine QDs and polymer-QD hybrids in films. Pristine QDs show huge aggregates and very poor film properties at nanoscale. However, in the hybrid, the particles are well dispersed within the film (vertically and horizontally) as shown in the top-view and cross-section TEM pictures. Using fluorescence microscopy, the film forming properties at microscale can be investigated, and the film of pristine QDs shows cracks, whereas the hybrid shows a very uniform film over several micrometers.

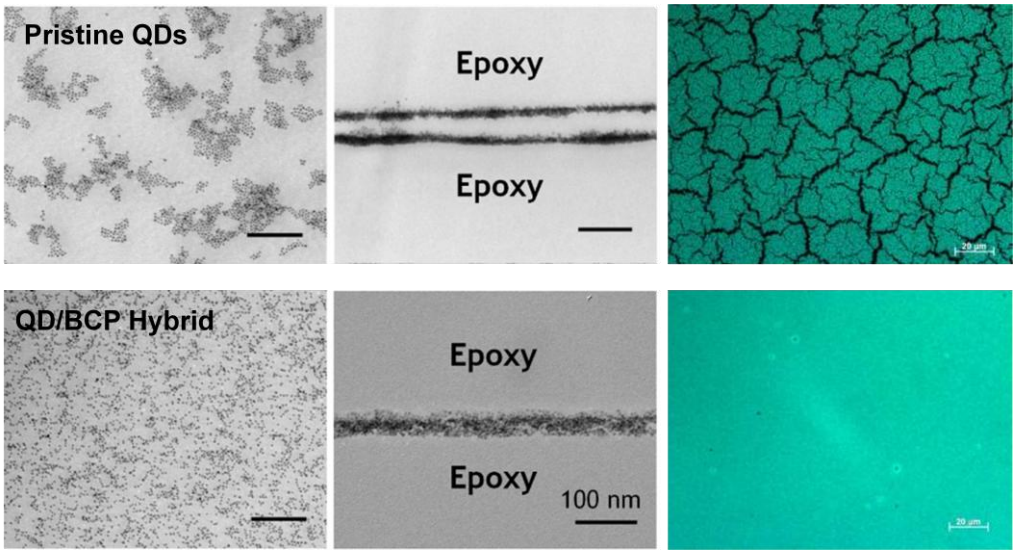

Figure 7. Pictures of QD-polymer hybrids (top) and pristine QDs (bottom). **Left:** TEM pictures of the top-view. **Middle:** TEM pictures of the cross-section. **Right:** Fluorescence microscope images.

1.4 Light Emitting Diodes

Officially, light emitting diodes (LEDs) celebrate their 50th birthday this year. However, Henry Round reported electroluminescence of a carborundum (silicon carbide) wire in 1907 and Oleg Losev published on the first LEDs in 1927. Their discoveries remained unused and Nick Holonyak and other researchers reported the first visible light LEDs in 1962.[88] Because the conventional light bulbs use too much energy, LEDs are considered the new light media. Amongst other things, they can be used in displays for electronic devices like smart phones, as large advertisement screens or as light sources for rooms. The color can be tuned to every wavelength according to the need. There are three different classes, namely i) conventional LEDs, ii) organic LEDs (OLDEs) and iii) quantum dot LEDs (QLEDs). The working principle is the same for all classes; a voltage is applied between two electrodes, the electrons are injected through the cathode, the holes through the anode, and they recombine inside the active layer where energy is released and a photon is emitted (Figure 8).

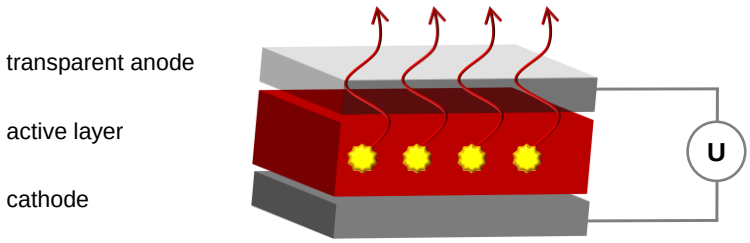

Figure 8. Schematic of a single layer LED.

Conventional LEDs are based on semiconductor layers of III-V elements, such as GaP or InGaN.[89-91] They emit light when the electrons jump from the conduction band to the valence band and recombine with the holes. All different colors can be produced by using different semiconducting materials. Even ultraviolet LEDs can be built using InAlGaN.[92]

In OLEDs, small organic molecules or polymers are used. For small organic molecules, most commonly tris-(8-hydroxyquinoline)aluminum (Alq_3),[93] cyclometalated iridium(III) or other coordination complexes are applied.[94, 95] For polymers, PPV is the most prominent example,[96] and by using polyethylene terephtalate as substrate and polyaniline as hole-injection electrode, flexible LEDs can be built.[97] Polyfluorenes are also applied in OLEDs, especially for blue and white light diodes.[98-100] The main advantage of the organic molecules is their easy tunability to cover the whole color range and the possibility to build flexible devices. Furthermore, printing can be used to fabricate large-area devices with low production costs.

An intermediate between conventional LEDs and OLEDs are the QLEDs. As described in paragraph 1.2.2, QDs find applications in LEDs due to their excellent optical properties. The first

QLEDs were reported in 1994,[25] and since then huge effort was devoted to improve their performance. Trilayer polymer-QD devices were found to show improved performance,[101] and multicolored bright QLEDs were reported in 2007.[102] White light emitting diodes were realized with red and green QDs as color converters on InGaN blue LEDs, and used as a white display backlight.[103] Recently, inverted structure devices using red, green and blue CdSe@ZnS core-shell QDs were reported and showed higher efficiencies and lifetimes.[46] In all these examples, the QDs and polymers or organic molecules are either blended with each other or deposited as different layers. Another approach is to use hybrids, in which the polymer is chemically bound to the QDs (paragraph 1.3). The devices showed improved performance compared to devices prepared with pristine QDs, and the hybrids exhibited excellent film forming properties, which allowed micropatterning.[104, 105]

1.5 Solar Cells

The light that the sun sends to the earth every day is more than enough to satisfy our energy needs if properly collected. It delivers $1.5 \cdot 10^{18}$ kW/h per year, which is much more than we need ($15 \cdot 10^{9}$ kW/h per year).[106, 107] Solar energy is available infinitely and is therefore very suitable to overcome our energy problems. Solar cells harvest the sunlight and transform it into electric energy. The different types of solar cells are presented in the following pages.

1.5.1 Semiconductor Solar Cells

Commercially available solar cells consist of silicon. It can either be crystalline,[108] amorphous,[109] or as wires.[110] Mono crystalline or poly crystalline solar cells have high power conversion efficiencies of up to 20%, but need a lot of energy for their production which makes a negative overall energy gain.[111]Also, small impurities have a large effect on the cell performance.[112] Amorphous silicon devices have lower power conversion efficiencies but are cheaper in production.[113] Mono- or multilayered solar cells (tandem-cells) based on III-V semiconductors show enhanced performances because the Shockley-Queisser[114] limit can be extended due to the multiple p-n junctions. They show the highest power conversion efficiencies with more than 40%.[115-120] They find applications in aeronautics, but their production costs are very high.

1.5.2 Dye sensitized Solar cells and Solid State DSSC

The first dye-sensitized solar cell (DSSC) was invented by O'Regan and Grätzel in 1991.[121] Nanoporous TiO_2 was used as an electron acceptor, a Ru(II) polypyridyl sensitizer as a light harvesting unit and I_3/I^- as a hole conductor. The major advantages of this system are that solar cells can be produced with affordable costs. Power efficiency conversions of 7% were achieved, and have now been raised to more than 12%.[122-124] Considerable research was devoted to the enhancement of the chromophore, which has to fulfill several requirements. Firstly, the absorption should ideally cover the whole solar spectrum and the extinction coefficient has to be very high. A high chemical and photochemical stability and an easy tuning are also preferable. Furthermore, the dye should have anchor groups (e.g. -COOH, $-H_2PO_3$) to bind to the surface of the electron acceptor. Various ruthenium-free DSSCs were built using other metal complexes based on osmium,[125] iron[126, 127] or copper.[128]Later, porphyrines[129] or phtalocyanines[130] were found to be suitable in DSSCs due to their intense absorption in the near-IR region. Highly efficient DSSCs with PCEs of 12% were built.[131] Organic dyes are also good candidates for DSSCs because they can easily be tuned, are cheaper than the noble metal complexes and they provide high molar extinction coefficients. The most successful strategy is the push-pull structure. Herein,

a donor-π-bridge-acceptor structure is the general character of the molecule.[132] A large variety of dyes, including coumarine,[133, 134] indoline[135, 136] or polymeric dyes,[137, 138] have been synthesized and tested in solar cells.[139] PCEs of up to 10% can now be achieved.[140] In addition to the adjustment of the sensitizer, other attempts to enhance the performance of DSSCs included using nanowires as electron acceptor units, because a higher electron transport rate was expected.[141] By using a specific perovskite ($CH_3NH_3PbI_2Cl$) as light absorber with intense visible to near-IR absorbitivity, a DSSC with a PCE of 10.9% was built.[142]

However, DSSCs suffer from a significant drawback: the possible leakage of the hole conductor I_3/I^- which is dissolved in a liquid. The stability of the cells against environmental stress is low. For this reason, solid-state DSSCs (ssDSSCs) were introduced.[143, 144] I_3/I^- was replaced by oligoethylene glycol methacrylate; ethylene glycol and lithium iodide were added to enhance the performance. In the following years different polymers,[145] organic molecules,[146] or inorganic nanoarrays[147] were introduced as *p*-type conductors. A quasi ssDSSC was reported with an amphiphilic ruthenium dye and a polymer as gel electrolyte with a PCE of more than 6%.[148] But even though the stability was enhanced, the power conversion efficiency was lower compared to the conventional DSSCs. One of the reasons was the low penetration rate of the sensitizer in the nanoporous TiO_2 layer. Recently, an all-solid-state dye-sensitized solar cell was reported where solution processable $CsSnI_3$ was used as a hole conductor. Power conversion efficiencies of around 10% could be achieved.[149]

1.5.3 Organic Solar Cells

In contrast to inorganic semiconductor solar cells, organic solar cells (OSCs) provide flexibility, can be print-processed and are cheaper to produce. On the other hand, they cannot reach their efficiencies. The main drawback is the recombination of the excitons. Even though powerful molecules with high absorption coefficients are used, the morphology at nanoscale is determining the performance. The exciton that forms at illumination can diffuse around 10 nm away before it recombines. Therefore, a highly ordered nanostructure of the donor and the acceptor metarials is desired to achieve efficient charge generation. Two-layer OSCs of a donor (D) and an acceptor (A) were found to have higher efficiencies than mono-layer devices,[150] but the charge percolation pathways were still not optimal. Bulk heterojunction (BHJ) solar cells were introduced and found to show enhanced performances.[151] However, the morphology is still quite poor and many excitons recombine within the material which leads to poor efficiencies. The well ordered structure is considered ideal for solar cells and is shown in Figure 9. In this case, the thicknesses of donor and acceptor layers are around 20 nm and the charge pathways for the electrons and holes designated. A highly efficient charge generation is expected. The choice of the

material is crucial for the efficiency of organic solar cells. The requirements for the light absorbing materials are a low bandgap of around 1.4 eV (determined by the Shockley-Quiesser equation[114]) in order to harvest a greater part of the solar spectrum, a high charge carrier mobility, and a favorable morphology when blended with the acceptor. Organic solar cells can be classified in three groups according to the materials that are used, and are described as follows.

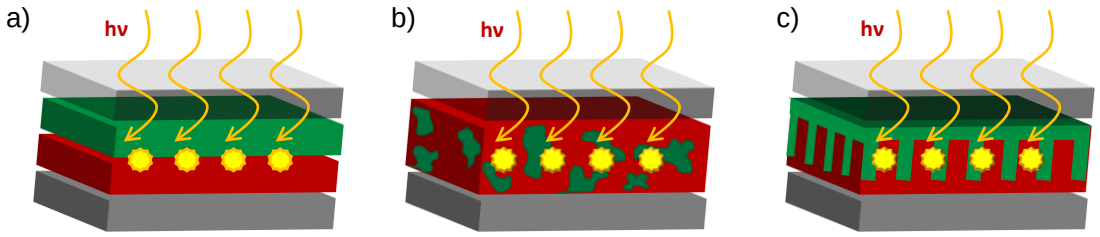

Figure 9. Schematic of different morphologies in organic solar cells. **a)** bilayer, **b)** bulk heterojunction and **c)** well ordered.

1.5.3.1 Polymer-Polymer Solar Cells

A relatively small group are the polymer-polymer solar cells. Herein, a donor and an acceptor polymer are either blended or covalently bound to each other (e.g. block copolymers). Beside the low production costs, the advantages are that both materials exhibit a very high absorption coefficient and can cover a wide part of the solar spectrum. Tuning of the polymers by changing the chemical structure is very easy so that optical properties and charge transfer as well as charge collection properties are optimized.[152] The first reported all-polymer solar cell was made with an alkyloxy substituted PPV as electron donor and a cyano substituted PPV as electron acceptor.[153] In the following years, the use of different polymers as well as the tuning of the chemical structure improved the performances of the devices. As an example, the application of PPV as donor and polyfluorene as acceptor gave power conversion efficiencies of 1.5%.[152] Later, the high regioregularity of a polythiophene derivative as donor in combination with a cyano-substituted PPV as acceptor increased the PCE to 2%,[154] and the application of a high molecular weight fluorine based copolymer and P3HT as donor yielded devices with a PCE of 2.7%.[155] Even though the idea of polymer-polymer based solar cells is very attractive, the current devices cannot compete with polymer-fullerene solar cells.

1.5.3.2 Polymer-Fullerene Solar Cells

Until now, polymer-fullerence bulk heterojunction solar cells show the highest efficiencies among organic solar cells. Semiconducting polymers are blended with a fullerene, typically $PC_{60}BM$. First attempts were made with PPV and C_{60} fullerene but gave poor results.[156] The most

prominent example are P3HT:PCBM bulk heterojunction solar cells. With these the hole conducting polymer P3HT and the electron conducting fullerene derivative PCBM are blended and annealed in order to get a good morphology at nanoscale. Power conversion efficiencies of 4-5% can be achieved.[157, 158] In order to further increase the performances, low band gap polymers were introduced to harvest more light.[159] To achieve the lower band gap, copolymers with donor and acceptor groups were synthesized. The push-pull effect lowered the band gap and increased the PCE to 5.5%.[160] Variations in the end groups also showed better performances due to a better morphology at nanoscale.[161] Another approach was the introduction of hetero atoms like nitrogen or selenium.[162, 163] State of the art polymer-fullerene solar cells show efficiencies of up to 7.3%,[164] and 7.6%.[165] Another key development was the design of inverted polymer solar cells. Herein, the anode and cathode are reversed. Record efficiencies of more than 9% could be achieved.[166-168] Even though the invention of new low bandgap polymers and new device engineering enhances performances, polymer solar cells still cannot reach the efficiencies of conventional silicon based solar cells. Another drawback is their short lifetimes, due to degradation of the polymers under irradiation with sun light.

1.5.3.3 Polymer-Inorganic Nanoparticle Hybrid Solar Cells

Another class of solar cell is the hybrid solar cell. They are composed of semiconducting polymers and semiconducting inorganic NCs. The morphology at nanoscale is again very important for an efficient charge separation. By simply blending the two materials together, undesired phase separation occurs which lowers the performance of the device. Therefore, the influence of the end group of the semiconducting polymer in CdSe QD solar cells was studied. It was found that the end group has an attribution to the performance. Br/allyl-terminated P3HT showed a higher PCE (0.9%) than H/Br-(0.45%) or H/thiol-terminated P3HT (0.6%).[169] Also, semiconducting P3HT were grafted to QDs and an enhancement in the efficiency of the solar cell compared to the physical blend was found.[170] In this case the two materials are covalently bound to each other and no phase separation can occur. The exciton can diffuse to the interface and charges can be generated. To further improve the performance, a low bandgap polymer (PCPDTBT) was used, so that more light can be harvested.[171] Instead of using spherical NCs, the use of semiconducting nanorods or wires of ZnO further increased the charge transport properties.[172] Hybrid CdSe nanorod-P3HT hybrid solar cells showed efficiencies of up to 1.7%.[29] CdTe or CdSe tetrapods are supposed to provide the best charge pathways since they can create interconnected networks. Solar cells with PPV and $CdSe_xTe_{1-x}$[173] or CdSe[174] as well as P3HT CdSe, CdTe or CdTe/CdSe tetrapod solar cells[175] were built and the efficiencies were enhanced. By using a low bandgap polymer with an amine end group and subsequent annealing, a PCE of 3.2% could be achieved with CdTe tetrapods.[176] The amine group plays an important

role in this device since it can bind to the tetrapod surface and thus enhance the interfacial donor-acceptor contact. The destructive effect of traps on the QD surface is dramatically illustrated in a recent publication, in which a hybrid ligand system consisting of organic molecules and halide ions on PbS nanocrystals leads to solar cells with a high PCE of more than 7%.

In order to better understand the comparably poor efficiencies of the polymer-polymer and polymer-inorganic nanocrystal solar cells compared with polymer-fullerene solar cells, transient photocurrent and photovoltage studies have been carried out.[177] It was shown that charge trapping does not significantly affect the P3HT-PCBM devices, whereas in P3HT-polyfluorene and P3HT-CdSe NC hybrid systems, the charge extraction is hindered by a rapid charge trapping. Overcoming this defect is a major goal of recent research.

In conclusion, semiconductor based solar cells still show the highest efficiencies, but dye sensitized solar cells or solar cells based on polymers or hybrid systems are promising low cost alternatives to overcome the energy needs of the world.

1.6 References

[1] C. K. Chiang, C. R. Fincher, Y. W. Park, A. J. Heeger, H. Shirakawa, E. J. Louis, S. C. Gau, A. G. Macdiarmid, *Phys. Rev. Lett.* **1977**, *39*, 1098.

[2] J. M. Warman, M. P. de Haas, G. Dicker, F. C. Grozema, J. Piris, M. G. Debije, *Chemistry of Materials* **2004**, *16*, 4600.

[3] A. J. Heeger, *Chemical Society Reviews* **2010**, *39*, 2354.

[4] R. Hoofman, M. P. de Haas, L. D. A. Siebbeles, J. M. Warman, *Nature* **1998**, *392*, 54.

[5] D. Adam, P. Schuhmacher, J. Simmerer, L. Haussling, K. Siemensmeyer, K. H. Etzbach, H. Ringsdorf, D. Haarer, *Nature* **1994**, *371*, 141.

[6] A. J. Heeger, *Angew. Chem.-Int. Edit.* **2001**, *40*, 2591.

[7] D. Braun, A. J. Heeger, *Appl. Phys. Lett.* **1991**, *58*, 1982.

[8] D. D. C. Bradley, *J. Phys. D-Appl. Phys.* **1987**, *20*, 1389.

[9] Y. Li, T. Pullerits, M. Zhao, M. Sun, *The Journal of Physical Chemistry C* **2011**, *115*, 21865.

[10] A. E. Siegrist, *Helv. Chim. Acta* **1981**, *64*, 662.

[11] H. Kretzschmann, H. Meier, *Tetrahedron Letters* **1991**, *32*, 5059.

[12] H. Mori, K. Takano, T. Endo, *Macromolecules* **2009**, *42*, 7342.

[13] M. Sommer, A. S. Lang, M. Thelakkat, *Angewandte Chemie International Edition* **2008**, *47*, 7901.

[14] G. Moad, M. Chen, M. Haussler, A. Postma, E. Rizzardo, S. H. Thang, *Polymer Chemistry* **2011**, *2*, 492.

[15] J. Chiefari, Y. K. Chong, F. Ercole, J. Krstina, J. Jeffery, T. P. T. Le, R. T. A. Mayadunne, G. F. Meijs, C. L. Moad, G. Moad, E. Rizzardo, S. H. Thang, *Macromolecules* **1998**, *31*, 5559.

[16] G. Moad, E. Rizzardo, S. H. Thang, *Aust. J. Chem.* **2006**, *59*, 669.

[17] G. Moad, E. Rizzardo, S. H. Thang, *Aust. J. Chem.* **2009**, *62*, 1402.

[18] M. Kato, M. Kamigaito, M. Sawamoto, T. Higashimura, *Macromolecules* **1995**, *28*, 1721.

[19] J.-S. Wang, K. Matyjaszewski, *Journal of the American Chemical Society* **1995**, *117*, 5614.

[20] K. Matyjaszewski, J. Xia, *Chemical Reviews* **2001**, *101*, 2921.

[21] E. Rizzardo, D. Solomon, *Polymer Bulletin* **1979**, *1*, 529.

[22] M. K. Georges, R. P. N. Veregin, P. M. Kazmaier, G. K. Hamer, *Macromolecules* **1993**, *26*, 2987.

[23] D. A. Shipp, *Journal of Macromolecular Science, Part C* **2005**, *45*, 171.

[24] J. Park, J. Joo, S. G. Kwon, Y. Jang, T. Hyeon, *Angew. Chem.-Int. Edit.* **2007**, *46*, 4630.

[25] V. L. Colvin, M. C. Schlamp, A. P. Alivisatos, *Nature* **1994**, *370*, 354.

[26] *Adv. Mater.* **2003**, *15*, 341.

[27] Y. Xia, P. Yang, Y. Sun, Y. Wu, B. Mayers, B. Gates, Y. Yin, F. Kim, H. Yan, *Adv. Mater.* **2003**, *15*, 353.

[28] J. Hu, L.-s. Li, W. Yang, L. Manna, L.-w. Wang, A. P. Alivisatos, *Science* **2001**, *292*, 2060.

[29] W. U. Huynh, J. J. Dittmer, A. P. Alivisatos, *Science* **2002**, *295*, 2425.

[30] V. I. Klimov, A. A. Mikhailovsky, S. Xu, A. Malko, J. A. Hollingsworth, C. A. Leatherdale, H.-J. Eisler, M. G. Bawendi, *Science* **2000**, *290*, 314.

[31] C. Z. Li, H. X. He, A. Bogozi, J. S. Bunch, N. J. Tao, *Appl. Phys. Lett.* **2000**, *76*, 1333.

[32] Y. Cui, Q. Wei, H. Park, C. M. Lieber, *Science* **2001**, *293*, 1289.

[33] H. Yan, R. He, J. Pham, P. Yang, *Adv. Mater.* **2003**, *15*, 402.

[34] D. Jariwala, V. K. Sangwan, L. J. Lauhon, T. J. Marks, M. C. Hersam, *Chemical Society Reviews* **2012**.

[35] A. Hagfeldt, M. Grätzel, *Chemical Reviews* **1995**, *95*, 49.

[36] X. Chen, S. S. Mao, *Chemical Reviews* **2007**, *107*, 2891.

[37] A. Mills, S. Le Hunte, *Journal of Photochemistry and Photobiology A: Chemistry* **1997**, *108*, 1.

[38] A. Fujishima, K. Honda, *Nature* **1972**, *238*, 37.

[39] A. L. Linsebigler, G. Lu, J. T. Yates, *Chemical Reviews* **1995**, *95*, 735.

[40] K. Nakata, A. Fujishima, *Journal of Photochemistry and Photobiology C: Photochemistry Reviews* **2012**, *13*, 169.

[41] C. J. Barbé, F. Arendse, P. Comte, M. Jirousek, F. Lenzmann, V. Shklover, M. Grätzel, *Journal of the American Ceramic Society* **1997**, *80*, 3157.

[42] Y. Hwu, Y. D. Yao, N. F. Cheng, C. Y. Tung, H. M. Lin, *Nanostructured Materials* **1997**, *9*, 355.

[43] H. Zhang, J. F. Banfield, *Journal of Materials Chemistry* **1998**, *8*, 2073.

[44] S. Shubra, P. Thiyagarajan, K. M. Kant, D. Anita, S. Thirupathiah, N. Rama, T. Brajesh, M. Kottaisamy, M. S. R. Rao, *Journal of Physics D: Applied Physics* **2007**, *40*, 6312.

[45] X. Wang, C. J. Summers, Z. L. Wang, *Nano Letters* **2004**, *4*, 423.

[46] J. Kwak, W. K. Bae, D. Lee, I. Park, J. Lim, M. Park, H. Cho, H. Woo, D. Y. Yoon, K. Char, S. Lee, C. Lee, *Nano Letters* **2012**, *12*, 2362.

[47] L. F. Dong, Z. L. Cui, Z. K. Zhang, *Nanostructured Materials* **1997**, *8*, 815.
[48] N.-G. Park, M. G. Kang, K. S. Ryu, K. M. Kim, S. H. Chang, *Journal of Photochemistry and Photobiology A: Chemistry* **2004**, *161*, 105.
[49] D. L. J. Thorek, A. Chen, J. Czupryna, A. Tsourkas, *Ann. Biomed. Eng.* **2006**, *34*, 23.
[50] C. Wang, J. C. Zhao, X. M. Wang, B. X. Mai, G. Y. Sheng, P. Peng, J. M. Fu, *Appl. Catal. B-Environ.* **2002**, *39*, 269.
[51] C. B. Murray, D. J. Norris, M. G. Bawendi, *Journal of the American Chemical Society* **1993**, *115*, 8706.
[52] L. Brus, *Applied Physics A* **1991**, *53*, 465.
[53] X. Michalet, F. F. Pinaud, L. A. Bentolila, J. M. Tsay, S. Doose, J. J. Li, G. Sundaresan, A. M. Wu, S. S. Gambhir, S. Weiss, *Science* **2005**, *307*, 538.
[54] M. Bruchez, M. Moronne, P. Gin, S. Weiss, A. P. Alivisatos, *Science* **1998**, *281*, 2013.
[55] W. C. W. Chan, S. Nie, *Science* **1998**, *281*, 2016.
[56] A. J. Nozik, *Physica E: Low-dimensional Systems and Nanostructures* **2002**, *14*, 115.
[57] T. H. Kim, K. S. Cho, E. K. Lee, S. J. Lee, J. Chae, J. W. Kim, D. H. Kim, J. Y. Kwon, G. Amaratunga, S. Y. Lee, B. L. Choi, Y. Kuk, J. M. Kim, K. Kim, *Nat. Photonics* **2011**, *5*, 176.
[58] A. L. Rogach, D. V. Talapin, E. V. Shevchenko, A. Kornowski, M. Haase, H. Weller, *Advanced Functional Materials* **2002**, *12*, 653.
[59] M. G. Bawendi, M. L. Steigerwald, L. E. Brus, *Annu. Rev. Phys. Chem.* **1990**, *41*, 477.
[60] B. O. Dabbousi, J. RodriguezViejo, F. V. Mikulec, J. R. Heine, H. Mattoussi, R. Ober, K. F. Jensen, M. G. Bawendi, *J. Phys. Chem. B* **1997**, *101*, 9463.
[61] P. Reiss, J. l. Bleuse, A. Pron, *Nano Letters* **2002**, *2*, 781.
[62] A. P. Alivisatos, *Science* **1996**, *271*, 933.
[63] M. Chen, Y. Xie, J. Lu, Y. Xiong, S. Zhang, Y. Qian, X. Liu, *Journal of Materials Chemistry* **2002**, *12*, 748.
[64] L. Manna, D. J. Milliron, A. Meisel, E. C. Scher, A. P. Alivisatos, *Nat Mater* **2003**, *2*, 382.
[65] H. Zhong, G. D. Scholes, *Journal of the American Chemical Society* **2009**, *131*, 9170.
[66] A. Fiore, R. Mastria, M. G. Lupo, G. Lanzani, C. Giannini, E. Carlino, G. Morello, M. De Giorgi, Y. Li, R. Cingolani, L. Manna, *Journal of the American Chemical Society* **2009**, *131*, 2274.
[67] D. V. Talapin, J. H. Nelson, E. V. Shevchenko, S. Aloni, B. Sadtler, A. P. Alivisatos, *Nano Letters* **2007**, *7*, 2951.
[68] J. Lim, W. K. Bae, K. U. Park, L. zur Borg, R. Zentel, S. Lee, K. Char, *submitted* **2012**.
[69] P. Reiss, E. Couderc, J. De Girolamo, A. Pron, *Nanoscale* **2011**, *3*, 446.
[70] J. Liu, T. Tanaka, K. Sivula, A. P. Alivisatos, J. M. J. FrÃ©chet, *Journal of the American Chemical Society* **2004**, *126*, 6550.
[71] I. Gur, N. A. Fromer, C.-P. Chen, A. G. Kanaras, A. P. Alivisatos, *Nano Letters* **2006**, *7*, 409.
[72] S. D. Oosterhout, M. M. Wienk, S. S. van Bavel, R. Thiedmann, L. Jan Anton Koster, J. Gilot, J. Loos, V. Schmidt, R. A. J. Janssen, *Nat Mater* **2009**, *8*, 818.
[73] M. C. Orilall, U. Wiesner, *Chemical Society Reviews* **2011**, *40*, 520.
[74] E. Holder, N. Tessler, A. L. Rogach, *Journal of Materials Chemistry* **2008**, *18*, 1064.
[75] M. Brinkmann, J. C. Wittmann, *Adv. Mater.* **2006**, *18*, 860.
[76] M. Brinkmann, D. Aldakov, F. Chandezon, *Adv. Mater.* **2007**, *19*, 3819.
[77] S. Gupta, Q. Zhang, T. Emrick, T. P. Russell, *Nano Letters* **2006**, *6*, 2066.
[78] L. Zhao, Z. Lin, *Adv. Mater.* **2012**, *24*, 4353.
[79] N. Hundt, K. Palaniappan, P. Sista, J. W. Murphy, J. Hao, H. Nguyen, E. Stein, M. C. Biewer, B. E. Gnade, M. C. Stefan, *Polymer Chemistry* **2010**, *1*, 1624.
[80] M. Zorn, R. Zentel, *Macromol. Rapid Commun.* **2008**, *29*, 922.
[81] D. J. Milliron, A. P. Alivisatos, C. Pitois, C. Edder, J. M. J. Fréchet, *Adv. Mater.* **2003**, *15*, 58.
[82] T. von Werne, T. E. Patten, *Journal of the American Chemical Society* **2001**, *123*, 7497.
[83] J. Raula, J. Shan, M. Nuopponen, A. Niskanen, H. Jiang, E. I. Kauppinen, H. Tenhu, *Langmuir* **2003**, *19*, 3499.
[84] H. Skaff, K. Sill, T. Emrick, *Journal of the American Chemical Society* **2004**, *126*, 11322.
[85] A. Watt, E. Thomsen, P. Meredith, H. Rubinsztein-Dunlop, *Chemical Communications* **2004**, 2334.
[86] A. Stavrinadis, R. Beal, J. M. Smith, H. E. Assender, A. A. R. Watt, *Adv. Mater.* **2008**, *20*, 3105.
[87] H. Zheng, R. K. Smith, Y.-w. Jun, C. Kisielowski, U. Dahmen, A. P. Alivisatos, *Science* **2009**, *324*, 1309.
[88] N. Holonyak, S. F. Bevacqua, *Appl. Phys. Lett.* **1962**, *1*, 82.
[89] S. Nakamura, T. Mukai, M. Senoh, *Appl. Phys. Lett.* **1994**, *64*, 1687.
[90] S. Nakamura, *Science* **1998**, *281*, 956.

[91] P. Waltereit, O. Brandt, A. Trampert, H. T. Grahn, J. Menniger, M. Ramsteiner, M. Reiche, K. H. Ploog, *Nature* **2000**, *406*, 865.
[92] H. Hirayama, *Journal of Applied Physics* **2005**, *97*, 19.
[93] V. A. Montes, G. Li, R. Pohl, J. Shinar, P. Anzenbacher, *Adv. Mater.* **2004**, *16*, 2001.
[94] R. C. Evans, P. Douglas, C. J. Winscom, *Coord. Chem. Rev.* **2006**, *250*, 2093.
[95] S. Lamansky, P. Djurovich, D. Murphy, F. Abdel-Razzaq, H.-E. Lee, C. Adachi, P. E. Burrows, S. R. Forrest, M. E. Thompson, *Journal of the American Chemical Society* **2001**, *123*, 4304.
[96] J. H. Burroughes, D. D. C. Bradley, A. R. Brown, R. N. Marks, K. Mackay, R. H. Friend, P. L. Burns, A. B. Holmes, *Nature* **1990**, *347*, 539.
[97] G. Gustafsson, Y. Cao, G. M. Treacy, F. Klavetter, N. Colaneri, A. J. Heeger, *Nature* **1992**, *357*, 477.
[98] T. Miteva, A. Meisel, W. Knoll, H. G. Nothofer, U. Scherf, D. C. Muller, K. Meerholz, A. Yasuda, D. Neher, *Adv. Mater.* **2001**, *13*, 565.
[99] G. L. Tu, C. Y. Mei, Q. G. Zhou, Y. X. Cheng, Y. H. Geng, L. X. Wang, D. G. Ma, X. B. Jing, F. S. Wang, *Advanced Functional Materials* **2006**, *16*, 101.
[100] L.-P. Lu, D. Kabra, K. Johnson, R. H. Friend, *Advanced Functional Materials* **2012**, *22*, 144.
[101] S. Chaudhary, M. Ozkan, W. C. W. Chan, *Appl. Phys. Lett.* **2004**, *84*, 2925.
[102] Q. Sun, Y. A. Wang, L. S. Li, D. Y. Wang, T. Zhu, J. Xu, C. H. Yang, Y. F. Li, *Nat. Photonics* **2007**, *1*, 717.
[103] E. Jang, S. Jun, H. Jang, J. Llim, B. Kim, Y. Kim, *Adv. Mater.* **2010**, *22*, 3076.
[104] M. Zorn, W. K. Bae, J. Kwak, H. Lee, C. Lee, R. Zentel, K. Char, *ACS Nano* **2009**, *3*, 1063.
[105] J. Kwak, W. K. Bae, M. Zorn, H. Woo, H. Yoon, J. Lim, S. W. Kang, S. Weber, H. J. Butt, R. Zentel, S. Lee, K. Char, C. Lee, *Adv. Mater.* **2009**, *21*, 5022.
[106] K. Kalyanasundaram, M. Gratzel, *Journal of Materials Chemistry* **2012**.
[107] A. J. Nozik, *Inorganic Chemistry* **2005**, *44*, 6893.
[108] J. H. Zhao, A. H. Wang, M. A. Green, F. Ferrazza, *Appl. Phys. Lett.* **1998**, *73*, 1991.
[109] D. E. Carlson, C. R. Wronski, *Appl. Phys. Lett.* **1976**, *28*, 671.
[110] B. Z. Tian, X. L. Zheng, T. J. Kempa, Y. Fang, N. F. Yu, G. H. Yu, J. L. Huang, C. M. Lieber, *Nature* **2007**, *449*, 885.
[111] A. V. Shah, H. Schade, M. Vanecek, J. Meier, E. Vallat-Sauvain, N. Wyrsch, U. Kroll, C. Droz, J. Bailat, *Progress in Photovoltaics: Research and Applications* **2004**, *12*, 113.
[112] J. R. Davis, A. Rohatgi, R. H. Hopkins, P. D. Blais, P. Raichoudhury, J. R. McCormick, H. C. Mollenkopf, *IEEE Trans. Electron Devices* **1980**, *27*, 677.
[113] J. Yang, A. Banerjee, S. Guha, *Appl. Phys. Lett.* **1997**, *70*, 2975.
[114] W. Shockley, H. J. Queisser, *Journal of Applied Physics* **1961**, *32*, 510.
[115] T. Takamoto, E. Ikeda, H. Kurita, M. Ohmori, *Appl. Phys. Lett.* **1997**, *70*, 381.
[116] P. Bermel, C. Luo, L. Zeng, L. C. Kimerling, J. D. Joannopoulos, *Opt. Express* **2007**, *15*, 16986.
[117] G. Conibeer, M. Green, R. Corkish, Y. Cho, E. C. Cho, C. W. Jiang, T. Fangsuwannarak, E. Pink, Y. D. Huang, T. Puzzer, T. Trupke, B. Richards, A. Shalav, K. L. Lin, *Thin Solid Films* **2006**, *511*, 654.
[118] K. A. Bertness, S. R. Kurtz, D. J. Friedman, A. E. Kibbler, C. Kramer, J. M. Olson, *Appl. Phys. Lett.* **1994**, *65*, 989.
[119] K. Tanabe, *Energies* **2009**, *2*, 504.
[120] W. Guter, J. Schone, S. P. Philipps, M. Steiner, G. Siefer, A. Wekkeli, E. Welser, E. Oliva, A. W. Bett, F. Dimroth, *Appl. Phys. Lett.* **2009**, *94*, 223504.
[121] B. O'Regan, M. Grätzel, *Nature* **1991**, *353*, 737.
[122] Y. Chiba, A. Islam, Y. Watanabe, R. Komiya, N. Koide, L. Y. Han, *Jpn. J. Appl. Phys. Part 2 - Lett. Express Lett.* **2006**, *45*, L638.
[123] F. Gao, Y. Wang, D. Shi, J. Zhang, M. Wang, X. Jing, R. Humphry-Baker, P. Wang, S. M. Zakeeruddin, M. Graỉˆtzel, *Journal of the American Chemical Society* **2008**, *130*, 10720.
[124] L. Han, A. Islam, H. Chen, C. Malapaka, B. Chiranjeevi, S. Zhang, X. Yang, M. Yanagida, *Energy & Environmental Science* **2012**, *5*, 6057.
[125] D. Kuciauskas, J. E. Monat, R. Villahermosa, H. B. Gray, N. S. Lewis, J. K. McCusker, *The Journal of Physical Chemistry B* **2002**, *106*, 9347.
[126] S. Ferrere, B. A. Gregg, *Journal of the American Chemical Society* **1998**, *120*, 843.
[127] S. Ferrere, *Inorganica Chimica Acta* **2002**, *329*, 79.
[128] T. Bessho, E. C. Constable, M. Graetzel, A. Hernandez Redondo, C. E. Housecroft, W. Kylberg, M. K. Nazeeruddin, M. Neuburger, S. Schaffner, *Chemical Communications* **2008**, 3717.

[129] W. M. Campbell, K. W. Jolley, P. Wagner, K. Wagner, P. J. Walsh, K. C. Gordon, L. Schmidt-Mende, M. K. Nazeeruddin, Q. Wang, M. GrÃ¤tzel, D. L. Officer, *The Journal of Physical Chemistry C* **2007**, *111*, 11760.
[130] P. Y. Reddy, L. Giribabu, C. Lyness, H. J. Snaith, C. Vijaykumar, M. Chandrasekharam, M. Lakshmikantam, J.-H. Yum, K. Kalyanasundaram, M. Grätzel, M. K. Nazeeruddin, *Angewandte Chemie International Edition* **2007**, *46*, 373.
[131] A. Yella, H.-W. Lee, H. N. Tsao, C. Yi, A. K. Chandiran, M. K. Nazeeruddin, E. W.-G. Diau, C.-Y. Yeh, S. M. Zakeeruddin, M. Grätzel, *Science* **2011**, *334*, 629.
[132] A. Hagfeldt, G. Boschloo, L. Sun, L. Kloo, H. Pettersson, *Chemical Reviews* **2010**, *110*, 6595.
[133] Z. S. Wang, Y. Cui, K. Hara, Y. Dan-oh, C. Kasada, A. Shinpo, *Adv. Mater.* **2007**, *19*, 1138.
[134] K. Hara, Z.-S. Wang, T. Sato, A. Furube, R. Katoh, H. Sugihara, Y. Dan-oh, C. Kasada, A. Shinpo, S. Suga, *The Journal of Physical Chemistry B* **2005**, *109*, 15476.
[135] T. Horiuchi, H. Miura, K. Sumioka, S. Uchida, *Journal of the American Chemical Society* **2004**, *126*, 12218.
[136] S. Ito, S. M. Zakeeruddin, R. Humphry-Baker, P. Liska, R. Charvet, P. Comte, M. K. Nazeeruddin, P. Péchy, M. Takata, H. Miura, S. Uchida, M. Grätzel, *Adv. Mater.* **2006**, *18*, 1202.
[137] X. Liu, R. Zhu, Y. Zhang, B. Liu, S. Ramakrishna, *Chemical Communications* **2008**, 3789.
[138] J. K. Mwaura, X. Zhao, H. Jiang, K. S. Schanze, J. R. Reynolds, *Chemistry of Materials* **2006**, *18*, 6109.
[139] J. N. Clifford, M. Planells, E. Palomares, *Journal of Materials Chemistry* **2012**, *22*, 24195.
[140] W. Zeng, Y. Cao, Y. Bai, Y. Wang, Y. Shi, M. Zhang, F. Wang, C. Pan, P. Wang, *Chemistry of Materials* **2010**, *22*, 1915.
[141] M. Law, L. E. Greene, J. C. Johnson, R. Saykally, P. D. Yang, *Nat. Mater.* **2005**, *4*, 455.
[142] M. M. Lee, J. Teuscher, T. Miyasaka, T. N. Murakami, H. J. Snaith, *Science* **2012**, *338*, 643.
[143] M. Matsumoto, H. Miyazaki, K. Matsuhiro, Y. Kumashiro, Y. Takaoka, *Solid State Ionics* **1996**, *89*, 263.
[144] U. Bach, D. Lupo, P. Comte, J. E. Moser, F. Weissortel, J. Salbeck, H. Spreitzer, M. Gratzel, *Nature* **1998**, *395*, 583.
[145] W. Zhang, Y. M. Cheng, X. O. Yin, B. Liu, *Macromol. Chem. Phys.* **2010**, *212*, 15.
[146] L. Schmidt-Mende, U. Bach, R. Humphry-Baker, T. Horiuchi, H. Miura, S. Ito, S. Uchida, M. Grätzel, *Adv. Mater.* **2005**, *17*, 813.
[147] C. Xu, J. Wu, U. V. Desai, D. Gao, *Nano Letters* **2012**, *12*, 2420.
[148] P. Wang, S. M. Zakeeruddin, J. E. Moser, M. K. Nazeeruddin, T. Sekiguchi, M. Gratzel, *Nat Mater* **2003**, *2*, 402.
[149] I. Chung, B. Lee, J. He, R. P. H. Chang, M. G. Kanatzidis, *Nature* **2012**, *485*, 486.
[150] C. W. Tang, *Appl. Phys. Lett.* **1986**, *48*, 183.
[151] G. Dennler, M. C. Scharber, C. J. Brabec, *Adv. Mater.* **2009**, *21*, 1323.
[152] M. M. Koetse, J. Sweelssen, K. T. Hoekerd, H. F. M. Schoo, S. C. Veenstra, J. M. Kroon, X. Yang, J. Loos, *Appl. Phys. Lett.* **2006**, *88*, 083504.
[153] J. J. M. Halls, C. A. Walsh, N. C. Greenham, E. A. Marseglia, R. H. Friend, S. C. Moratti, A. B. Holmes, *Nature* **1995**, *376*, 498.
[154] T. W. Holcombe, C. H. Woo, D. F. J. Kavulak, B. C. Thompson, J. M. J. Fréchet, *Journal of the American Chemical Society* **2009**, *131*, 14160.
[155] D. Mori, H. Benten, H. Ohkita, S. Ito, K. Miyake, *ACS Applied Materials & Interfaces* **2012**, *4*, 3325.
[156] N. S. Sariciftci, D. Braun, C. Zhang, V. I. Srdanov, A. J. Heeger, G. Stucky, F. Wudl, *Appl. Phys. Lett.* **1993**, *62*, 585.
[157] W. Ma, C. Yang, X. Gong, K. Lee, A. J. Heeger, *Advanced Functional Materials* **2005**, *15*, 1617.
[158] G. Li, V. Shrotriya, J. Huang, Y. Yao, T. Moriarty, K. Emery, Y. Yang, *Nat Mater* **2005**, *4*, 864.
[159] C. J. Brabec, S. Gowrisanker, J. J. M. Halls, D. Laird, S. J. Jia, S. P. Williams, *Adv. Mater.* **2012**, *22*, 3839.
[160] F. Liu, Y. Gu, C. Wang, W. Zhao, D. Chen, A. L. Briseno, T. P. Russell, *Adv. Mater.* **2012**, *24*, 3947.
[161] C. Shim, M. Kim, S.-G. Ihn, Y. S. Choi, Y. Kim, K. Cho, *Chemical Communications* **2012**, *48*, 7206.
[162] H.-Y. Chen, J. Hou, S. Zhang, Y. Liang, G. Yang, Y. Yang, L. Yu, Y. Wu, G. Li, *Nat Photon* **2009**, *3*, 649.
[163] L. Dou, W.-H. Chang, J. Gao, C.-C. Chen, J. You, Y. Yang, *Adv. Mater.* **2012**, n/a.
[164] C. M. Amb, S. Chen, K. R. Graham, J. Subbiah, C. E. Small, F. So, J. R. Reynolds, *Journal of the American Chemical Society* **2011**, *133*, 10062.

[165] L. Huo, S. Zhang, X. Guo, F. Xu, Y. Li, J. Hou, *Angewandte Chemie International Edition* **2011**, *50*, 9697.
[166] Z. He, C. Zhong, S. Su, M. Xu, H. Wu, Y. Cao, *Nat Photon* **2012**, *6*, 591.
[167] J. Sun, Y. Zhu, X. Xu, L. Lan, L. Zhang, P. Cai, J. Chen, J. Peng, Y. Cao, *The Journal of Physical Chemistry C* **2012**, *116*, 14188.
[168] Y. Sun, J. H. Seo, C. J. Takacs, J. Seifter, A. J. Heeger, *Adv. Mater.* **2011**, *23*, 1679.
[169] K. Palaniappan, J. W. Murphy, N. Khanam, J. Horvath, H. Alshareef, M. Quevedo-Lopez, M. C. Biewer, S. Y. Park, M. J. Kim, B. E. Gnade, M. C. Stefan, *Macromolecules* **2009**, *42*, 3845.
[170] S. Ren, L.-Y. Chang, S.-K. Lim, J. Zhao, M. Smith, N. Zhao, V. Bulović, M. Bawendi, S. Gradečak, *Nano Letters* **2011**, *11*, 3998.
[171] Y. Zhou, M. Eck, C. Veit, B. Zimmermann, F. Rauscher, P. Niyamakom, S. Yilmaz, I. Dumsch, S. Allard, U. Scherf, M. Krüger, *Sol. Energy Mater. Sol. Cells* **2011**, *95*, 1232.
[172] A. L. Briseno, T. W. Holcombe, A. I. Boukai, E. C. Garnett, S. W. Shelton, J. J. M. Frechet, P. D. Yang, *Nano Letters* **2009**, *10*, 334.
[173] Z. Yi, L. Yunchao, Z. Haizheng, H. Jianhui, D. Yuqin, Y. Chunhe, L. Yongfang, *Nanotechnology* **2006**, *17*, 4041.
[174] B. Sun, E. Marx, N. C. Greenham, *Nano Letters* **2003**, *3*, 961.
[175] H. Lee, S. Kim, W. S. Chung, K. Kim, D. Kim, *Sol. Energy Mater. Sol. Cells* **2011**, *95*, 446.
[176] H. C. Chen, C. W. Lai, I. C. Wu, H. R. Pan, I. W. P. Chen, Y. K. Peng, C. L. Liu, C. H. Chen, P. T. Chou, *Adv. Mater.* **2011**, *23*, 5451.
[177] Z. Li, F. Gao, N. C. Greenham, C. R. McNeill, *Advanced Functional Materials* **2011**, *21*, 1419.
[178] K. Suzuki, A. Kobayashi, S. Kaneko, K. Takehira, T. Yoshihara, H. Ishida, Y. Shiina, S. Oishi, S. Tobita, *Physical Chemistry Chemical Physics* **2009**, *11*, 9850.

2. Aim of work

The objective of this work is to synthesize new semiconducting block copolymers for the functionalization of inorganic nanocrystals. The polymers consist of a long, solubility enhancing block and a short anchor group block. The main focus of this work is the investigation of the self-organization of the hybrid materials in order to create excellent morphologies at nanoscale. Furthermore, the properties of the polymer are fine-tuned for the application's purpose. This can either be the self-organization of conjugated polymers to create advanced morphologies, or adjustment of the band gap for the improvement of light emitting diodes. The use of new semiconducting inorganic nanocrystals is important for achieving better optical properties or better charge pathways. To this end, cadmium selenide tetrapods are applied.

The characterization of the improved materials is essential. To achieve this, new techniques can be applied. Hybrid materials suitable for application in solar cells can be characterized with Kelvin probe force microscopy in order to detect local charge generations and separations. Another significant part is the application of these materials in optoelectronic devices like light emitting diodes. The effect of the fine-tuning can then be understood.

3. Results and Discussion

This work deals with the synthesis of new functional semiconducting block copolymers and the subsequent functionalization of various inorganic nanostructures with them. In addition, the morphology at nanoscale and applications of the new hybrid materials in optoelectronic devices is demonstrated. In the following chapters, two different classes of semiconducting polymers are presented.

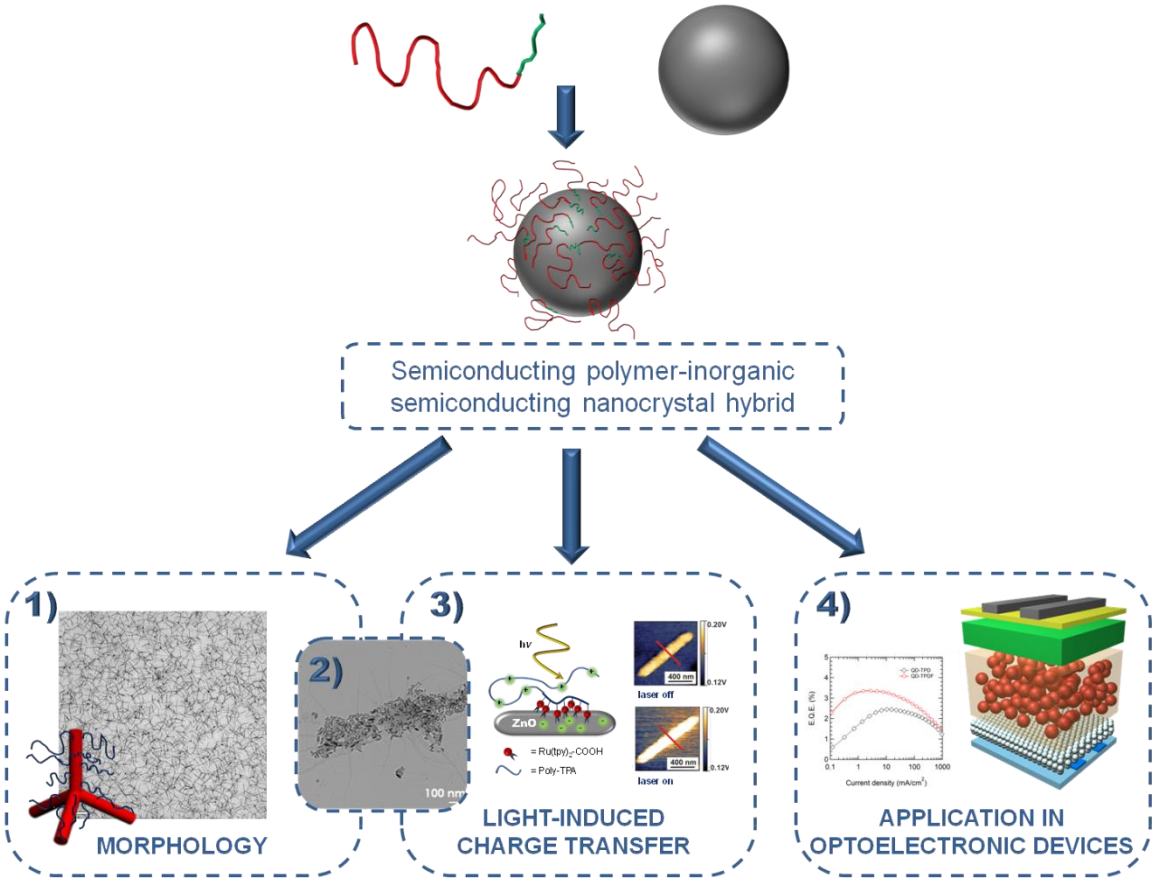

Figure 10. Overview of the different topics presented in this work. **1)**Morphology control of CdSe tetrapod-semiconducting polymer hybrids. **2)** Incorporation of TiO_2 nanorods into fibers of semiconducting polymer and subsequent investigation of light-induced charge transfer. **3)** Light-induced charge transfer of a donor-chromophore acceptor system based on a semiconducting polymer, a bis-terpyridyl ruthenium(II) dye and ZnO nanorods. **4)** Effect of the band gap alignment of hole transporting polymers in quantum dot light emitting diodes.

Firstly, poly(*para*-phenylene vinylene) which was synthesized by Siegrist polycondensation and secondly poly(vinyltriphenylamine) derivatives synthesized by RAFT polymerization. The work in general shows the effect and importance of the anchor groups in the semiconducting block copolymers for the example of tetrapods. The aspect of self-assembly is further extended for the example of a polymer that forms fibers and is loaded with nanoparticles. New functional structures at nanoscale were obtained, that showed an efficient charge transfer at irradiation, which makes them suitable for organic solar cells. The light induced charge transfer is then presented at a new donor-chromophore-acceptor nanocomposite, where the direct binding of the chromophore to both, the donor and the acceptor, is beneficial. The effect of the band gap alignment of the hole transporting polymers is further on presented. These different projects will be presented in detail in the following section.

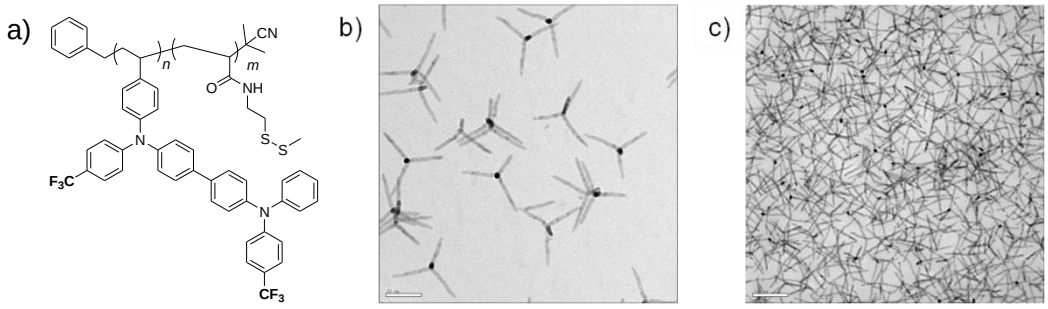

Figure 11. a) Structure of the polymer used for the functionalization of semiconducting nanosized tetrapods, **b)** TEM picture of the as-synthesized tetrapods and **c)** TEM picture of the polymer-tetrapod hybrids film.

In the first chapter, a new class of semiconducting organic-inorganic hybrids is presented. Monodisperse CdSe tetrapods, synthesized with different arm lengths, are functionalized with a semiconducting block copolymer, poly(TPDF-b-SSMe) (Figure 11). The vinyltriphenylamine dimer units provide the semiconducting character and the disulfide groups anchor to the surface of the tetrapods. Three different arm lengths of tetrapods (100 nm, 70 nm and 40 nm) were used for this study, and different mixing ratios of polymers and tetrapods (90:10, 80:20, 70:30 and 50:50, respectively) were fabricated. As reference sample, the same materials were fabricated but the polymer had no anchor groups. The morphology was investigated by TEM. All samples made of hybrid material showed excellent morphologies in terms of dispersion/aggregation of the tetrapods. However, the physical mixtures showed aggregation of tetrapods and cracks in the film. The good control about morphology was extended in the second project.

A new PPV derivative, which gels in organic solvents and forms networks of thin fibers, was transformed into a functional block copolymer carrying anchor groups, poly(*para*-(2,5-bis pentyloxy)phenylene vinylene-*b*-dopamine acrylamide) (Figure 12). It was further on loaded with TiO_2 nanorods. Different fascinating superstructures were found. In a mixture of 90% hybrid and

only 10% homopolymer, the nanorods were incorporated into the network of the polymer fibers. When the polymer content was increased, different superstructures like long strands, loaded with nanorods, or micelles, filled with nanorods, could be seen in the TEM images. Kelvin probe force microscopy (KPFM) was used to verify the suitability of this system for solar cells. A light-induced charge transfer was observed, accompanied with a charge separation: the polymer transferred electrons to the TiO_2 nanorods. Additionally charge transport along the fibers for up to 150 nm was observed.

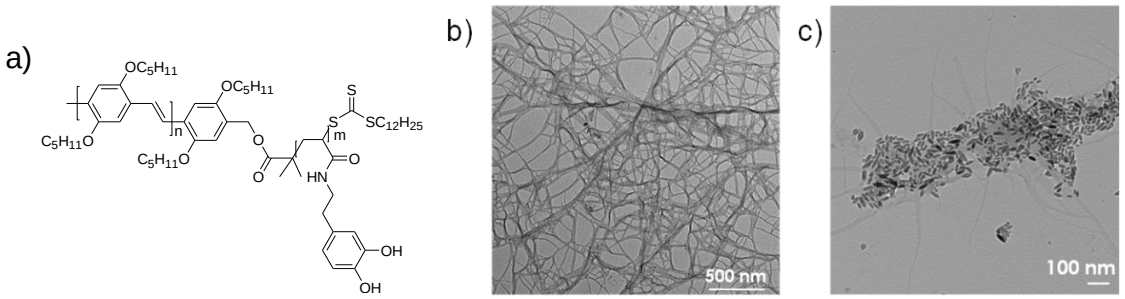

Figure 12. a) Structure of the semiconducting block copolymer that forms gels with a thin fibrous structure, **b)** TEM image of the fibrous network formed by the polymer and **c)** TEM image of the polymer fiber loaded with TiO_2 nanorods.

The third project of this work deals again with light-induced charge transfer, but demonstrated at different systems. A new donor-chromophore-acceptor system was synthesized, in which all three components were attached covalently to each other. Poly(vinyltriphenylamine-*b*-pentafluorophenyl acrylate) (Figure 13) was reacted with a bis(terpyridine)ruthenium(II) chromophore. The chromophore carried an amino group on one side, which was used to attach it to the polymer, and a carboxyl group on the other side, which can anchor to oxidic surfaces. This functional block copolymer was then attached to ZnO nanorods. Charge transfer and separation was investigated by photoluminescence spectroscopy and KPFM. Both methods confirmed a charge transfer, when the sample was illuminated with light of the absorption maximum of the chromophore. KPFM measurements showed a positive charging of the polymer corona on the surface of the ZnO nanorods.

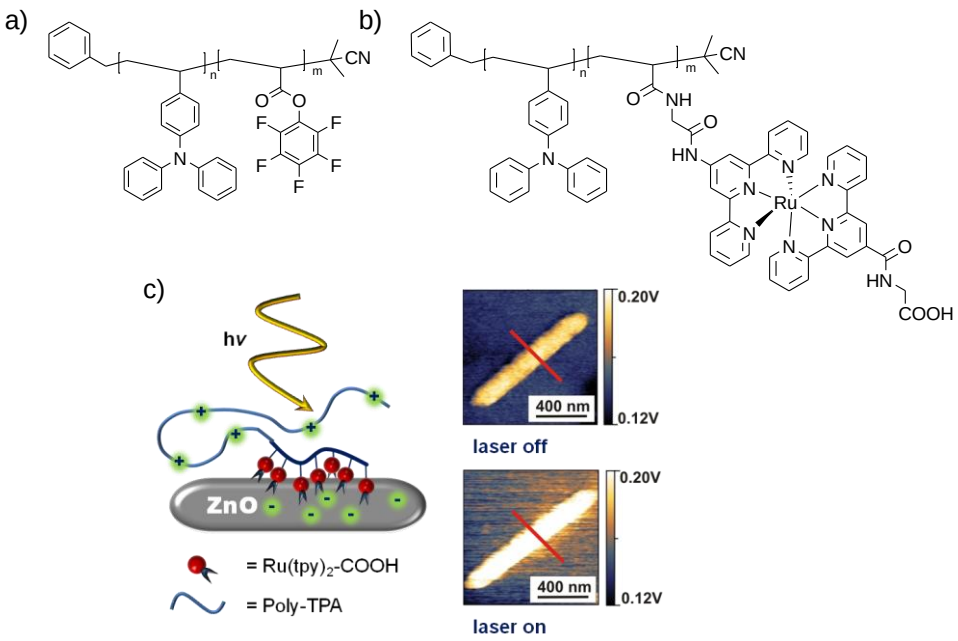

Figure 13. a) Reactive ester block copolymer, **b)** Semiconducting ruthenium(II)-chromophore containing block copolymer and **c)** schematic of the donor-chromophore-acceptor system and KPFM images of the sample in dark (top) and irradiated (bottom).

In the last project of this work, the effect of the band gap alignment of the hole transporting polymer was investigated. It is important for the fabrication of highly efficient QLEDs to understand this influence. First, two different semiconducting block copolymers were synthesized: One with an electron donating methoxy group and the other one with an electron withdrawing trifluoromethyl group (Figure 14). Both polymers carried the same disulfide anchor groups in the second block. The HOMO levels were calculated by cyclovoltammetry, and a difference of 0.7 eV was found. Hybridization of CdSe/CdS/CdZnS red QDs was the following step. The chemical bonding of the polymers to the QDs was checked by solubility change and by TEM. After having proven the success of the hybridization, inverted structure QLEDs were fabricated. Both devices showed good performances, but the device built with the polymer with the lower HOMO level showed a better external quantum efficiency and turn-on voltage. In the latter case, a direct and non-disturbed hole transport from the anode to the active material. In the case of the polymer with the electron donating groups, the HOMO level is too high to provide a smooth hole transport. Hence, we can say that the alignment of the HOMO level of the hole transporting material is crucial for the performance of QLEDs.

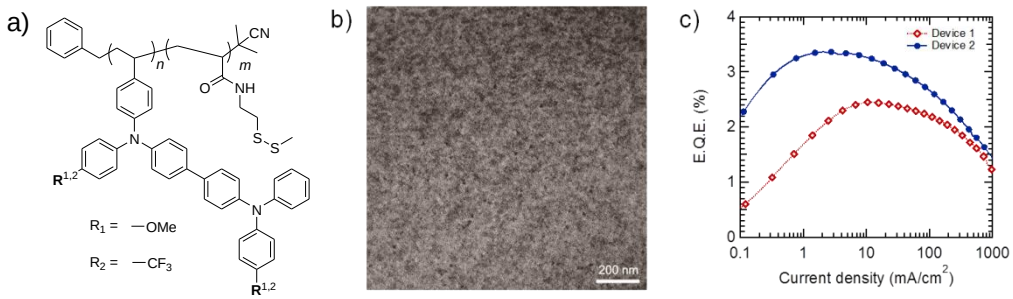

Figure 14. a) Chemical structure of the polymers used for this project, **b)** TEM image of a spin-coated film of polymer-QD hybrids and **c)** device performance of QLED built with the two different polymers: external quantum efficiency versus the current density.

All these projects demonstrate clearly the beneficial effect of anchor groups in the block copolymer, but also show the synthesis of new materials for either solar cells or light emitting diodes.

3.1 Annealing-Free Enhanced Morphology of Semiconducting Polymer-Inorganic Tetrapod Hybrids

L. zur Borg, J. Lim, K. Char, R. Zentel

Abstract

The functionalization of monodisperse CdSe tetrapods with a semiconducting block copolymer which is chemically bound to the surface is demonstrated. The influence of the polymer loading and different arm lengths of the tetrapods in order to get a uniform distribution is investigated.

Introduction

Creating a well defined morphology at nanoscale of two different materials is challenging. It is especially important in optoelectronic devices like organic solar cells. Among them, hybrid solar cells play a significant role. They are made with semiconducting inorganic nanocrystals and semiconducting organic materials, mostly polymers. Creating a well defined interface is especially complex due to the strong aggregation forces of the inorganic materials and the crystalline areas of the polymers resulting in a phase-separation of the materials. However, hybrid solar cells are still considered a good alternative to polymer-fullerene bulk heterojunction solar cells for several reasons. Firstly, the inorganic materials provide a better photostability and high charge carrier mobility. For example, the photo induced charge carrier transfer from quantum dots (QDs) to organic materials is in the picoseconds range.[1] Furthermore, the organic materials have very high absorption coefficients[2] and low cost solution based techniques such as inkjet-printing or roll to roll techniques can be applied.[3] Hybrid solar cells can be made with different inorganic nanocrystals. QDs made of cadmium sulfide (CdS) or cadmium selenide (CdSe) have been used with poly(3-hexylthiophene) (P3HT) as donor material. Efficiencies between less than 1% and up to 4.1% are reported, depending on the morphology at nanoscale.[4, 5] The best performance was achieved by binding CdS QDs to P3HT nanowires through solvent-assisted grafting and ligand exchange. Other complex nanocrystals include nanorods. Due to their anisotropy, they provide a better charge transfer to the electrodes.[6] More complex systems, due to their branched structure, are tetrapods. They are ideal for hybrid solar cells because their arms can create an excellent pathway for the charge transport. Additionally, the large surface provides a bettter interface for

the charge separation. Tetrapods have first been applied in solar cells with poly(*para*-phenylene vinylene) as an electron donor.[7, 8] By using a low bandgap polymer the efficiency was enhanced.[9] The efficiency was low because of the phase separation of the materials. Since the interface between the organic donor and the inorganic acceptor materials is so fundamental, another approach is to chemically bind polymers to the surface of the inorganic nanocrystals. The grafting-to or grafting-from approaches are useful to create hybrid materials with enhanced interfacial contact.[10] Using block copolymers which carry one long, solubilizing and one short, anchoring block, a variety of nanocrystals, like nanorods[11] or QDs,[12, 13] were functionalized. For the same reasons, the influence of the end groups of the polymers on the performance of the hybrid solar cells was also found to be important. By using specific end groups, the interfacial contact, and thereby the efficiency, could be improved.[14, 15]

Herein, we present hybrid systems made with highly uniform CdSe tetrapods and a semiconducting block copolymer that carries anchor groups. Tetrapod arm length and the amount of polymer loading was varied in order to find the ideal morphology for hybrid solar cells. The hybrids were characterized through transmission electron microscopy (TEM), fluorescence optical microscopy (FOM), and thermal gravimetric analysis (TGA). Additionally, polymer with no anchor groups was also mixed with tetrapods to study the effect of the anchor groups on the morphology. We found that in all samples the block copolymer-tetrapod mixture ("hybrid") showed much better film qualities and tetrapod distributions within the film compared to the homopolymer-tetrapod mixture ("blend"), which showed aggregations and cracks in the films.

Results and Discussion

The polymer poly(TPDF-*b*-SSMe) was synthesized via reversible addition fragmentation chain transfer (RAFT) polymerization, as previously reported (Scheme 1).[16] RAFT polymerization is suitable for the synthesis of well defined polymers with a narrow molecular weight distribution and a functional end group, which allows the synthesis of block copolymers. The monomer *N*,*N*'-2-bis(4-trifluoromethylphenyl)-*N*-phenyl-*N'*-4-vinylphenyl(1,12-biphenyl)-4,4-diamine was polymerized with dithiobenzoic acid benzyl ester as chain transfer agent. Characterization by GPC showed a M_n of 25,000 g mol^{-1} with a polydispersity index (PDI) of 1.09. This macro-chain transfer agent was subsequently used in the block copolymer synthesis, in which the active ester pentafluorophenyl acrylate was polymerized. Characterization by GPC showed a M_n of 26,000 g mol^{-1}, which corresponds to 4 anchor groups, and a PDI of 1.10. Post polymerization functionalization with cysteamine disulfide gave the functional block copolymer poly(TPDF-*b*-SSMe). Disulfide groups are known to anchor to CdSe surfaces without cross linking the polymer intermolecularly.[17]

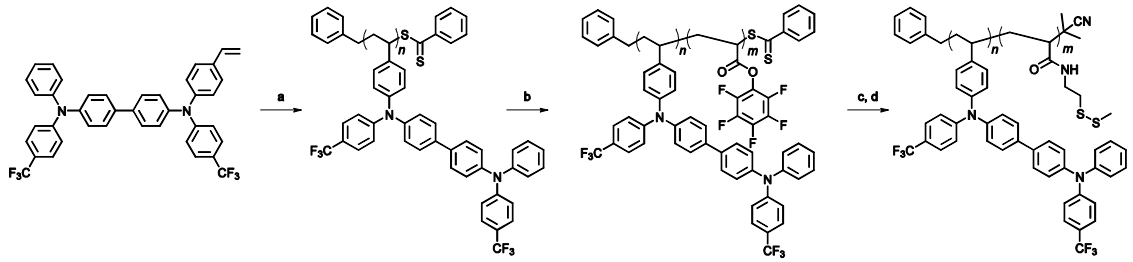

Scheme 1. Synthesis of poly(TPDF-*b*-SSMe). **a)** Dithiobenzoic acid benzyl ester, AIBN, 80 °C, 48 h; **b)** Pentafluorophenyl acrylate, AIBN, 80 °C, 48 h; **c)** AIBN, 80 °C, 3 h; **d)** Cysteaminmethyl disulfide, NEt_3, 45 °C, 12 h.

The tetrapods were synthesized via continuous precursor injection (CIP).[18] This route gives highly uniform samples with more than 93% shape selectivity. By systematically varying the reaction and injection times, tetrapods with different arm lengths could be synthesized. For a good understanding of the aggregation behavior of the tetrapods, 40 nm, 70 nm, and 100 nm long tetrapods were chosen.

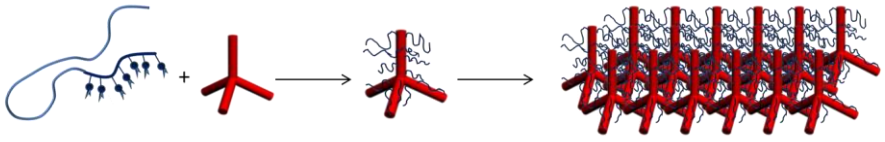

Figure 1. Schematic of the hybridization of tetrapods with the semiconducting block copolymer.

The effect of the arm length on the morphology and the dispersion/aggregation behavior in dependence of the polymer content was investigated. For that, the polymer was dissolved in toluene and added to the pristine tetrapods in different amounts (50%, 70%, 80%, 90% polymer) (Figure 1). Hybridization was achieved by redispersing the tetrapods in the polymer solution, followed by precipitation by ethanol and centrifugation. The samples were then redispersed in toluene to have a concentration of 30 mg mL^{-1}. The same procedure was applied for the blend systems. The samples were then spin-coated at 2000 rpm for 40 sec for the TEM measurements. The results are shown in Figures 2-4. Figure 2 shows hybrid and blend samples made from tetrapods with 40 nm arm length. For the hybrid, all samples formed uniform films with well dispersed tetrapods. In the case of 50% polymer and 50% tetrapods, the difference between the hybrid and the blend film was insignificant. Both showed densly packed tetrapods and good films. But with increasing polymer content, tetrapod aggregations appear more frequently, even though the film shows no cracks.

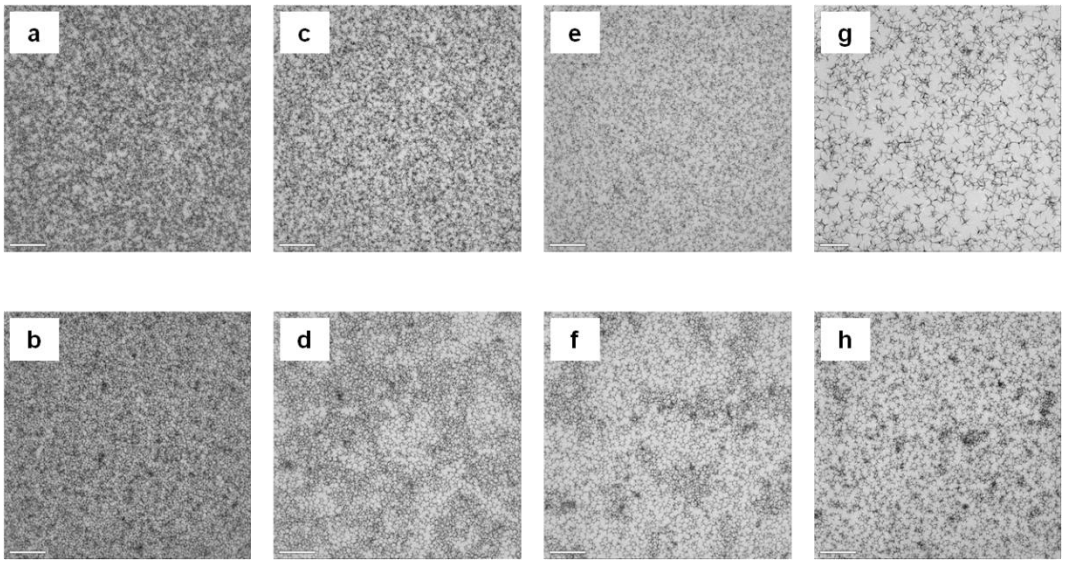

Figure 2. TEM images of the 40 nm arm length tetrapods with polymer in different variations. Top: hybrid samples, bottom: blend samples, ratio polymer:tetrapod: **a)** and **b)** 50:50, **c)** and **d)** 70:30, **e)** and **f)** 80:20, **g)** and **h)** 90:10. Scale bar: 0.5 µm.

Figure 3 displays the 70 nm arm length samples. Again, the hybrid samples show a very high film quality and no aggregation of the tetrapods; they form a perfectly interconnected system. At high tetrapod concentrations of 50% the blend sample develops a good morphology. But with an increasing amount of polymer, the tetrapods tend to aggregate more.

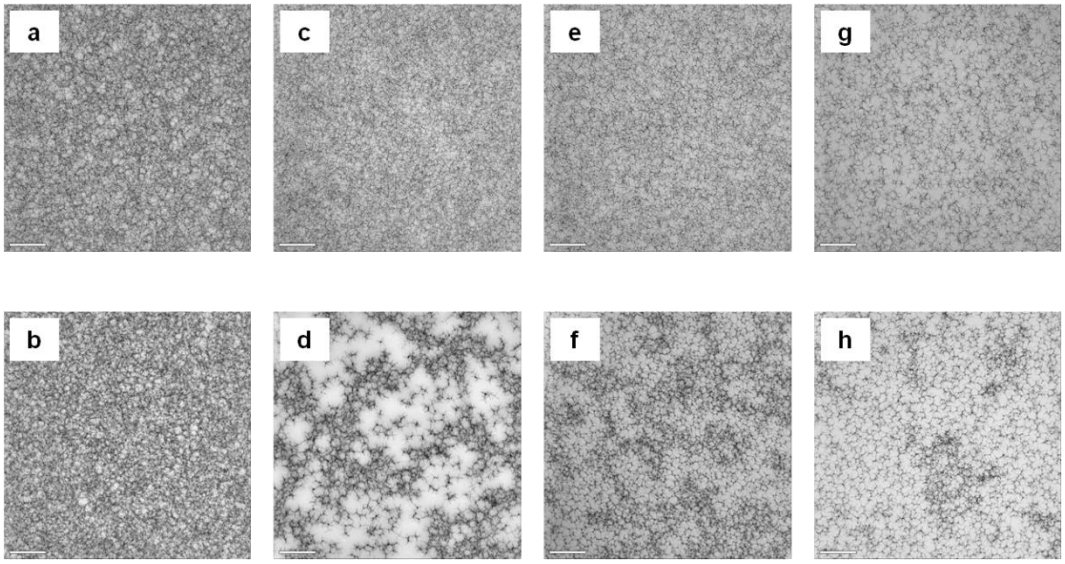

Figure 3. TEM images of the 70 nm arm length tetrapods with polymer in different variations. Top: hybrid samples, bottom: blend samples, ratio polymer:tetrapod: **a)** and **b)** 50:50, **c)** and **d)** 70:30, **e)** and **f)** 80:20, **g)** and **h)** 90:10. Scale bar: 0.5 µm.

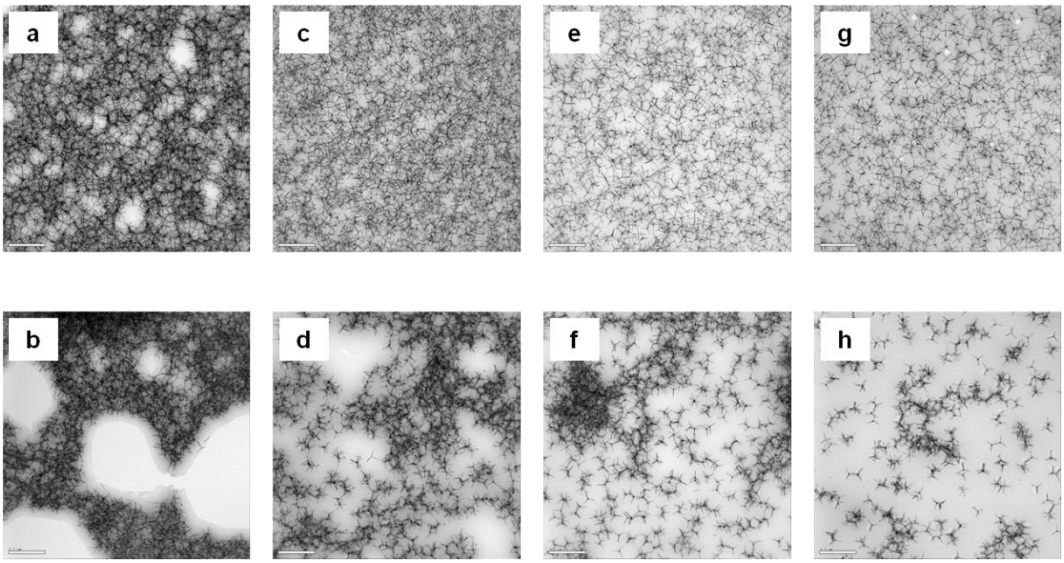

Figure 4. TEM images of the 100 nm arm length tetrapods with polymer in different variations. Top: hybrid samples, bottom: blend samples, ratio polymer:tetrapod: **a)** and **b)** 50:50, **c)** and **d)** 70:30, **e)** and **f)** 80:20, **g)** and **h)** 90:10. Scale bar: 0.5 µm.

The most drastic difference between hybrid and blend was observed with the 100 nm arm length tetrapods (Figure 4). In the 50% tetrapod hybrid sample, some defects were observed. However, the film was still very stable. In contrast to that, the blend sample showed massive cracks, and aggregation was predominantly found. No stable film was formed. This is also the case in the 70% polymer sample. In comparison, the hybrid sample of the same concentration shows a defect-free uniform distribution. With increasing polymer content, the hybrid samples show very good film qualities. The blend samples show better film qualities with fewer cracks, but the tetrapods aggregate within the film and no uniform distribution was found.

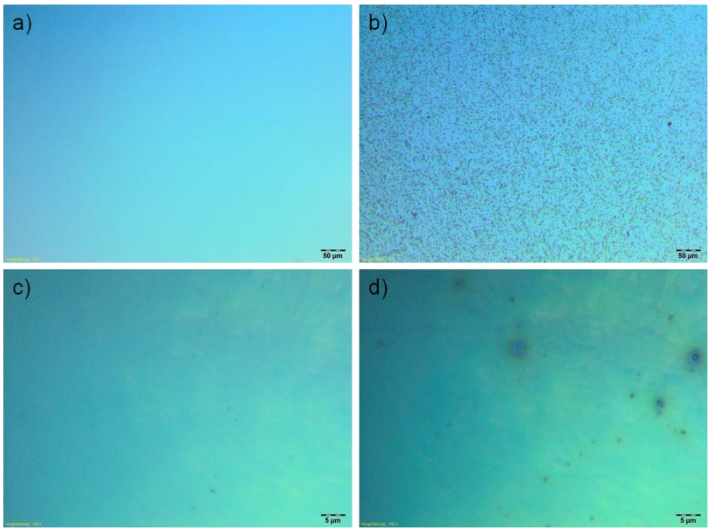

Figure 5. Fluorescence optical microscope images of 50:50 hybrids and blends. **a)** 100 nm hybrid, **b)** 100 nm blend, **c)** 40 nm hybrid and **d)** 40 nm blend.

Fluorescence optical microscope (FOM) images were taken to check the film qualities at microscale. For that, the hybrid and blend samples (50:50) were spin-coated on glass substrates in the same conditions as for the TEM measurements. Figure 5 a) shows the image of the film obtained with the 100 nm hybrid sample. A uniform film with no cracks or aggregation of tetrapods was found. However, in the analogue blend sample (b), massive aggregations of several micrometer size were visible. In the case of 40 nm tetrapods, the hybrid forms a uniform film. In the case of the blend sample, the film has large areas of good qualities, but also some impurities / aggregations. The quality in general is much better compared to that of the longer tetrapods. This result confirms the conclusion of the TEM images, that the shorter tetrapods form better films and fewer aggregates than the longer ones.

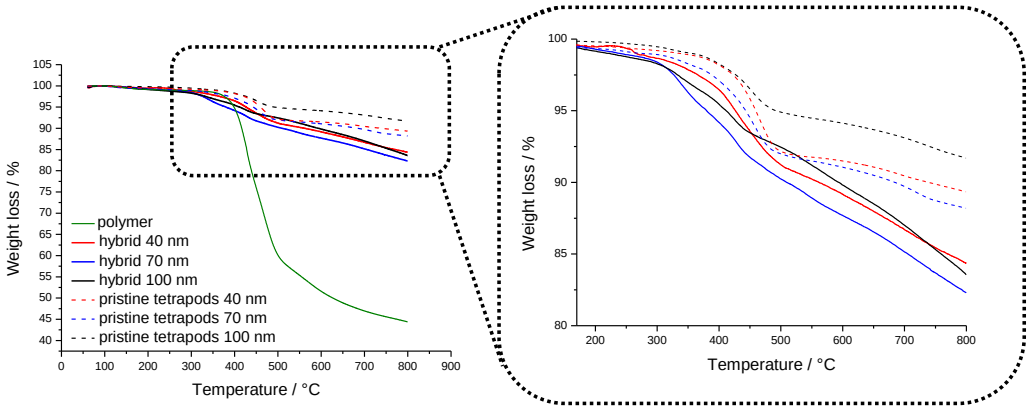

Figure 6. Thermal gravimetric analysis of the hybrid samples of different tetrapod arm lengths, the pristine tetrapods and the polymer (right image: zoom).

To get an idea of the amount of polymer loaded onto the tetrapods, thermal gravimetric analysis (TGA) was carried out. Therefore, the hybrid samples (50:50) were washed with acetone in order to remove excess polymer that was not bound to the tetrapods. For a good comparison, as-synthesized tetrapods with organic ligands (OA) and the polymer poly(TPDF-*b*-SSMe) were also measured. All samples were stable up to 300 °C and started degrading above this temperature. The polymer degraded partly, but 40wt% were left at 800 °C. This can be caused by the formation of graphite. The hybrid samples and pristine tetrapods showed some weight loss above 300 °C, which is referred to the organic material, e.g. polymer or OA. In all cases, hybrids lost more weight (16-18wt%) compared to pristine tetrapods (8-12wt%).

Conclusion

In summary, we presented a new semiconducting polymer-CdSe tetrapod hybrid system and showed the unique morphology at nanoscale. The samples do not need to be annealed, the

organization is self-assembled. In contrast, we showed the morphology of a blend system, in which the polymer does not carry anchoring groups. The effects were drastic in terms of tetrapod aggregation and film quality. By varying the amount of polymer and the tetrapod arm length, we found the optimal conditions to obtain a well connected network of tetrapods, optimal for applications in hybrid solar cells.

Experimental Details

Materials and Instrumentation:

Unless otherwise mentioned, all chemical reagents were used as purchased without any further purification. Pentafluorophenol was obtained from Fluorochem (UK). Anhydrous THF and dioxane were freshly distilled from sodium. 2,2'-Azobis(isobutyronitrile) (AIBN) was recrystallized from diethyl ether and stored at -18 °C.

Synthesis: The polymers polyTPDF and poly(TPDF-*b*-SSMe) were synthesized according to literature.[16] The synthesis of CdSe tetrapods is described in the supporting information.

Synthesis of the hybrids and blends. A general procedure is described here, details can be found in Table 1. The polymer was dissolved in toluene (0.5 mL) and centrifuged at 13.300 rpm for 2 min to remove dust or colloidal impurities. Ethanol was added to the dispersion of tetrapods in hexanes followed by centrifugation at 4000 rpm for 10 min in order to precipitate them. The residual solvent was removed and the polymer solution was added. The tetrapods (100 nm, 70 nm and 40 nm) were redispersed by vortexing. Ethanol was added and the hybrids/blends were precipitated by centrifugation at 4000 rpm for 10 min. The residual solvent was removed and the resulting hybrid was redispersed in toluene (1 mL) and kept at 4 °C.

Preparation of the TEM samples. The hybrid/blend dispersions (c = 30 mg mL^{-1}) were spin coated on Mica (2000 rpm for 40 sec). The film was subsequently floated on water and collected with the TEM grid.

Table 1. Details of the synthesis of hybrid and blend material

polymer /wt%	**m /mg**	**tetrapod /wt%**	**m /mg**
90	25.2	10	2.8
80	22.4	20	5.6
70	19.6	30	8.4
50	14.0	50	14.0

Preparation of the samples for TGA measurements. The hybrid samples (0.3 mL of the toluene dispersion; ratio 50:50, all different arm lengths) were precipitated with ethanol and subsequent centrifugation at 4.500 rpm for 10 min. The supernatant was removed and the solid hybrid was dispersed in 0.3 mL acetone and 1 drop ethanol. They were centrifuged at 13.300 rpm for 15 min. The supernatant, containing free polymer, was removed and the washing cycle repeated for four times, until no more polymer was found in the supernatant (checked with a UV lamp). The hybrids were then dried at 45 °C for 12

References

1. J. Huang, Z. Huang, Y. Yang, H. Zhu and T. Lian, *J. Am. Chem. Soc.*, 2010, **132**, 4858-4864.
2. M. M. Koetse, J. Sweelssen, K. T. Hoekerd, H. F. M. Schoo, S. C. Veenstra, J. M. Kroon, X. Yang and J. Loos, *Applied Physics Letters*, 2006, **88**, 083504-083503.
3. F. C. Krebs, *Solar Energy Materials and Solar Cells*, 2009, **93**, 394-412.
4. S. Ren, L.-Y. Chang, S.-K. Lim, J. Zhao, M. Smith, N. Zhao, V. BulovicÌ, M. Bawendi and S. Gradecak, *Nano Letters*, 2011, **11**, 3998-4002.
5. S. H. Choi, H. J. Song, I. K. Park, J. H. Yum, S. S. Kim, S. H. Lee and Y. E. Sung, *J. Photochem. Photobiol. A-Chem.*, 2006, **179**, 135-141.
6. D. Celik, M. Krueger, C. Veit, H. F. Schleiermacher, B. Zimmermann, S. Allard, I. Dumsch, U. Scherf, F. Rauscher and P. Niyamakom, *Solar Energy Materials and Solar Cells*, 2012, **98**, 433-440.
7. B. Sun, E. Marx and N. C. Greenham, *Nano Letters*, 2003, **3**, 961-963.
8. Z. Yi, L. Yunchao, Z. Haizheng, H. Jianhui, D. Yuqin, Y. Chunhe and L. Yongfang, *Nanotechnology*, 2006, **17**, 4041.
9. S. Dayal, N. Kopidakis, D. C. Olson, D. S. Ginley and G. Rumbles, *Nano Letters*, 2009, **10**, 239-242.
10. L. Zhao and Z. Lin, *Advanced Materials*, 2012, **24**, 4346-4346.
11. M. Zorn and R. Zentel, *Macromol. Rapid Commun.*, 2008, **29**, 922-927.
12. H. Skaff, K. Sill and T. Emrick, *J. Am. Chem. Soc.*, 2004, **126**, 11322-11325.
13. M. Zorn, W. K. Bae, J. Kwak, H. Lee, C. Lee, R. Zentel and K. Char, *ACS Nano*, 2009, **3**, 1063-1068.
14. J. S. Liu, T. Tanaka, K. Sivula, A. P. Alivisatos and J. M. J. Frechet, *J. Am. Chem. Soc.*, 2004, **126**, 6550-6551.
15. H.-C. Chen, C.-W. Lai, I. C. Wu, H.-R. Pan, I. W. P. Chen, Y.-K. Peng, C.-L. Liu, C.-h. Chen and P.-T. Chou, *Advanced Materials*, 2011, **23**, 5451-5455.
16. L. zur Borg, D. Lee, J. Lim, W. K. Bae, M. Park, S. Lee, C. Lee and K. Char, *submitted*, 2012.
17. M. Zorn, S. A. L. Weber, M. N. Tahir, W. Tremel, H. J. Butt, R. Berger and R. Zentel, *Nano Letters*, 2010, **10**, 2812-2816.
18. J. Lim, W. K. Bae, K. U. Park, L. zur Borg, R. Zentel, S. Lee and K. Char, *submitted*, 2012.

3.2 Photoinduced Charge Separation of Self-Organized Semiconducting Superstructures Composed of a Functional Polymer-TiO_2 Hybrid

Lisa zur Borg, Anna L. Domanski, Rüdiger Berger and Rudolf Zentel

Abstract:

This paper describes the incorporation of TiO_2 nanoparticles into thin but long (several μm) fibers of a gel forming poly-*para*-phenylene vinylene (PPV) derivative. For that purpose we synthesized a PPV with pentyloxy side groups using Siegrisd polycondensation, reduced the aldehyde end-group to an alcohole and attached a chain transfer agent. Subsequent reversible addition–fragmentation chain transfer (RAFT) polymerization gave a PPV block copolymer, poly(bis(2,5-pentyloxy)-*p*-phenylene vinylene-*b*-pentafluorphenyl acrylate). The pentafluorophenyl groups were then replaced with dopamine to introduce the anchor groups to the oxidic TiO_2 surface. These block copolymers can be used to coat the TiO_2 nanoparticles (grafting to) with a PPV layer leading to fluorescence quenching. Due to compatibilization by the PPV layer the modified nanoparticles can be well dispersed within a matrix of the PPV homopolymer.

Independently we observed the homopolymer poly(bis(2,5-pentyloxy)-*p*-phenylene vinylene) gels in various organic solvents forming long fibers of several μm length. By mixing the PPV homopolymer with the TiO_2 PPV hybrid, we were able to incorporate the nanoparticles into the fibrous network, as shown in transmission electron microscope (TEM) and scanning electron microscope (SEM) images. Photo-induced charge separation at a single nanoparticle level was measured by Kelvin probe force microscopy. Upon illumination the polymer fibers with 488 nm light we observed positive charges even at distances of around 300 nm from TiO_2 particles. From these results we infer charge transport along the polymer fibers.

Introduction:

Since first reported in 1977,[1] electrically conducting polymers are of great interest. Today they attract most attention because of their semiconducting properties and their possible use in organic light emitting diodes (OLED), thin film transistors (TFT) or organic photovoltaics (OPV). For

these applications it is often necessary to mix different semiconducting materials on the nano-scale. This necessity is most obvious for OPVs, which rely on the formation of a nanosized p-n junction (bulk-heterojunction) to separate the charges. The formation of the bulk-heterojunction is usually achieved by de-mixing during film formation. The nanostructure formed is therefore difficult to control, as it depends on the special conditions during de-mixing and it may change afterwards during annealing, e.g. during operation. For this reason methods to achieve better control of the nanostructure are highly desirable. In addition to the control of the nanostructure it is also important to control the morphology over larger distances (up to μm) to offer a direct path for the separated charges to the electrodes. Therefore self-assembled one dimensional fibers are desirable.

The use of block-copolymers, in which two (semiconducting) polymers are linked covalently to each other, is an attractive method to control the nanostructure and to prevent demixing during annealing/operation. To study the control of the morphology, blockcopolymers are often used, in which only one block is semiconducting, e.g. rod-coil polymers[2, 3] with a semiconducting rod and a flexible coil[4] like poly(*para*-phenylene vinylene)[5-8] (PPV) block copolymers with styrene[9] or isoprene[10] . In addition organic D-A polymers like poly(vinyl triphenylamine-*b*-perylene bisimide acrylate) and derivatives were reported.[11, 12] Further examples are poly(3-hexylthiophene-*b*-C_{60}),[13-16] poly(3-hexylthiophene-*b*-perylene)bis acrylamide),[17] or poly(fluorene-*b*-triphenylamine). [18]

D-A materials composed of organic-inorganic nanostructures are of great interest. They offer the possibility to combine the high charge carrier mobility of the inorganic materials with the flexibility and processibility of polymers.[19] Such D-A systems composed of PPV or P3HT and inorganic semiconducting quantum dots have been synthesized by the grafting-from approach.[20, 21] In addition hybrid solar cells composed of a blend of PPV and CdTe nanocrystals like spheres and tetrapods have been reported.[22, 23]

One approach to improve the morphology in the μm-range is to utilize the self-assembly of particular materials into fibers and gels (organogels) to create better charge percolation pathways. It has been shown that self-organized, well packed structures show higher charge-carrier mobilities compared to the amorphous materials.[24] The gelation of P3HT in different organic solvents has been investigated thoroughly.[25-27] Also, other semiconducting polymers, like polyfluorenes, show gelation behavior.[28-32] PPVs are especially interesting as they often pack in a board-like fashion (analogy to sanidic LC-phases),[33] which facilitates intermolecular hopping of charges. Generally such organogels can include inorganic nanoparticles like gold[34] or ZnO.[35]

Herein, we present the synthesis of a PPV block copolymer carrying anchor groups, which also self-assembles into fibers, as well as the functionalization and incorporation of TiO_2 nanoparticles into the polymer. For that purpose PPV was end functionalized with a chain transfer agent (CTA) suitable for RAFT polymerization and an active ester monomer was grafted to the polymer. Subsequent polymer analogue reaction with a bifunctional anchor molecule gave the functional block copolymer. It was then tethered to TiO_2 nanoparticles to form a hybrid material. These nanoparticles can be well dispersed within polymer matrix of the homopolymer. The polymer showed fiber formation in organic solvents as well as a gelling behavior. When the hybrid material was mixed with the polymer, incorporation of the nanoparticles into the fibrous network occurred. Kelvin probe force microscopy (KPFM) measurements show a charging of the PPV fibers under laser illumination (wavelength 488 nm), which extends over more than 100 nm. The KPFM results indicate charge transfer from the PPV to the TiO_2 nanoparticles and an effective charge transfer within the PPV fibers.

Results and Discussion:

In order to synthesize a PPV block copolymer with a functionalizable moiety, we chose the route via transformation of the terminal hydroxyl group of the PPV into a macro chain-transfer agent followed by RAFT polymerization[36-38] of an active ester monomer, pentafluorophenyl acrylate[39] (Scheme 1). The monomer *N*-[[2,5-bis(pentyloxy)-4-methylphenyl]methylene]was synthesized in three steps according to published procedures[40-42] (detailed description can be found in the supporting information) and polymerized by Siegrist polycondensation[42, 43] using potassium *tert*-butylate in DMF. The average molecular weight M_n was calculated via ^1H NMR spectroscopy by comparing the integration of the terminal aldehyde group with the signals of the repetition units to be 3.500 g/mol with a degree of polymerization of 12. The polymer was further characterized by GPC (Figure 1). A narrow polydispersity index (PDI) of 1.2 was observed, referred to a polystyrene standard. Since polystyrene is coiled in THF, and PPV is rod-like, we expect the PDI to be higher in reality because the polycondensation mechanism is not well controlled.

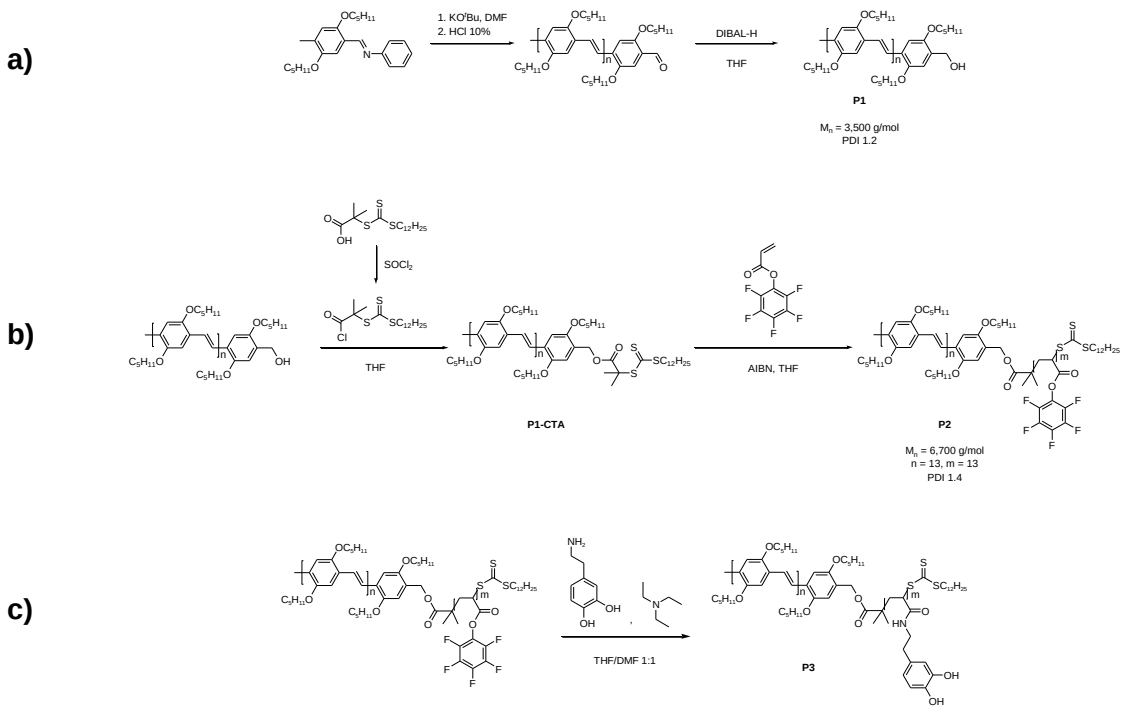

Scheme 1. a) Siegrist polycondensation and end group functionalization of **P1**. **b)** Synthesis of **P1-CTA** followed by the synthesis of **P2** via RAFT polymerization. **c)** Polymer analog reaction of **P2** with dopamine to form **P3**.

The small shoulder at higher molecular weight indicated that some polymer chains recombined before the reaction was quenched. Siegrist polycondensation route yields polymers with well defined end groups which can be further functionalized. The terminal imine group of the dark red polymer was transformed into an aldehyde by stirring it in aqueous hydrochloric acid. ^{1}H NMR spectra showed the signal of the terminal aldehyde at 10.4 ppm and the complete disappearance of the signal of the imine. Further reaction with diisobutylaluminium hydride reduced the terminal aldehyde to give BPO-PPV-OH (**P1**) with a terminal hydroxide group. The reaction was tracked by ^{1}H NMR spectroscopy. A new signal at 4.6 ppm of the two protons next to the alcohol appeared and the signal of the aldehyde at 10.4 ppm disappeared entirely (Figure 1). This proves a quantitative reaction within the detection threshold of the NMR spectra. In order to introduce anchor groups to the polymer, an active ester block was grafted onto the homopolymer **P1**. For this it was transformed into a macro chain transfer agent (**P1-CTA**) for subsequent RAFT polymerization by reacting it with an excess of 2-dodecylsulfanylthiocarbonylsulfanyl-2-methyl-propionic acid chloride. The formation of the ester group was proven by ^{1}H NMR spectroscopy. The signal from the protons next to the terminal hydroxyl group at 4.6 ppm disappeared and a new signal at 5.2 ppm appeared because of the ester group. After several steps of purification no free CTA was found in the sample. This was very important because otherwise they would react in the next step and form undesired homopolymers.

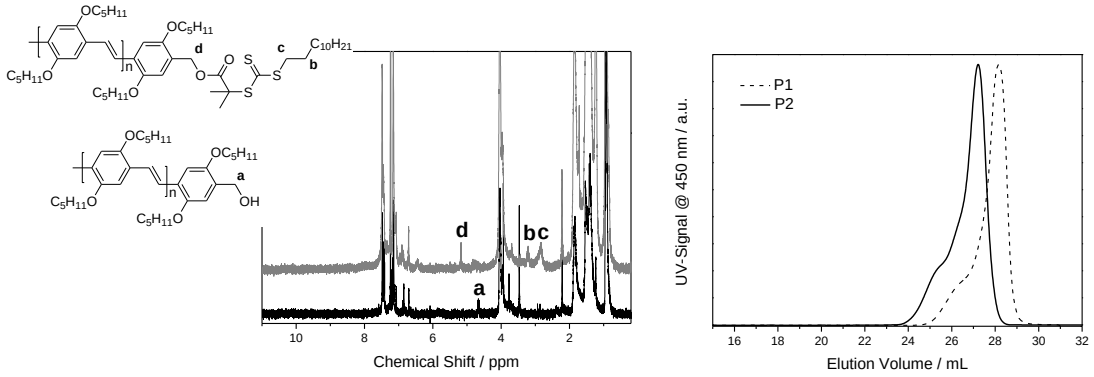

Figure 1. ^{1}H NMR spectra of **P1** (black) and **P1-CTA** (grey) (left) and GPC trace of **P1** and the corresponding block copolymer **P2** (right).

The RAFT polymerization was carried out at 70 °C (12 h) with pentafluorophenyl acrylate as the active ester. The success of the synthesis was checked by GPC and a shift to higher molecular weight was detected. For verifying that this signal corresponds to the desired block copolymer, we set the UV detector to 450 nm at which wavelength only the PPV absorbs. The observation of a signal at the same elution time verifies the formation of the block copolymer and excludes free poly(pentafluorophenyl acrylate). ^{19}F NMR measurement showed the three signals of the pentafluorophenyl groups, and the ester band was found in the IR (supporting information). After having proven the chemical structure of the block copolymer, the active ester moieties were substituted with dopamine, since catechol groups are known to bind to the oxidic surface of the inorganic material.[44, 45] The success of the reaction was confirmed by FT-IR measurements, as the ester band disappeared and the new amide band emerged. ^{19}F NMR also confirmed the absence of any fluorine in the sample. UV-Vis absorption spectroscopy measurements of **P1** and **P2** showed the same absorption maximum and intensity, which shows that the radicals formed during the RAFT polymerization, did not harm the aromatic system of the PPV backbone. Thus the desired block copolymer from PPV and a short anchor block based on dopamine has been successfully synthesized.

The TiO_2 nanorods used for this study had been synthesized as previously described.[44, 46] They were 50-80 nm long and 15 nm wide. The nanoparticles were coated with **P3** by sonicating them in a polymer solution followed by several washing steps. The resulting hybrid system contained 36 wt% of polymer per TiO_2 as determined by thermogravimetric measurements. This high functionalization is in agreement with earlier work,[47] which showed that especially short polymers with short anchor blocks bind very efficiently onto TiO_2 nanoparticles. In this case, the amount of bound polymer may be further increased by physisorbed polymer (see the gelling experiments later). TEM measurements performed on drop cast films from a diluted dispersion of

the nanoparticles in *o*-DCB showed that the nanoparticles are well dispersed and do not aggregate (Figure S 1).

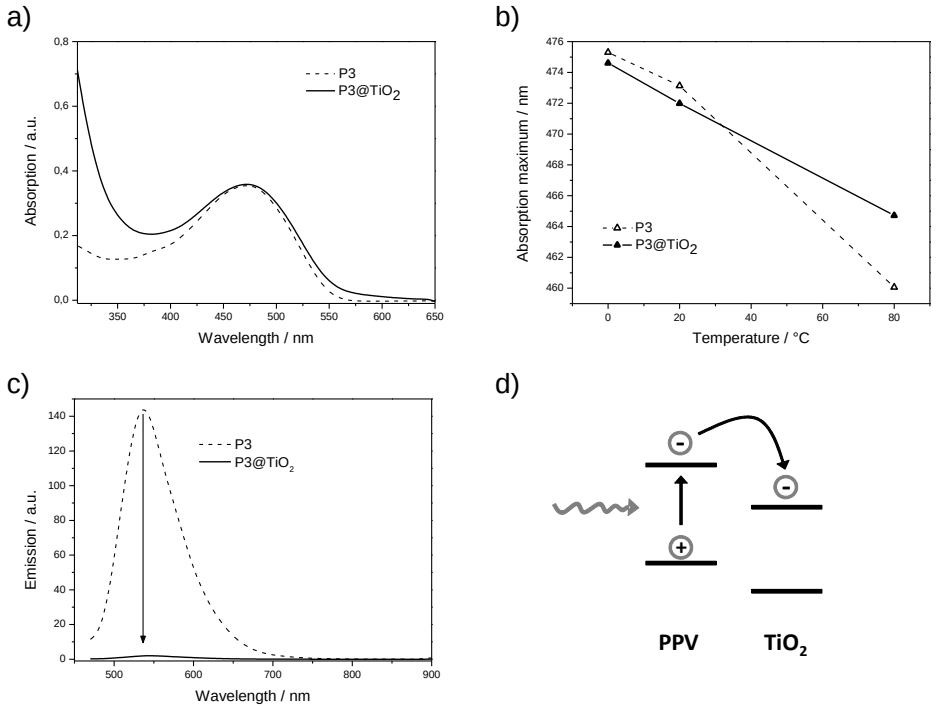

Figure 2. a) Absorption spectra of **P3** and **P3@TiO$_2$** in *o*-DCB, **b)** Temperature dependent absorption of **P3** and **P3@TiO$_2$**, **c)** PL spectra of **P1** and **P3@TiO$_2$** solution/dispersion in *o*-DCB and **d)** Schematic of the charge separation at the interface of PPV and TiO_2.

Figure 2 shows the room-temperature UV-Vis measurements of pristine **P1** and of the hybrid material **P3@TiO$_2$**, as well as the temperature dependence of the absorption maximum of the materials and the photoluminescence (PL) spectra (all measured in *o*-DCB). **P1** exhibits a broad absorption maximum at 450 nm, which does not change when the inorganic nanoparticles are attached. The TiO_2 nanoparticles have an absorption edge at 350 nm, which is also visible in the spectrum of the hybrid. Thermochromic behavior was found in both materials, the absorption shifts to higher energy with increasing temperatures. This is as expected since PPV polymers are known to show thermochromic behavior.[48] The absorption maxima of the block copolymer **P3** shifted by 15.5 nm from 475.5 nm to 460.0 nm and from 473.5 nm by 8.8 nm to 464.7 nm in case of **P3@TiO$_2$**. The conjugation length probably decreases with increasing temperature. Since the energy levels of the BPO-PPV make it a good hole conductor and TiO_2 is a typical electron acceptor, energy transfer between these two materials is expected. When **P1** was excited at its absorption maximum of 450 nm, it emitted green light with a wavelength of 550 nm. In the case of **P3@TiO$_2$** fluorescence is quenched. This is a first hint for the charge transfer, which is determined later by KPFM measurements (2.4.)

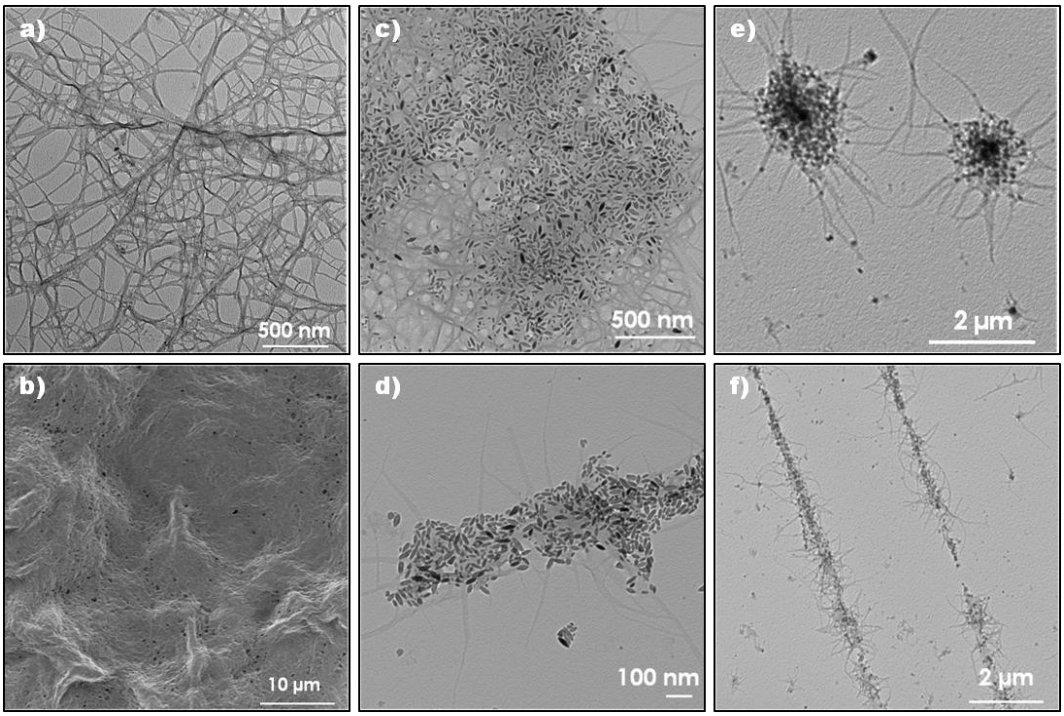

Figure 3. a) TEM image of **P1**, 5 mg/mL. **b)** SEM image of **P1**, 30 mg/mL. **c)** and **d)** TEM pictures of **P3@TiO$_2$** mixed with 10 wt% **P1**, 10 mg/mL. **e)** and **f)** TEM pictures of **P3@TiO$_2$** mixed with 50 wt% **P1**, 10 mg/mL. All samples were drop cast from *o*-DCB.

A gelling behavior of **P1** was observed in many organic solvents like chloroform, THF or *o*-dichlorobenzene (*o*-DCB). E.g. the polymer dispersion in *o*-DCB was heated up until it became a clear solution and was then slowly cooled down to room temperature. Gelling was observed above a concentration of 30 mg/mL. The solution solidified and could be placed upside down without inducing flow. SEM pictures made of this gel (Figure 3b) showed the three-dimensional sponge-like structure. TEM images obtained from drop cast samples of more diluted solutions showed the thin and fibrous structure within the gel at the nanoscale (Figure 3a). The fibers of the polymer were between 30-100 nm thin and many µm long.

Since the TiO_2 nanoparticles were well dispersed within the polymer matrix (paragraph 2.2), we wanted to incorporate them into the fibers of the gel. For that, we mixed 10 wt% of **P1** with the hybrid dispersion **P3@TiO$_2$** in *o*-DCB. The mixture was heated up to 90 °C, cooled down to room temperature and allowed to gel for 4 h. TEM measurements of a diluted aliquot (Figure 3) showed that a network of polymer was formed again and the nanoparticles were firmly attached to the polymer fibers. We could find networks, in which the nanoparticles were incorporated and large fibers (~200 nm wide) with nanoparticles sticking onto them. By increasing the amount of **P1** to 50 wt%, different superstructures were observed since there was an excess of free homopolymer. We found micelles with long polymer arms that had the same thickness as in the pure polymer gel. Again, the nanoparticles were obviously attached to the

polymer fibers. We also found several micrometer long strands of polymer which were filled with the TiO_2 nanoparticles.

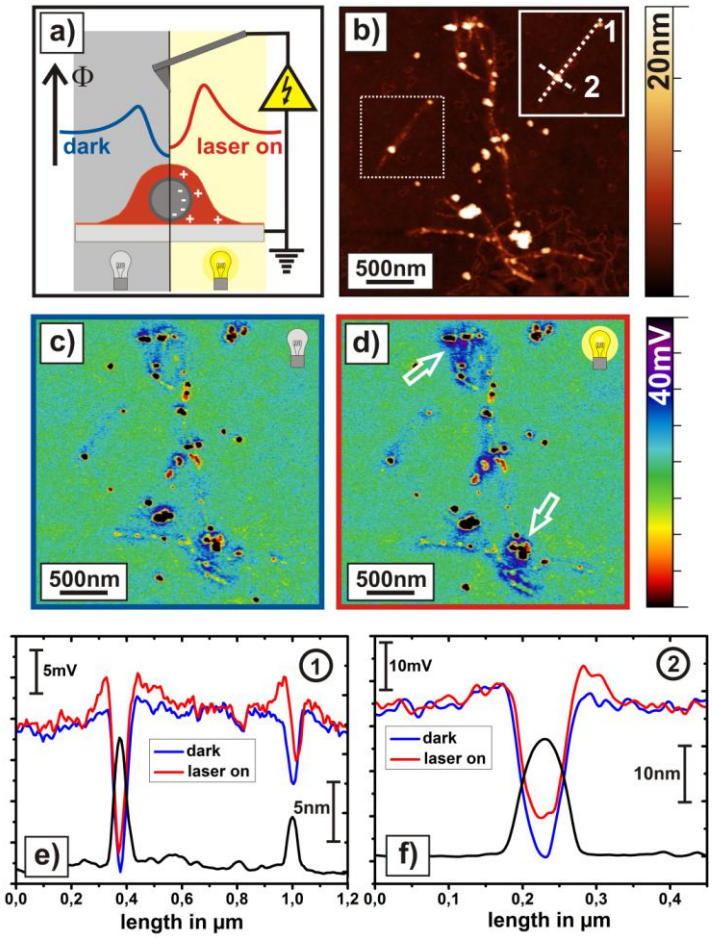

Figure 4. Study of interfacial charge transfer by KPFM on **P3@TiO_2** / **P1** (70 wt%/ 30 wt%, 5 mg/mL, drop cast from *o*-DCB) in dark and under laser illumination (λ = 488 nm). **a)** Schematic of the KPFM measurement on polymer (orange) functionalized TiO_2 particle (grey) in dark and under laser illumination through the carbon coated glass substrate. The increase in surface potential upon illumination is qualitatively depicted in the upper graph (in dark: blue; laser on: red). **b)** Topography image: TiO_2 particles (white ellipsoids) are dispersed within the polymer network (light brown lines). Areas of the uncovered carbon coated glass substrate appear in dark brown. **Inset:** dotted square marks the position of area shown in the inset in the upper right corner. Lines 1 and 2 correspond to the line profiles depicted in the graphs in (e) and (f), respectively. **c)** and **d)** Corresponding surface potential maps measured in dark (blue frame) and under illumination (red frame) on the same position. The images were corrected by background subtraction. White arrows in (d) indicate regions of large photo-response. **e)** and **f)** Line profiles taken along the two isolated TiO_2 particles that are connected by a single PPV fiber (profile 1 in (b)) and across one TiO_2 particle and the surrounding PPV matrix (profile 2 in (b)) on the topography (black), and the surface potentials measured in dark (blue) and under illumination (red).

The hybrid material also formed physical gels when the content of the PPV homopolymer was higher than 30 wt%. The gelation effect was thermo reversible. By warming the gel above 45 °C, it became liquid. It gelled again within seconds while it was cooled down to room temperature again. Figure S 2 shows SEM pictures taken of the hybrid gel. The gel was heated up and a drop of the warm mixture was placed onto the substrate. At low magnifications, a rough surface and a three-dimensional sponge-like structure were visible. When magnified, the nanoparticles could be distinguished from the polymer matrix. They were well dispersed within the matrix, and no phase-separation was found. These gels are self-organized on two levels, first with regard to the incorporation of inorganic nanoparticles into the organic matrix and then with regard to the fiber like self-organization of the PPV chains, which allows it to span large distances (μm).

The quenching of the photoluminescence as a result of the covalent binding of **P3** to the TiO_2 particles (Figure 2c) was already a strong indication for an efficient charge transfer at the interface between polymer and TiO_2. In order to further investigate this photo-induced charge transfer, KPFM measurements were carried out. KPFM is a very powerful tool to detect local variations of the contact potential difference (CPD) in the nanometer regime.[49, 50] Illuminating samples with light allows studying the photo-response of optoelectronic materials.[51-56] We have used this so-called photo-KPFM in order to investigate the light-induced charge separation of polymer functionalized ZnO nanorods[57] on a single particle level. In the existing setup the sample illumination was realized by placing a laser source underneath the sample (Figure 4a). For sample preparation, **P3@TiO_2**/ **P1** (70 wt%/ 30 wt%, 5 mg/mL) was drop cast from *o*-DCB on a transparent carbon coated glass substrate. Typically the surface areas were probed several times consecutively with laser on and then off, from which we attributed the changes in the measured CPD to the photo-induced change in the surface potential of the same particles. Initially, the investigation of the topography revealed either single TiO_2 particles with ellipsoidal shape with a height of around 20 nm and a length of 50-100 nm or larger aggregates (Figure 4b). The TiO_2 particles were connected through a network of thin PPV block-copolymer fibers on the uncovered carbon substrate. Upon laser illumination at a wavelength of 488 nm excitons are created in the PPV and are separated at the interface of the TiO_2 particle. The electrons are transferred to the LUMO level of the TiO_2 whereas the holes remain in the HOMO level of the polymer as depicted in the energy level diagram (Figure 2d). By first measuring the surface potential in darkness (Figure 4a) and subsequently comparing that to the surface potential recorded under illumination, the photo-response of the polymer functionalized TiO_2 particles can be determined. The surface potential map recorded in darkness (Figure 4c) exhibited an approximately 30 mV lower surface potential on the TiO_2 particles than on the surrounding polymer matrix which reflected the lower HOMO level of TiO_2 compared to PPV. Upon illumination, the surface potential increased

especially in the polymer regions close to larger TiO_2 aggregates. This effect was completely reversible after switching off the laser. In order to quantitatively exhibit this photo-response, the topography and two surface potential profiles were analyzed in detail along one TiO_2 particle (Figure 4e). The surface potential line profiles along the polymer fiber and across one polymer embedded TiO_2 particle show an increase in the surface potential of up to 10 mV both on top of the TiO_2 particle and the surrounding PPV upon illumination. The increase in surface potential in the PPV is attributed to the build-up of positive charges in the polymer as a consequence of the charge separation at the interface. Furthermore, negative charges on top of the TiO_2 could not be detected by KPFM. This observation indicates that the covalent binding of the PPV block copolymer to the TiO_2 leads to a densely packed and thick polymer layer. Thus, the effect of the build-up of electrons inside the particles on the surface potential is shielded by the positive charges of the PPV.[58] Furthermore, the surface potential difference of the hybrid material is maximal close to the TiO_2 particles which can be attributed to (i) the small exciton diffusion length of around 6 nm in PPV derivates[59] and (ii) to the electrostatic interaction. However, the light-induced change in the surface potential can be observed up to a distance of around 300 nm away from the TiO_2 particle which proves a hole transport along the polymer fibers. Finally, an additional control experiment performed on films of non-functionalized **P1** showed no photo-response (Figure S 4).

Conclusion:

Semiconducting PPV block copolymers with an activated ester block can be prepared via Siegrist polycondensation and subsequent RAFT polymerization. By post polymerization reaction dopamine anchor groups can be introduced. These polymers chemisorb onto TiO_2 nanoparticles and allow the preparation of TiO_2 –PPV hybrid systems, which can be well dispersed in a sample of PPV. Independent of the presence of nanoparticles the pentyloxy-PPV self-organizes into long fiber like aggregates. In the presence of nanoparticles they get self-organized on two levels, first with regard to the incorporation of inorganic nanoparticles into the organic matrix and then with regard to the fiber like self-organization of the PPV chains, which allows it to span large distances (μm). KPFM measurements show that illumination in the absorption range of PPV leads to charge transfer from PPV to the TiO_2 nanoparticles. The positive charge accumulating in the surrounding PPV matrix can migrate up to 300 nm away from the TiO_2 nanoparticles along the PPV fibers.

Experimental:

Materials. Unless otherwise mentioned, all chemical reagents were used as purchased without any further purification. Pentafluorophenol was obtained from Fluorochem (UK). Anhydrous THF and dioxane were freshly distilled from sodium. DMF was freshly distilled from calcium hydride and not exposed to light until it was used. 2,2'-Azobis(isobutyronitrile) (AIBN) was recrystallized from diethyl ether and stored at -18 °C.

Instrumentation. All ^{1}H and ^{13}C NMR spectra were recorded on a Bruker 300 MHz FT NMR spectrometer. All ^{19}F NMR spectra were recorded on a Bruker 400 MHz FT NMR spectrometer. Chemical shifts (δ) are given in parts per million relative to TMS. Samples were prepared in deuterated solvents and their signals referenced to residual nondeuterated solvent signals. The polymers' molecular weight was determined by gel permeation chromatography (GPC) in tetrahydrofuran (THF) as solvent and with the following parts: pump PU 1580, auto sampler AS1555, UV detector UV 1575 (detection at 254 nm), RI detector RI 1530 from JASCO. Columns were used from MZ-Analysentechnik: MZ-Gel SDplus 10 2 Å and MZ-Gel SDplus 10 6 Å. Calibration was done using polystyrene standards purchased from Polymer Standard Services. IR spectra were recorded on Perkin-Elmer 100 FTIR spectrometer using an ATR unit. UV-Vis spectra were recorded using a Jasco V-630 spectrophotometer (1 cm x 1 cm quartz cell). Emission spectra were recorded on a Varian Cary Eclipse. TEM pictures were taken on a Philips EM-420: 120kV with CCD-Camera. SEM pictures were taken with a Zeiss Gemini 1530. Kelvin probe force microscopy measurements were performed at a MFP-3D standalone setup (Asylum Research, Santa Barbara). In order to prevent any degradation of the sample during the KPFM measurements the setup was placed in a glove box that was continuously purged with dry nitrogen (humidity <0.1%, oxygen <0.01%). For simultaneous sample illumination during the KPFM measurement the setup was equipped with a diode laser (Point Source, iFLEX2000) with a wavelength of 488 nm, a power of 13.3 mW, and intensity on the sample of <10 W/cm^2. We used Pt/Ir coated cantilevers with a nominal vertical resonance frequency of 70 kHz (Nanosensors, PPP-EFM). The measurements were performed in the dual pass mode at a lift height of 5 nm and with an AC voltage of 1.5 V. In KPFM, the contact potential difference is measured which is defined as the difference in the work function between tip and sample. By using the amplitude modulation mode for KPFM both the tip apex and the cantilever contribute to the measured CPD.[60] Thus, local changes in the CPD are not exclusively related to the sample area underneath the tip apex but also to the one underneath the cantilever. In case, the work function of the tip remains constant it is possible to attribute changes in the measured CPD owing to sample illumination to changes in the surface potential of the sample.[61] However, studies on P3HT:PCBM blends have shown that the CPD changes significantly for consecutive scanning on

the same position. These shifts of the measured CPDs can be attributed to changes in the cantilever tip, such as coating thickness and adsorbates. Thus, it is important to have one surface within the scan area that does not participate in the photo-induced reaction and can therefore serve as internal reference[62, 63] . In this study, we could use the carbon coated glass substrate in order to correct for changes in the tip work function. For sample preparation, the solution of 5 mg/mL 70wt% / 30wt% **P3@TiO$_2$/P1** in *o*-DCB was drop cast on a glass slide coated with a thin layer of evaporated carbon (evaporation time: 7 s, Balzers BAE250). The carbon coated glass substrate was cleaned in Ar plasma (PDC-002, Harrick plasma) for 2 min prior to the drop coating.

Syntheses. TiO_2 nanoparticles,[47, 49] pentafluorophenyl acrylate[39] and 2-dodecylsulfanylthiocarbonylsulfanyl-2-methyl-propionic acid chloride[64, 65] were synthesized as published elsewhere. The synthesis of *N*-[[2,5-bis(pentyloxy)-4-methylphenyl]methylene] is described in the supporting information.

Synthesis of **P1**. For the synthesis of **P1**, we followed an already published procedure.[42] Potassium *tert*-butylate (2.36 g, 21.0 mmol, 3 eq) was dissolved in 150 mL anhydrous DMF and stirred for 30 min at 30 °C in a N_2 atmosphere. Then, *N*-[[2,5-bis(pentyloxy)-4-methylphenyl]methylene] (2.57 g, 7.0 mmol, 1 eq), dissolved in 50 mL anhydrous DMF was added quickly. The solution turned from colorless to dark brown / red immediately and was stirred at 30 °C for 30 min. The polymerization was quenched by pouring it into 600 mL 5% hydrochloric acid. The polymer precipitated instantly. The mixture was then stirred for 30 min to complete the end group conversion from the imine to the aldehyde. The precipitate was collected by filtration, dissolved in a few mL anhydrous THF and precipitated in methanol. The polymer was collected by centrifugation. The washing cycle was carried out three times and the red polymer was dried at 45 °C for 12 h under 10 mbar vacuum. Yield: 1.50 g, 94%; GPC: M_n = 3500 g/mol, M_w = 4000 g/mol, PDI = 1.2; ^{1}H NMR (300 MHz, $CDCl_3$, δ): 10.45, 7.57, 7.23, 3.99, 1.83, 1.53, 1.38, 1.02, 0.92.

End group functionalization of **P1**. To reduce the terminal aldehyde, **P1** (1.50 g, 0.4 mmol, 1 eq) was dissolved in anhydrous THF in a N_2 atmosphere. Diisobutylaluminium hydride 1 M in THF (15 mL, 12.9 mmol, 30 eq) was added and the solution was stirred over night at room temperature. Water was then added drop by drop until all excess of the hydride was reacted. 10% sulfuric acid was added until the precipitate was dissolved. The red solution was washed with water/chloroform three times. The organic fractions were collected and dried over magnesium sulfate. The solvent was removed under low pressure and the polymer BPO-PPV-OH was dried at 45 °C for 12 h under 10 mbar vacuum. Yield: quantitative. ^{1}H NMR (300 MHz, $CDCl_3$, δ): 7.57, 7.23, 4.64, 3.99, 1.83, 1.53, 1.38, 1.02, 0.92. For the synthesis of **P1-CTA**, **P1** (0.9 g, 0.3 mmol, 1 eq) was placed in a Schlenk tube in N_2 atmosphere and a solution of 2-

dodecylsulfanylthiocarbonylsulfanyl-2-methyl-propionic acid chloride (1.18 g, 3.1 mmol, 12 eq) in anhydrous THF(3 mL) was added. Pyridine (0.9 g, 11.6 mmol, 45 eq) was added and the solution was stirred for 24 h at 40 °C. For the purification, the polymer was precipitated in methanol for four times. After drying for 12 h at 45 °C under 10 mbar vacuum, the macro chain transfer agent was obtained as a red powder. Yield: quantitative. ^{1}H NMR (300 MHz, $CDCl_3$, δ): 7.57, 7.23, 5.18, 3.99, 3.22, 2.84, 1.83, 1.53, 1.38, 1.02, 0.92.

Block copolymer synthesis of **P2**. For the synthesis of the block copolymer, **P1-CTA** (0.4 g, 0.1 mmol, 1 eq), pentafluoro phenyl acrylate (1.36 g, 5.7 mmol, 50 eq) and AIBN (0.2 mg, 0.01 mmol, 0.01 eq) were dissolved in anhydrous dioxane (10 mL) in a Schlenk tube equipped with a stir bar. Oxygen was removed by three freeze-pump-thaw cycles and the polymerization was carried out at 70 °C for 12 h. The polymer was precipitated in methanol and collected by centrifugation. For further purification, it was redissolved in THF and precipitated in methanol. This cycle was repeated three times. The resulting dark orange powder was dried for 12 h at 45 °C under 10 mbar vacuum. Yield: 433 mg. GPC: M_n = 6700 g/mol, M_w = 9400 g/mol, PDI = 1.39; ^{19}F NMR (376 MHz, $CDCl_3$, δ): -152.5 (2H), -157.5 (1H),-162.32 (2H); IR (ATR): ν = 2928 (m), 1779 (s, COOR), 1675 (m), 1515 (s, ArF), 1422 (s), 1203 (s), 1080 (m), 989 (m).

Synthesis of **P3**. **P2** (0.10 g, 0.02 mmol, 1 eq) was dissolved in anhydrous THF (3 mL). Dopamine hydrochloride (0.19 g, 1.0 mmol, 60 eq) and triethylamine (0.10 g, 1.0 mmol, 60 eq) were dissolved in anhydrous DMF (2 mL) and added to the polymer solution. The red reaction mixture was stirred at 45 °C over night in a N_2 atmosphere. The resulting polymer was precipitated in methanol and collected by centrifugation. After redissolving in THF and reprecipitation in methanol, the block copolymer was obtained as a dark orange powder after drying it for 12 h at 45 °C under 10 mbar vacuum. Yield: 80 mg. ^{19}F NMR (376 MHz, $CDCl_3$, δ): no signal; IR (ATR): ν = 3367 (w, Ar-OH), 2928 (m), 1649 (w), 1509 (s), 1415 (s), 1199 (s), 1020 (m), 601 (s).

Functionalization of TiO_2 nanoparticles with **P3**. The TiO_2 nanoparticles (70 mg) and the block copolymer **P3** (35 mg) were dispersed in *o*-DCB (1 mL) in a Schlenk tube equipped with a stir bar in a N_2 atmosphere and immersed in an ultra sonification bath for 15 min. The tube was then placed in an oil bath and kept at 65 °C for 3 h. The functionalized nanoparticles were precipitated by adding a small amount of ethanol. They were collected by centrifugation (13,000 rpm). For further purification, they were redispersed in *o*-DCB and the washing cycle was repeated for four times. The resulting dark red precipitate was finally redispersed in 1.5 mL *o*-DCB and kept under N_2 at room temperature.

Synthesis of the organogel and the hybrid organogel. For the synthesis of the organogel, **P1** (30 mg, 2.1wt %) was dissolved in *o*-DCB (1 mL) in a vial and heated to 85 °C. As soon as the solution became clear, the vial was removed from the heat and allowed to cool down to room

temperature. The gel formed within minutes. When warmed up, the gel became liquid when the temperature exceeded 45 °C and gelated within seconds when removed from the heat. For the synthesis of the hybrid organogel, **P3@TiO$_2$** (30 mg) and **P1** (30 mg) were dissolved in o-DCB (1 mL). The concentration of the gelator was 2.4 wt% and of the total amount 4.6 wt%. The same procedure as for the organogel was applied.

Acknowledgements

This work was financially supported by the International Research Training Group (IRTG): "Self Organized Materials for Optoelectronics" (GRK 1404) jointly supported by the Deutsche Forschungsgemeinschaft (DFG). We thank Annette Kelsch for the SEM measurements and Dr. Nawaz Tahir for the synthesis of the TiO_2 nanoparticles. Furthermore, we thank Christoph Sieber for the preparation of the carbon coated glass substrates. In addition we thank Stefan Weber, Esha Sengupta and Maria Untch for discussions and the BMBF (contract # 03SF0334) for partial financial support in building up the photo KPFM.

References

[1] H. Shirakawa, E. J. Louis, A. G. Macdiarmid, C. K. Chiang, A. J. Heeger, *J. Chem. Soc.-Chem. Commun.* 1977, 578.
[2] G. Sauvé, R. D. McCullough, *Advanced Materials* 2007, *19*, 1822.
[3] M. C. Iovu, C. R. Craley, M. Jeffries-El, A. B. Krankowski, R. Zhang, T. Kowalewski, R. D. McCullough, *Macromolecules* 2007, *40*, 4733.
[4] A. de Cuendias, R. C. Hiorns, E. Cloutet, L. Vignau, H. Cramail, *Polym. Int.* 2010, *59*, 1452.
[5] J. H. Burroughes, D. D. C. Bradley, A. R. Brown, R. N. Marks, K. Mackay, R. H. Friend, P. L. Burns, A. B. Holmes, *Nature* 1990, *347*, 539.
[6] K. D. Gourley, C. P. Lillya, J. R. Reynolds, J. C. W. Chien, *Macromolecules* 1984, *17*, 1025.
[7] Y. Suzuki, K. Hashimoto, K. Tajima, *Macromolecules* 2007, *40*, 6521.
[8] D. Braun, A. J. Heeger, *Applied Physics Letters* 1991, *58*, 1982.
[9] N. Sary, R. Mezzenga, C. Brochon, G. Hadziioannou, J. Ruokolainen, *Macromolecules* 2007, *40*, 3277.
[10] B. D. Olsen, R. A. Segalman, *Macromolecules* 2007, *40*, 6922.
[11] M. Sommer, S. Huettner, M. Thelakkat, *Journal of Materials Chemistry* 2010, *20*, 10788.
[12] M. Sommer, S. M. Lindner, M. Thelakkat, *Advanced Functional Materials* 2007, *17*, 1493.
[13] J. U. Lee, A. Cirpan, T. Emrick, T. P. Russell, W. H. Jo, *Journal of Materials Chemistry* 2009, *19*, 1483.
[14] C. Yang, J. K. Lee, A. J. Heeger, F. Wudl, *Journal of Materials Chemistry* 2009, *19*, 5416.
[15] R. C. Hiorns, E. Cloutet, E. Ibarboure, A. Khoukh, H. Bejbouji, L. Vignau, H. Cramail, *Macromolecules* 2010, *43*, 6033.
[16] K. Sivula, Z. T. Ball, N. Watanabe, J. M. J. Fréchet, *Advanced Materials* 2006, *18*, 206.
[17] Q. Zhang, A. Cirpan, T. P. Russell, T. Emrick, *Macromolecules* 2009, *42*, 1079.
[18] Y. Tan, Z. Gu, K. Tsuchiya, K. Ogino, *Polymer* 2012, *53*, 1444.
[19] I. Y. Jeon, J. B. Baek, *Materials* 2010, *3*, 3654.
[20] H. Skaff, K. Sill, T. Emrick, *Journal of the American Chemical Society* 2004, *126*, 11322.
[21] J. Xu, J. Wang, M. Mitchell, P. Mukherjee, M. Jeffries-El, J. W. Petrich, Z. Q. Lin, *Journal of the American Chemical Society* 2007, *129*, 12828.
[22] S. Kumar, T. Nann, *J. Mater. Res.* 2004, *19*, 1990.
[23] Y. Zhou, Y. C. Li, H. Z. Zhong, J. H. Hou, Y. Q. Ding, C. H. Yang, Y. F. Li, *Nanotechnology* 2006, *17*, 4041.

[24] H. Sirringhaus, P. J. Brown, R. H. Friend, M. M. Nielsen, K. Bechgaard, B. M. W. Langeveld-Voss, A. J. H. Spiering, R. A. J. Janssen, E. W. Meijer, P. Herwig, D. M. de Leeuw, *Nature* 1999, *401*, 685.
[25] S. Malik, T. Jana, A. K. Nandi, *Macromolecules* 2000, *34*, 275.
[26] M. Koppe, C. J. Brabec, S. Heiml, A. Schausberger, W. Duffy, M. Heeney, I. McCulloch, *Macromolecules* 2009, *42*, 4661.
[27] S. Berson, R. De Bettignies, S. Bailly, S. Guillerez, *Advanced Functional Materials* 2007, *17*, 1377.
[28] Z.-Q. Lin, N.-E. Shi, Y.-B. Li, D. Qiu, L. Zhang, J.-Y. Lin, J.-F. Zhao, C. Wang, L.-H. Xie, W. Huang, *The Journal of Physical Chemistry C* 2011, *115*, 4418.
[29] C. C. Kitts, D. A. Vanden Bout, *Polymer* 2007, *48*, 2322.
[30] M. Iyoda, M. Hasegawa, H. Enozawa, *Chem. Lett.* 2007, *36*, 1402.
[31] M. Hasegawa, M. Iyoda, *Chemical Society Reviews* 2010, *39*, 2420.
[32] S. H. Kang, B. M. Jung, J. Y. Chang, *Advanced Materials* 2007, *19*, 2780.
[33] W. Pisula, M. Zorn, J. Y. Chang, K. Müllen, R. Zentel, *Macromol. Rapid Commun.* 2009, *30*, 1179.
[34] J. Puigmarti-Luis, A. P. Del Pino, E. Laukhina, J. Esquena, V. Laukhin, C. Rovira, J. Vidal-Gancedo, A. G. Kanaras, R. J. Nichols, M. Brust, D. B. Amabilino, *Angew. Chem.-Int. Edit.* 2008, *47*, 1861.
[35] R. K. Das, S. Bhat, S. Banerjee, C. Aymonier, A. Loppinet-Serani, P. Terech, U. Maitra, G. Raffy, J.-P. Desvergne, A. Del Guerzo, *Journal of Materials Chemistry* 2011, *21*, 2740.
[36] J. Chiefari, Y. K. Chong, F. Ercole, J. Krstina, J. Jeffery, T. P. T. Le, R. T. A. Mayadunne, G. F. Meijs, C. L. Moad, G. Moad, E. Rizzardo, S. H. Thang, *Macromolecules* 1998, *31*, 5559.
[37] G. Moad, E. Rizzardo, S. H. Thang, *Aust. J. Chem.* 2006, *59*, 669.
[38] G. Moad, E. Rizzardo, S. H. Thang, *Aust. J. Chem.* 2009, *62*, 1402.
[39] M. Eberhardt, R. Mruk, R. Zentel, P. Theato, *Eur. Polym. J.* 2005, *41*, 1569.
[40] B. D. Olsen, R. A. Segalman, *Macromolecules* 2005, *38*, 10127.
[41] A. Rieche, H. Gross, E. Höft, *Chemische Berichte* 1960, *93*, 88.
[42] H. Kretzschmann, H. Meier, *Tetrahedron Lett.* 1991, *32*, 5059.
[43] A. E. Siegrist, *Helv. Chim. Acta* 1981, *64*, 662.
[44] S. Meuer, P. Oberle, P. Theato, W. Tremel, R. Zentel, *Advanced Materials* 2007, *19*, 2073.
[45] M. N. Tahir, M. Eberhardt, P. Theato, S. Faiss, A. Janshoff, T. Gorelik, U. Kolb, W. Tremel, *Angew. Chem.-Int. Edit.* 2006, *45*, 908.
[46] S. Meuer, K. Fischer, I. Mey, A. Janshoff, M. Schmidt, R. Zentel, *Macromolecules* 2008, *41*, 7946.
[47] M. Zorn, S. Meuer, M. N. Tahir, Y. Khalavka, C. Sonnichsen, W. Tremel, R. Zentel, *Journal of Materials Chemistry* 2008, *18*, 3050.
[48] C. C. Wang, Y. Gao, A. P. Shreve, C. Zhong, L. Wang, K. Mudalige, H. L. Wang, M. Cotlet, *J. Phys. Chem. B* 2009, *113*, 16110.
[49] M. Nonnenmacher, M. P. O'Boyle, H. K. Wickramasinghe, *Applied Physics Letters* 1991, *58*, 2921.
[50] R. Berger, H.-J. Butt, M. B. Retschke, S. A. L. Weber, *Macromol. Rapid Commun.* 2009, *30*, 1167.
[51] V. Palermo, G. Ridolfi, A. M. Talarico, L. Favaretto, G. Barbarella, N. Camaioni, P. Samorì, *Advanced Functional Materials* 2007, *17*, 472.
[52] J. M. R. Weaver, H. K. Wickramasinghe, *Journal of Vacuum Science & Technology B: Microelectronics and Nanometer Structures* 1991, *9*, 1562.
[53] H. Hoppe, T. Glatzel, M. Niggemann, A. Hinsch, M. C. Lux-Steiner, N. S. Sariciftci, *Nano Lett.* 2005, *5*, 269.
[54] L. S. C. Pingree, O. G. Reid, D. S. Ginger, *Advanced Materials* 2009, *21*, 19.
[55] S. Sadewasser, M. C. Lux-Steiner, *Journal of Vacuum Science & Technology B: Microelectronics and Nanometer Structures* 2010, *28*, C4D29.
[56] E. J. Spadafora, R. Demadrille, B. Ratier, B. Grevin, *Nano Letters* 2010, *10*, 3337.
[57] M. Zorn, S. A. L. Weber, M. N. Tahir, W. Tremel, H. J. Butt, R. Berger, R. Zentel, *Nano Lett.* 2010, *10*, 2812.
[58] S. V. Kalinin, D. A. Bonnell, *Nano Letters* 2004, *4*, 555.
[59] D. E. Markov, J. C. Hummelen, P. W. M. Blom, A. B. Sieval, *Physical Review B* 2005, *72*, 045216.
[60] S. V. Kalinin, D. A. Bonnell, *Physical Review B* 2001, *63*, 125411.
[61] V. Palermo, M. Palma, P. Samorì, *Advanced Materials* 2006, *18*, 145.
[62] E. Sengupta, A. L. Domanski, S. A. L. Weber, M. B. Untch, H.-J. Butt, T. Sauermann, H. J. Egelhaaf, R. Berger, *The Journal of Physical Chemistry C* 2011, *115*, 19994.

[63] A. L. Domanski, E. Sengupta, K. Bley, M. B. Untch, S. A. L. Weber, K. Landfester, C. K. Weiss, H.-J. Butt, R. Berger, *Langmuir* 2012, *28*, 13892.
[64] J. T. Lai, D. Filla, R. Shea, *Macromolecules* 2002, *35*, 6754.
[65] M. H. Stenzel, T. P. Davis, A. G. Fane, *Journal of Materials Chemistry* 2003, *13*, 2090.

3.3 Light-Induced Charge Separation in a Donor-Chromophore-Acceptor Nanocomposite Poly[TPA-Ru(tpy)$_2$]@ZnO

Lisa zur Borg, Anna L. Domanski,[‡] Aaron Breivogel,[‡] Mareike Bürger, Rüdiger Berger, Katja Heinze and Rudolf Zentel

Abstract:

In this work, we present the synthesis and characterization of a new donor-chromophore-acceptor system based on poly(vinyltriphenylamine) as electron donor and a glycine-functionalized bis(2,2';6',2''-terpyridine)ruthenium(II) acting both as chromophore and as anchor group attached to ZnO nanorods as electron acceptor. The TPA-containing block copolymer was synthesized by RAFT polymerization and the metal complex chromophores were attached via post-polymerization esterification. GPC, IR and UV-Visible spectroscopy were used to characterize the multifunctional polymer. ZnO nanorods were functionalized with the block copolymer by multisite adsorption via the glycine COOH groups. The functionalized nanoparticles were well dispersible in organic solvents. Photoluminescence studies showed a complete quenching of the phosphorescence of the ruthenium chromophore (^{3}MLCT state). Kelvin probe Force Microscopy was used to confirm that under continuous excitation of the Ru complex (^{1}MLCT) the polymer corona develops a positive charge and thus efficient charge separation between ZnO and polymer is achieved.

Introduction:

Since O'Regan and Grätzel reported the first dye-sensitised solar cells (DSSCs) in 1991,[1] much effort has been devoted to enhancing their efficiency. The benefit to our environment is obvious, but the DSSCs suffer from the possibility of leaking of the I_3^-/I^- hole conductor dissolved in liquid solvent. To avoid leaking, solid state dye-sensitised solar cells (ssDSSCs) were introduced in 1996.[2] Oligoethylene glycol methacrylate doped with lithium ions was used as p-type conductor. In the following years, different polymers were used to improve the efficiency.[3, 4] Conducting polymers like poly(vinyltriphenylamine) (PTPA), poly(*para*-phenylene vinylene) (PPV) or

poly(3-hexylthiophene) (P3HT) have been used as hole transporting layers.[5] Transient absorption spectroscopy studies showed that the dye regeneration in ssDSSCs was at least one order of magnitude faster than in conventional DSSCs. However, the efficiencies of ssDSSCs remained low. The major drawback in this system is the low penetration rate of the polymer within the mesoporous film of TiO_2 nanoparticles. Several approaches were reported to increase the penetration. P3HT with carboxylate end groups has been synthesised and was used as a sensitiser in ssDSSCs.[6] A higher adsorption of the polymer onto the TiO_2 was observed compared to methyl terminated P3HT. Oligotriarylamine groups were directly bound to ruthenium(II) polypyridine dyes, enhancing the contact between the donor and the chromophore.[7-11] Furthermore, it has been shown that these systems show higher extinction coefficients compared to standard polypyridine complexes.[12] To further improve the ssDSSCs, a tris(2,2'-bipyridine) ruthenium(II) dye was incorporated directly inside a hole transporting PTPA and indeed these devices showed enhanced performances.[13]. However, they carry only a single ruthenium(II) complex within each polymer chain. To increase the amount of the chromophore in each polymeric chain, block copolymers with the first block based on a semiconducting PTPA and a second block with perylene units as chromophores and separated dopamine units as anchor groups were synthesised.[14] These polymers were attached to ZnO nanorods and characterised by Kelvin probe force microscopy (KPFM) on the level of the individual nanoparticle. A negative charging of the inorganic nanoparticles and a positive charging of the polymer corona was observed upon laser irradiation.[14] However, a more proximate contact of the dye with the ZnO is desirable for a more efficient electron injection.

Herein, we present the synthesis of a nanoscale donor-chromophore-acceptor (D-C-A) system with a PTPA based block copolymer carrying several directional bis(terpyridine)ruthenium(II) side groups in the second block. A carboxyl group is attached to each Ru^{II} dye which binds to the oxidic surface of ZnO nanorods. This allows for a large amount of dyes in proximity to the surface of the ZnO with the direct binding of the dye to the acceptor being beneficial for an efficient electron injection and charge separation. The TPA polymer acts as hole transporting matrix and the directional ruthenium complexes act both as light harvesting units and as anchor groups. Upon irradiation into the dye MLCT absorption band, charges are created and separated, as proven by Photoluminescence (PL) spectra and KPFM measurements.

Experimental

Materials. Unless otherwise mentioned, all chemical reagents were used as purchased without any further purification. Pentafluorophenol was obtained from Fluorochem (UK). Anhydrous THF and dioxane were freshly distilled from sodium. DMF was freshly distilled from calcium hydride and not exposed to light until it was used. 2,2'-Azobis(isobutyronitrile) (AIBN) was recrystallised

from diethyl ether and stored at -18 °C. Diphenyl-(4-vinyl-phenyl)-amine[15a] and ZnO nanorods[15b] were synthesised as reported in the literature.

Instrumentation. ^{1}H NMR spectra were recorded on a Bruker 300 MHz FT NMR spectrometer. Chemical shifts (δ) are given in parts per million relative to TMS. Samples were prepared in deuterated solvents and their signals referenced to residual nondeuterated solvent signals. ^{19}F NMR spectra were recorded on a Bruker 400 MHz FT NMR spectrometer. The molecular weight of the polymers was determined by gel permeation chromatography (GPC) in THF as solvent and with the following equipment: pump PU 1580, auto sampler AS1555, UV detector UV 1575 (detection at 254 nm), RI detector RI 1530 from JASCO. Columns were used from MZ-Analysentechnik: MZ-Gel SDplus 10 2 Å and MZ-Gel SDplus 10 6 Å. Calibration was done using polystyrene standards purchased from Polymer Standard Services. IR spectra were recorded on Perkin-Elmer 100 FTIR spectrometer using an ATR unit. UV-Vis spectra were recorded using a Jasco V-630 spectrophotometer (1 cm x 1 cm quartz cell). Emission spectra were recorded on a Varian Cary Eclipse spectrometer. Quantum yields were calculated by comparing the areas under the emission spectra on an energy scale/cm^{-1} recorded for optically matched solutions of the sample and the reference $[Ru(bpy)_3]Cl_2$ = 0.094 in CH_3CN.[16] ESI MS spectra were recorded on a Micromass Q-TOF-Ultima spectrometer. TEM pictures were taken on a Philips EM-420: 120kV with CCD-Camera.

KPFM measurements were performed at a MFP-3D standalone setup (Asylum Research, Santa Barbara). In order to prevent any degradation of the sample during the KPFM measurements the setup was placed in a glove box that was continuously purged with dry nitrogen (H_2O <0.1%, O_2 <0.01%). For simultaneous sample illumination during the KPFM measurement the setup was equipped with a diode laser (Point Source, iFLEX2000) with a wavelength of 488 nm, an intensity of 13.3 mW on the sample, and a spot diameter of 640 µm.[17a] We used Pt/Ir coated cantilevers with a nominal vertical resonance frequency of 70 kHz (Nanosensors, PPP-EFM). The measurements were performed in the dual pass mode at a lift height of 5 nm and with an AC voltage of 1.5 V. In KPFM, the contact potential difference (CPD) is measured which is defined as the difference in the work function between tip and sample. By using the amplitude modulation mode for KPFM both the tip apex and the cantilever contribute to the measured CPD.[17b] Thus, local changes in the CPD are not exclusively related to the sample area underneath the tip apex but also to the one underneath the cantilever. In case, the work function of the tip remains constant it is possible to attribute changes in the measured CPD owing to sample illumination to changes in the surface potential of the sample.[20] However, studies on P3HT:PCBM blends have shown that the CPD changes significantly for consecutive scanning on the same position. These shifts of the measured CPDs can be attributed to changes in the cantilever tip, such as coating thickness and adsorbates. Thus, it is important to have one surface within the scan area that does not participate in the photo-induced reaction and can therefore serve

as internal reference.[21, 22] For sample preparation, glass substrates were coated with 100 nm of ITO (99.9%, MaTeck GmbH) and cleaned in Ar plasma (PDC-002, Harrick plasma) for 2 min prior to their usage. The ITO surface acted as a reference surface for the KPFM study. A highly diluted dispersion of **P3a@ZnO** in THF was spin cast on the substrates.

Synthesis of chromophore **A**. The ruthenium dye [(H_2N-CH_2-CONH-tpy)Ru(tpy-CONH-CH_2-COOH)](PF_6)$_2$ (**A**) was synthesised from [(H_2N-tpy)Ru(tpy-COOH)](PF_6)$_2$ according to a solid phase peptide synthesis procedure.[18, 19] After cleavage from the TentaGel S Wang solid phase chromophore **A** was precipitated as its PF_6 salt by adding aqueous NH_4PF_6 to give **A** as dark red powder. ν_{max}/cm^{-1} 3090w (=C-H), 2920w (C-H), 1717m (C=O(acid)), 1663m (amide I), 1603m (C=C stretching), 1528s (amide II), 1477s (C=C stretching), 1427s, 1354s, 1289s, 1260, 1095m, 1028s, 826vs (PF_6), 789s, 752s, 555s (see Fig. S1). ^{1}H NMR: δ_H (600 MHz; CD_3CN; Me_4Si) 9.09 (s, 2H, H^2), 9.05 (s, 2H, $H^{2'}$), 8.59 (s, 1H, NH^b), 8.59 (m, 2H, H^5), 8.41 (m, 2H, $H^{5'}$), 8.16 (m, 1H, NH^a), 7.95 (m, 2H, H^6), 7.93 (m, 2H, $H^{6'}$), 7.44 (m, 2H, H^8), 7.31 (m, 2H, $H^{8'}$), 7.21 (m, 2H, H^7), 7.12 (m, 2H, $H^{7'}$), 4.32-4.30 (m, 2H, $CH_2{}^a$), 4.32-4.30 (m, 2H $CH_2{}^b$), NH_2 not observed probably due to protonation (for atom numbering see Supporting Information). $\lambda_{abs,max}$(DMF)/nm (ε/dm^3 mol^{-1} cm^{-1}) 279 (87900, $\pi\rightarrow\pi^*$), 311 (72600, $\pi\rightarrow\pi^*$), 498 (29400, MLCT), c = 0.09 mg ml^{-1}. $\lambda_{em,max}$(DMF)/nm 667 (λ_{ex}/nm 498). Quantum yield $\Phi = 1.4 \cdot 10^{-3}$). MS (ESI$^+$): *m*/*z* = 370.6 (22%) [**M**-(PF_6)$_2$]$^{2+}$, 886.1 (100%) [**M**-PF_6]$^+$.

Synthesis of **P1**. Diphenyl-(4-vinyl-phenyl)-amine (1.71 g, 6.3 mmol), dithiobenzoic acid benzyl ester (6.6 mg, 0.03 mmol), and 2,2'-azobis(2-methylpropionitrile) (AIBN) (0.6 mg, 4.5 µmol) were placed in a Schlenk tube and equipped with a stir bar. Dioxane (9 mL) was added and the solution was degassed by three freeze-pump-thaw cycles. The flask was then immersed in a preheated oil bath at 75 °C and the polymerisation was carried out for 42 h. The polymer was precipitated in methanol, collected by centrifugation, redissolved in THF and reprecipitated in methanol. This procedure was repeated three times. The light yellow powder **P1** (540 mg, 32%) was dried at 45 °C under reduced pressure for 12 h. λ_{max}(THF)/nm 300 (ε/dm^3 mol^{-1} cm^{-1} 205 800, c = 0.13 mg ml^{-1}). GPC: M_n = 12.800, M_w = 15.600 PDI: 1.2.

Synthesis of **P2**. **P1** (180 mg, 0.01 mmol), pentafluorophenyl acrylate (90 mg, 0.4 mmol) and AIBN (0.2 mg, 1.5 µmol) were placed in a Schlenk tube and equipped with a stir bar. Dioxane (2 mL) was added and the solution was degassed by three freeze-pump-thaw cycles. The flask was then immersed in a preheated oil bath at 80 °C and the polymerisation was carried out for 48 h. The polymer was precipitated in methanol, collected by centrifugation, redissolved in THF and reprecipitated in methanol. This procedure was repeated three times. The light yellow powder (171 mg) was dried at 45 °C under reduced pressure for 12 h. To remove the end group, the polymer (171 mg) was dissolved in dioxane (2 mL) and AIBN (47 mg, 0.28 mmol) was added. The solution was immersed ina preheated oil bath at 80 °C and stirred for 4 h. The polymer was

precipitated in methanol, collected by centrifugation, redissolved in THF and reprecipitated in methanol. This procedure was repeated three times. The light yellow powder **P2** (151 mg) was dried at 45 °C under reduced pressure for 12 h. ν_{max}/cm^{-1} 3082w (=C-H), 2914w (C-H), 1784m (COOR), 1587vs, 1515 vs (Ar-F), 1507vs, 1489vs, 1312s, 1272s, 1175s, 1029s, 835s, 750vs, 692vs, 623vs. ^{1}H NMR: δ_H (300 MHz; $CDCl_3$; Me_4Si) 1.55 (br, s), 1.97 (br, s), 6.54 (br), 6.87 (br). ^{19}F NMR δ_F (400 MHz; $CDCl_3$; Me_4Si) -153.21 (2F, br, s, F_{ortho}), -157.36 (1F, br, d, F_{para}), -164.28 (2F, br, s, F_{meta}). GPC: M_n = 14.900, M_w = 19.000 PDI: 1.3.

Synthesis of **P3a**. **P2** (37 mg, 2.8 µmol) was dissolved in dry THF (0.5 mL) in a nitrogen atmosphere. **A** (88 mg, 90 µmol) was dissolved in dry DMF (0.5 mL) in a nitrogen atmosphere and triethylamine (0.01 mg, 10 µmol) was added. The solutions were combined and stirred at 45 °C for 90 h. A white precipitate was observed after some time. The polymer was precipitated in methanol, redissolved in THF and reprecipitated in methanol seven more times until the supernatant was colourless. The dark red polymer **P3a** (18 mg) was dried under reduced pressure at 45 °C for 12 h. λ_{max}(THF)/nm 300, 498 (MLCT). ν_{max}/cm^{-1} 3082w (=C-H), 2914w (C-H), 1664m (amide I), 1587vs (amide II), 1402s, 1507vs, 1489vs, 1312s, 1272s, 1175s, 835s, 780 s, 750vs, 692vs, 623vs. GPC: M_n = 18.000, M_w = 22.000 PDI: 1.2. ^{19}F NMR δ_F (400 MHz; $CDCl_3$; Me_4Si) no signal.

Synthesis of **P3b**. **P2** (300 mg, 0.02 mmol), 4-(Aminomethyl)benzoic acid (139 mg, 0.9 mmol) and triethylamine (0.1 mL, 0.9 mmol) were placed in a Schlenk tube and dispersed in anhydrous DMF (2 mL). The suspension was stirred for 21 h at 80 °C in a nitrogen atmosphere and the resulting polymer was purified by dialysis against methanol (molecular weight cut off of 3.500 g/mol). **P3b** (275 mg) was obtained as light brown powder after drying in a vacuum at 45 °C for 12 h. λ_{max}(THF)/nm (ε/dm^3 mol^{-1} cm^{-1}) 301 (102 400), c = 0.16 mg ml^{-1}. ν_{max}/cm^{-1} 3082w (C=C), 2914w (C-C), 1700m (amide I), 1655m (amide I), 1587vs (amide II), 1507vs, 1489vs, 1312s, 1272s, 1175s, 1029s, 835s, 750vs, 692vs, 623vs. ^{19}F NMR δ_F (400 MHz; $CDCl_3$; Me_4Si) no signal.

Functionalisation of ZnO with **P3a** and **P3b**. For both polymers **P3a** and **P3b** the same procedure was applied. **P3a** (15 mg) or **P3b** (15 mg) and ZnO nanorods (15 mg) were dispersed in THF (1 mL) in a Schlenk tube and degassed by three freeze-pump-thaw cycles. The tube was then immersed in a preheated oil bath at 65 °C and stirred for 18 h. The dispersion was then centrifuged at 4000 rpm for 5 min to remove the non-functionalised nanorods which precipitated. A few drops of ethanol were then added to the supernatant and the dispersion was centrifuged at 13.000 rpm for 5 min. The supernatant was removed and the precipitate redispersed in THF (0.5 mL). The washing cycle was repeated four more times. The functionalised nanoparticles **P3a@ZnO** and **P3b@ZnO** were dispersed in 1 mL anhydrous THF and kept under nitrogen and in the dark until they were used. **P3a@ZnO:** λ_{max}(THF)/nm 300, 498 (MLCT). $\lambda_{em,max}$(DMF)/nm practically no emission observed (λ_{ex}/nm 498).

Results and discussion

Polypyridine complexes of ruthenium(II) have been extensively used as photoactive compounds in light to energy conversion devices. Compared to organic dyes they exhibit higher photo and thermal stabilities.[23] In many cases, ruthenium(II) polypyridine complexes contain bidentate (e. g. 2,2'-bipyridine) and monodentate ligands (e. g. pyridine, NCS^-). Especially monodentate ligands are believed to cause long term stability problems because of photo-induced and thermal ligand dissociation and degradation.[24-26] We employed tridentate 2,2';6',2''-terpyridine (tpy) ligands in the ruthenium complex **A** which imparts high photo and thermal stability because of the chelating effect.[19,27,28] In addition, the 4'-substituents on the $[Ru(tpy)_2]^{2+}$ core lead to a push-pull system with the two amide substituents pointing in the same direction. This vectorial arrangement is beneficial for charge separation and charge injection into inorganic semiconductors like ZnO or TiO_2.

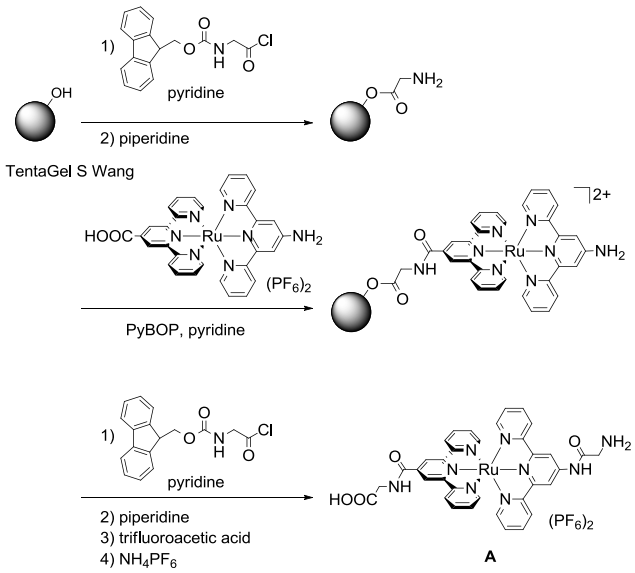

Scheme 1. Synthesis of directional chromopore **A** by SPPS.

The ruthenium dye conjugate $[(H_2N\text{-}CH_2\text{-}CONH\text{-}tpy)Ru(tpy\text{-}CONH\text{-}CH_2\text{-}COOH)](PF_6)_2$ (**A**) was obtained via solid phase peptide synthesis (SPPS) (Scheme 1) with a TentaGel S Wang resin used as the solid phase and Fmoc proteting group strategy.[18] SPPS allows high yield and high purity over several reaction steps because the reagents can be used in excess and purification is done by a simple washing procedure. A glycine unit was attached to the resin before the ruthenium(II) complex $[(H_2N\text{-}tpy)Ru(tpy\text{-}COOH)](PF_6)_2$ was anchored to the solid support by an amide bond. As aromatic amino groups are known to be less reactive towards activated esters[29] the amino group of the complex was decorated with a further glycine at the *N*-terminus which provides a reactive aliphatic amine functionality. In the last step the complex was cleaved from

the solid phase by trifluoroacetic acid and precipitated by addition of an aqueous NH_4PF_6 solution.

The polymer poly(vinyltriphenylamine) PTPA (**P1**) was prepared by Reversible Addition Fragmentation Chain Transfer (RAFT) polymerisation from vinyltriphenylamine (Scheme 2). PTPA is well known as a p-type semiconducting polymer and has already been used in solar cells.[30] The controlled radical polymerisation allows a good control of the molecular weight, a narrow polydispersity index (PDI) and the possibility to synthesise block copolymers. **P1** had a molecular weight of 13.000 g mol^{-1} (by GPC, polystyrene standard) and a PDI of 1.2. The second block was subsequently grafted onto **P1**, using pentafluorophenyl acrylate as monomer and giving block copolymer **P2**. Characterisation of **P2** by GPC (Fig. 1) showed a small shift to higher molecular weight and by referring it to the polystyrene standard, the degree of polymerisation of the first block was calculated to be around 50 ($n \approx 50$) and of the second block around 10 ($m \approx 10$). The ^{19}F NMR spectrum shows the expected resonances of the five fluorine nuclei attached to the aromatic ring (Fig. S2). The activated pentafluorophenyl ester of **P2** can subsequently be treated with primary amines to introduce functionalities in quantitative yields.[31, 32] The activated ester block was chosen to be relatively short ($m \approx 10$), since short anchor blocks were shown to bind the most effectively to ZnO surfaces.[33]

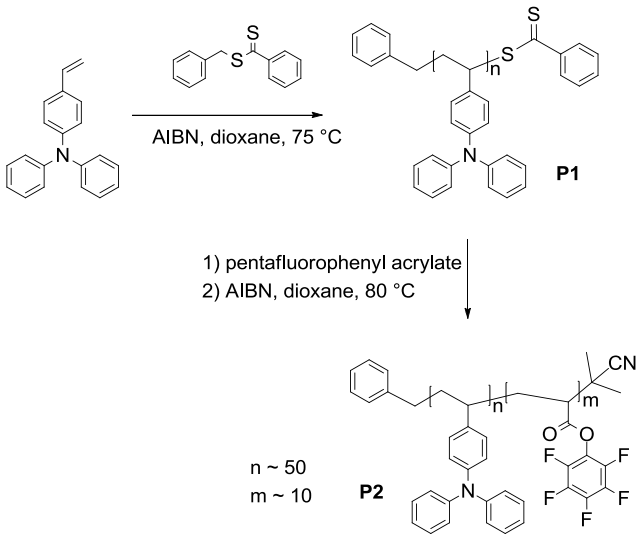

Scheme 2. Synthesis of **P1** and **P2** by RAFT polymerisation.

In order to attach the ruthenium dye **A** to polymer **P2** a polymer analog reaction was carried out. The amine functionality of dye **A** readily reacts with the activated ester moieties of **P2** (Scheme 3). An excess of the dye and the polymer were dissolved in *N,N'*-dimethylformamide and heated to 45°C for 90 h. Excessive washing by precipitation/dissolving yielded the pure dark red block copolymer **P3a**. Characterisation by Fourier transform infrared (FT-IR) spectroscopy

showed the absence of the ester band at 1784 cm^{-1} and the new band of amide bonds at 1664 cm^{-1} (Fig. S2). Additionally, a ^{19}F NMR spectrum proves that all pentafluorophenyl groups were removed from the polymer (Fig. S3). Furthermore, the PF_6 counterions were exchanged by other anions as judged by the absence of a resonance at -73.2 ppm. A significantly higher molecular weight of **P3a** was observed by GPC (Fig. 1) compared to the block copolymer **P2**, so that the covalent attachment of the dye to the polymer is proven. As a control, **P2** was treated with 4-(aminomethyl)benzoic acid giving **P3b**. The synthesis and characterisation of **P3b** is analogous to the reaction of **P2** with **A**. The carboxyl groups of **P3b** can also adsorb to ZnO surfaces but no charge generation is expected under irradiation with visible light.

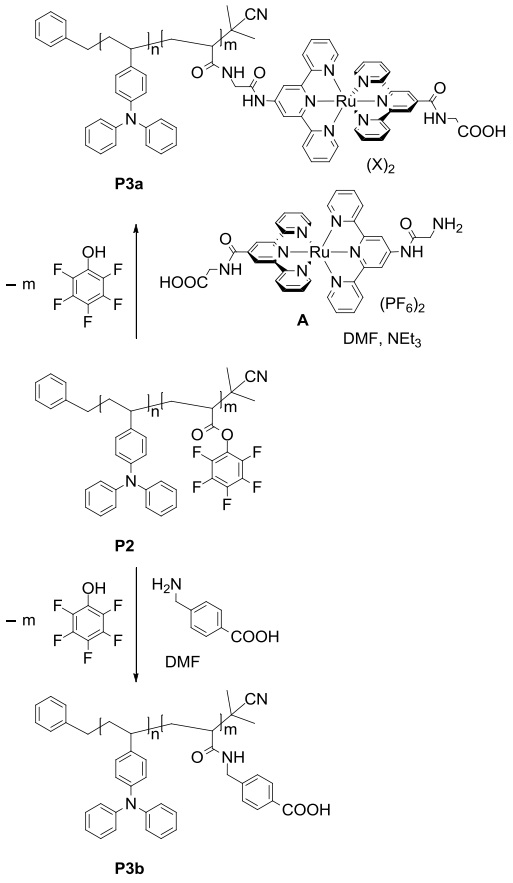

Scheme 3. Functionalisation of **P2** with **A** to give **P3a** (top) and with 4-(aminomethyl)benzoic acid to give **P3b** (bottom).

UV-Visible and photoluminescence (PL) measurements were carried out (Fig. 2). In the absorption spectrum of **P3a** the bands at 250-350 nm arise from $\pi \rightarrow \pi^*$ transitions mainly of the triphenylamine groups and a small contribution from the ruthenium dye. The absorption of the dye is the visible region was observed at 498 nm and is attributed to the characteristic metal-to-ligand charge transfer (MLCT) of the complex.[18] For **P3b** no absorption is observed in that spectral region (Fig. S8). Photoluminescence measurements in THF (λ_{exc} = 498 nm) show that the

dye functionalised polymer **P3a** emits at 667 nm, which is the same value as for the pristine dye **A** (667 nm in DMF). Thus the emission of the dye is not reductively quenched by the TPA polymer.

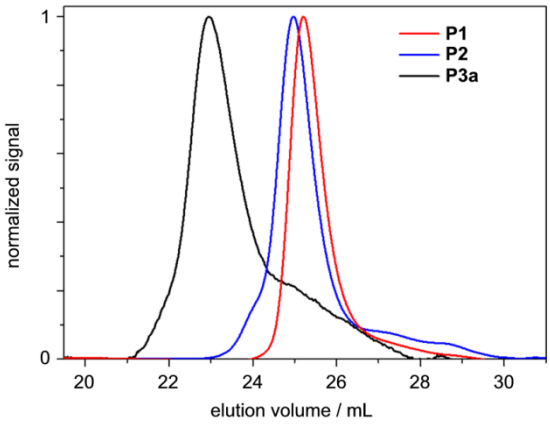

Fig. 1 GPC traces of **P1** (red), **P2** (blue) and **P3a** (black).

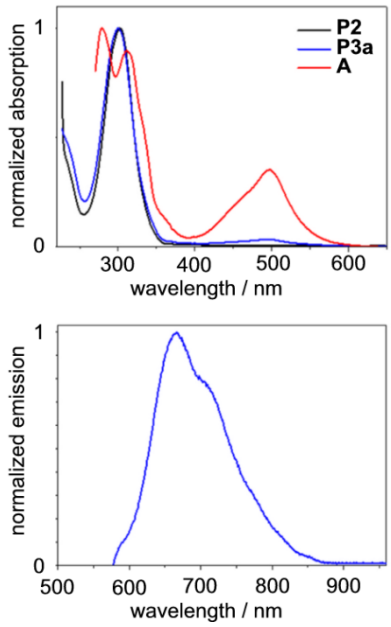

Fig. 2 UV-Vis spectra of **P2** in THF (black), **P3a** in THF (blue) and **A** in DMF (red) (top) and PL spectrum of **P3a** in THF at 498 nm excitation (bottom).

ZnO nanorods were synthesised according to the literature with a sise distribution of several hundreds of nanometers to two micrometers.[15b] For functionalisation with polymers **P3a** and **P3b**, the nanorods were dispersed in a small amount of THF and the respective polymer was added subsequently. The dispersion was stirred at 65 °C over night under an inert atmosphere. Centrifugation (4000 rpm) for 2 min removed all insufficiently functionalised nanoparticles. Ethanol was then added to the clear dispersion to precipitate the nanocomposite. Subsequent centrifugation, redispersion and repetition of the washing cycle for several times gave the pure

hybrid materials **P3a@ZnO** and **P3b@ZnO**, respectively. **P3a@ZnO** was a stable red dispersion, which showed some scattering of the light due to the large nanoparticles (length > 800 nm). TEM images drop cast from the THF dispersion showed that **P3a@ZnO** nanoparticles were well dispersed and did not aggregate. In contrast, the as-synthesised sample of pristine ZnO showed strong aggregation (Fig. S4).

The Jablonski diagram of the nanocomposite (Fig. 3) shows the estimated energy levels of the system **P3a@ZnO** together with the possible charge separation/recombination pathways in the D-C-A array.[43] Irradiation of ZnO-<Ru>$^{2+}$-TPA at 498 nm leads to the singlet MLCT excited state ZnO-^{1}<Ru>$^{2+*}$-TPA (2.49 eV), which subsequently undergoes intersystem crossing (ISC) to the triplet excited state ^{3}MLCT ZnO-^{3}<Ru>$^{2+*}$-TPA (1.86 eV) typically with unit efficiency. Both MLCT states are thermodynamically competent to inject an electron into ZnO or to accept an electron from TPA. Photoluminescence measurements show that the phosphorescence of **P3a@ZnO** is indeed efficiently quenched as compared to **P3a** lacking the ZnO acceptor. From the singlet and triplet MLCT excited states ZnO-^{1}<Ru>$^{2+*}$-TPA / ZnO-^{3}<Ru>$^{2+*}$-TPA the fully charge separated state ZnO(e^-)-<Ru>$^{2+}$-TPA(h^+)[14,34] can principally be populated via the partially charge separated states ZnO-<Ru>$^{+}$-TPA(h^+) (1.45 eV) or ZnO(e^-)-<Ru>$^{3+}$-TPA (1.57 eV).[18] In the fully charge separated state ZnO(e^-)-<Ru>$^{2+}$-TPA(h^+) (0.88 eV), the ZnO carries the negative and the TPA the positive charge.

By performing PL measurements the quantum yield of **P3a** was determined to be $\Phi = 2.0 \cdot 10^{-3}$ which is very similar to the value of **A** without TPA attachment ($\Phi = 1.4 \cdot 10^{-3}$).[18] This shows that no luminescence quenching occurs when the dye is bound to the polymer backbone i.e. photo-induced electron transfer from TPA to the excited ruthenium units ^{1}<Ru>$^{2+*}$ and ^{3}<Ru>$^{2+*}$ is inefficient in this polymer. However, after anchoring of **P3a** to ZnO, the quantum yield of the hybrid **P3a@ZnO** drops below $\Phi = 6.5 \cdot 10^{-5}$. This low quantum yield clearly corroborates the efficiency of the oxidative quenching in the system, i.e. the first electron transfer step after excitation is electron injection into ZnO, likely followed by dye regeneration by TPA.

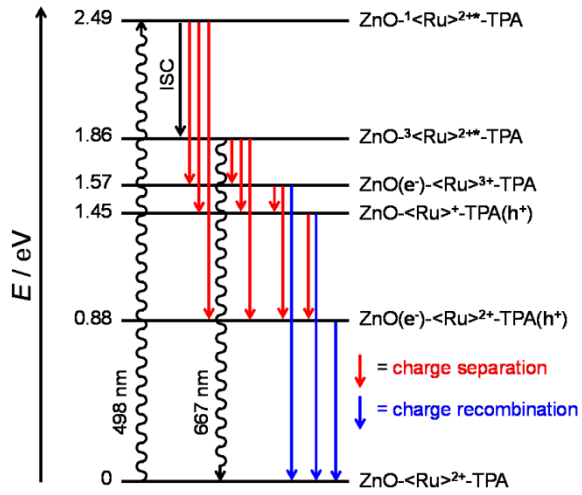

Fig. 3 Jablonski diagram of **P3a@ZnO**.

In order to study the photo-induced interfacial charge transfer in more detail on a single particle level KPFM measurements were carried out in analogy to the measurements we performed on the D-C-A system consisting of a PTPA-perylene block copolymer covalently bound to ZnO[14] and on PPV-TiO_2 hybrid systems.[35] KPFM is a very powerful tool to detect local variations of the surface potential in the nanometer regime.[36] Illuminating samples with light allows studying the photo-response of optoelectronic materials.[37-42] Sample illumination of **P3a@ZnO** is realised from underneath the sample through transparent indium tin oxide (ITO) (Fig. 4a) The surface potential was first measured without illumination (Fig. 4b) on a single particle with the length of around 1 µm and a diameter of approximately 120 nm (Fig. S5). The particle displays an approximately 45 mV higher surface potential than the surrounding ITO substrate. By subsequently comparing that to the surface potential recorded under illumination with λ = 488 nm (Fig. 4c), the photo-induced change in the surface potential of the **P3a@ZnO** particles is determined. Upon illumination, the surface potential on the **P3a@ZnO** particle increases. This effect was completely reversible after switching off the laser and could be observed for all particles at different positions. Upon laser illumination at a wavelength of 488 nm an electron of the chromophore is excited. Charge separation occurs at the interface of the ZnO particle by transfer of the electron to the conduction band of the ZnO. The oxidised ruthenium dye regenerates by collecting an electron from the HOMO level of the TPA polymer.

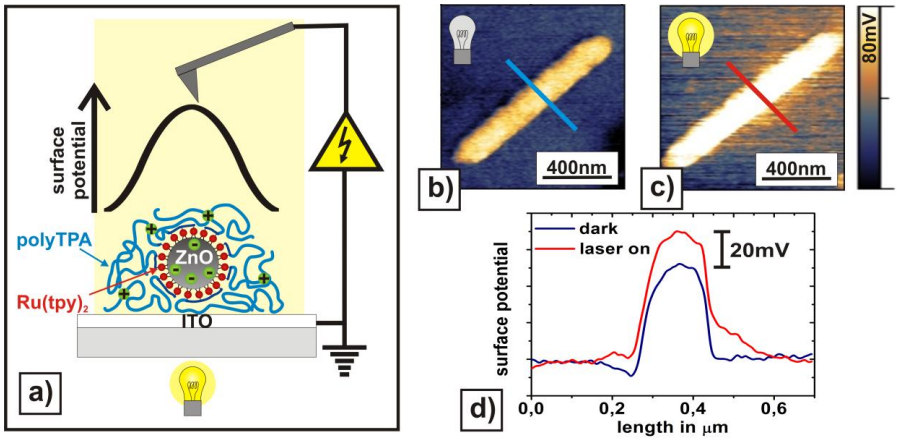

Fig. 4 Study of interfacial charge transfer by KPFM on **P3a@ZnO** spun cast from THF in the dark and under laser illumination (λ = 488 nm). **a)** Schematic of the KPFM measurement on D-C-A system (TPA in blue, $Ru(tpy)_2$ in red and ZnO in grey) under laser illumination through the ITO coated glass substrate. The surface potential on the functionalised ZnO particle upon illumination is qualitatively depicted in the upper graph. **b)** and **c)** Surface potential maps measured in the dark and under illumination on the same position. The measured potential values were adjusted relative to the constant potential value of the ITO at large distance from the **P3a@ZnO**. **d)** Line profiles of the surface potentials taken across the particle show an increase in surface potential of around 20 mV upon illumination.

In order to quantitatively discuss this photo response, the surface potential profile was analyzed in detail across the particle as indicated by the blue and red line for laser off and on in the corresponding surface potential images (Fig. 4d). The increase in surface potential of around 20 mV on the **P3a@ZnO** particle and up to a distance of around 100 nm around the particle was attributed to the build-up of positive charges in the TPA block as a consequence of the charge separation at the interface. Negative charges of the ZnO particle could not be detected by KPFM. This observation indicates a high grafting density of the **P3a** to the ZnO and therefore results in a densely packed and thick polymer layer. Thus, the effect of the build-up of electrons inside the ZnO on the surface potential change is shielded by the positive charges of the TPA.[44]

The estimated energy level difference of 0.88 eV between the ground state ZnO-$<Ru>^{2+}$-TPA and the charge separated state ZnO(e^-)-$<Ru>^{2+}$-TPA(h^+) (Fig. 3) is significantly larger than the value obtained by KPFM. We attribute this difference to the screening of the positively charged TPA by the counter ions of the $<Ru>^{2+}$ which diffuse from the D-A interface into the polymer matrix. Finally, an additional control experiment performed on **P3b@ZnO** showed no photo-response under irradiation with λ = 488 nm (Fig. S6). Without the chromophore as anchoring group at the interface between ZnO and TPA no excitons can be generated under similar conditions. Thus, for an efficient charge transfer the complete donor-chromophore-acceptor system is required.

Conclusions

Herein we demonstrated the synthesis and characterisation of a new nanoscale D-C-A system with polytriphenylamine as electron donor (D) and a directional $[Ru^{II}(tpy)_2]^{2+}$ complex as chromophore (C) which is directly bound to ZnO nanorods as electron acceptor (A).

The ruthenium complex $[Ru^{II}(tpy)_2]^{2+}$ with tridentate ligands has a higher thermal and photo stability compared to organic dyes or 2,2'-bipyridine ruthenium(II) complexes. Additionally, the push-pull substituted terpyridine ligands induce spatially separated frontier orbitals which support the charge separation at the interphase. Since the polymer carries several chromophores within each chain, the local concentration of the light harvesting units at the ZnO surface is very high. The chromophore-acceptor contact is very intimate through the direct attachment via the carboxyl groups of the Ru^{II} complex. The donor-chromophore contact on the other side is enhanced by the covalent binding of the triphenylamine polymer to the chromophores. Charge separation occurs under light excitation of the chromophore and was proven by phosphorescence quenching and KPFM measurements. Based on these results, we believe that the system is especially suitable to build high performance ssDSSCs.

Acknowledgement

This work was financially supported by the International Research Training Group (IRTG): Self Organized Materials for Optoelectronics supported by the Deutsche Forschungsgemeinschaft (DFG). We thank Dr. Stefan Frank for the synthesis of the ZnO nanorods and Gabi Herrmann for the preparation of the ITO coated glass substrates. In addition, we thank Esha Sengupta and Stefan Weber for discussions and the BMBF (contract # 03SF0334) for partial financial support in building up the photo KPFM.

Notes and references

ǂAuthors contributed equally to this work.

1. B. O'Regan and M. Grätzel, *Nature*, 1991, **353**, 737-740.
2. M. Matsumoto, H. Miyazaki, K. Matsuhiro, Y. Kumashiro and Y. Takaoka, *Solid State Ionics*, 1996, **89**, 263-267.
3. U. Bach, D. Lupo, P. Comte, J. E. Moser, F. Weissortel, J. Salbeck, H. Spreitzer and M. Grätzel, *Nature*, 1998, **395**, 583-585.
4. J. Boucle and J. Ackermann, *Polym. Int.*, 2012, **61**, 355-373.
5. W. Zhang, Y. Cheng, X. Yin and B. Liu, *Macromol. Chem. Phys.*, 2011, **212**, 15-23.
6. R. H. Lohwasser, J. Bandara and M. Thelakkat, *J. Mater. Chem.*, 2009, **19**, 4126-4130.
7. K. C. D. Robson, B. D. Koivisto, T. J. Gordon, T. Baumgartner and C. P. Berlinguette, *Inorg. Chem.*, 2010, **49**, 5335-5337.
8. K. C. D. Robson, B. Sporinova, B. D. Koivisto, E. Schott, D. G. Brown and C. P. Berlinguette, *Inorg. Chem.*, 2011, **50**, 6019-6028.

9. C. S. Karthikeyan, K. Peter, H. Wietasch and M. Thelakkat, *Sol. Energy Mater. Sol. Cells*, 2007, **91**, 432-439.
10. J.-H. Yum, S.-J. Moon, C. S. Karthikeyan, H. Wietasch, M. Thelakkat, S. M. Zakeeruddin, M. K. Nazeeruddin and M. Grätzel, *Nano Energy*, 2012, **1**, 6-12.
11. Z. Jin, H. Masuda, N. Yamanaka, M. Minami, T. Nakamura and Y. Nishikitani, *Chem. Lett.*, 2009, **38**, 44-45.
12. H. J. Snaith, C. S. Karthikeyan, A. Petrozza, J. Teuscher, J. E. Moser, M. K. Nazeeruddin, M. Thelakkat and M. Grätzel, *J. Phys. Chem. C*, 2008, **112**, 7562-7566.
13. K. Peter and M. Thelakkat, *Macromolecules*, 2003, **36**, 1779-1785.
14. M. Zorn, S. A. L. Weber, M. N. Tahir, W. Tremel, H. J. Butt, R. Berger and R. Zentel, *Nano Lett.*, 2010, **10**, 2812-2816.
15. a) M. Behl, E. Hattemer, M. Brehmer and R. Zentel, *Macromol. Chem. Phys.*, 2002, **203**, 503-510; b) B. Cheng, Shi, J. M. Russell-Tanner, L. Zhang and E. T. Samulski, *Inorg. Chem.*, 2006, **45**, 1208-1214.
16. K. Suzuki, A. Kobayashi, S. Kaneko, K. Takehira, T. Yoshihara, H. Ishida, Y. Shiina, S. Oishi and S. Tobita, *Phys. Chem. Chem. Phys.*, 2009, **11**, 9850-9860.
17. a) S. L. Weber, H.-J. Butt and R. Berger, Electrical Characterization of Solar Cell Materials Using Scanning Probe Microscopy. In *Scanning Probe Microscopy in Nanoscience and Nanotechnology 3*, Bhushan, B., Ed. Springer Berlin Heidelberg: 2013; pp 551-573; b) S. V. Kalinin and D. A. Bonnell, *Phys. Rev. B*, 2001, **63**, 125411.
18. K. Heinze and K. Hempel, *Chem. – Eur. J.*, 2009, **15**, 1346-1358.
19. K. Heinze, K. Hempel and M. Beckmann, *Eur. J. Inorg. Chem.*, 2006, **2006**, 2040-2050.
20. V. Palermo, M. Palma and P. Samorì, *Adv. Mater.*, 2006, **18**, 145-164.
21. E. Sengupta, A. L. Domanski, S. A. L. Weber, M. B. Untch, H.-J. Butt, T. Sauermann, H. J. Egelhaaf and R. Berger, *J. Phys. Chem. C*, 2011, **115**, 19994-20001.
22. A. L. Domanski, E. Sengupta, K. Bley, M. B. Untch, S. A. L. Weber, K. Landfester, C. K. Weiss, H.-J. Butt and R. Berger, *Langmuir*, 2012, **28**, 13892-13899.
23. A. Reynal and E. Palomares, *Eur. J. Inorg. Chem.*, 2011, **2011**, 4509-4526.
24. P. T. Nguyen, B. X. T. Lam, A. R. Andersen, P. E. Hansen and T. Lund, *Eur. J. Inorg. Chem.*, 2011, **2011**, 2533-2539.
25. T. P. Brewster, W. Ding, N. D. Schley, N. Hazari, V. S. Batista and R. H. Crabtree, *Inorg. Chem.*, 2011, **50**, 11938-11946.
26. S. Kämper, A. Paretzki, J. Fiedler, S. Záliš and W. Kaim, *Inorg. Chem.*, 2012, **51**, 2097-2104.
27. A. Breivogel, C. Förster and K. Heinze, *Inorg. Chem.*, 2010, **49**, 7052-7056.
28. A. Breivogel, K. Hempel and K. Heinze, *Inorg. Chim. Acta*, 2011, **374**, 152-162.
29. K. Nilles and P. Theato, *J. Polym. Sci. Pol. Chem.*, 2010, **48**, 3683-3692.
30. M. Sommer, S. M. Lindner and M. Thelakkat, *Adv. Funct. Mater.*, 2007, **17**, 1493-1500.
31. M. Eberhardt, R. Mruk, R. Zentel and P. Théato, *Eur. Polym. J.*, 2005, **41**, 1569-1575.
32. M. Eberhardt and P. Theato, *Macromol. Rapid Commun.*, 2005, **26**, 1488-1493.
33. M. Zorn, S. Meuer, M. N. Tahir, Y. Khalavka, C. Sonnichsen, W. Tremel and R. Zentel, *J. Mater. Chem.*, 2008, **18**, 3050-3058.
34. E. Hattemer, Johannes Gutenberg-Universität, Mainz, 2000.
35. L. zur Borg, A. L. Domanski, R. Berger and R. Zentel, *submitted*, 2012.
36. M. Nonnenmacher, M. P. O'Boyle and H. K. Wickramasinghe, *Appl. Phys. Lett.*, 1991, **58**, 2921-2923.
37. J. M. R. Weaver and H. K. Wickramasinghe, *J. Vac. Sci. Technol. B: Microelectronics and Nanometer Structures*, 1991, **9**, 1562-1565.
38. H. Hoppe, T. Glatzel, M. Niggemann, A. Hinsch, M. C. Lux-Steiner and N. S. Sariciftci, *Nano Lett.*, 2005, **5**, 269-274.
39. J. Cao, J.-Z. Sun, J. Hong, X.-G. Yang, H.-Z. Chen and M. Wang, *Appl. Phys. Lett.*, 2003, **83**, 1896-1898.
40. V. Palermo, G. Ridolfi, A. M. Talarico, L. Favaretto, G. Barbarella, N. Camaioni and P. Samorì, *Adv. Funct. Mater.*, 2007, **17**, 472-478.
41. S. Sadewasser and M. C. Lux-Steiner, *J. Vac. Sci. Technol. B: Microelectronics and Nanometer Structures*, 2010, **28**, C4D29-C24D33.
42. E. J. Spadafora, R. Demadrille, B. Ratier and B. Grevin, *Nano Lett.*, 2010, **10**, 3337-3342.
43. The energy levels of the Jablonski diagram were estimated from the absorption and emission maxima (ZnO-^{1}<Ru>$^{2+}$*-TPA: 498 nm; 2.49 eV; ZnO-^{3}<Ru>$^{2+}$*-TPA: 667 nm; 1.86 eV) as well as from potential differences of literature known energy levels and redox potentials. The conduction band of ZnO is at -4.4 eV vs. vacuum[14]. The oxidation potential of the TPA units in **P3@ZnO** is

estimated to be +0.84 V vs. NHE which is the oxidation potential of monomeric tolyldiphenylamine.[34] The oxidation and reduction potentials of the <Ru> unit in **P3@ZnO** were estimated to be +1.285 and -0.850 V vs. SCE, respectively, from the values of the molecular ruthenium dye $[(H_3C\text{-}CONH\text{-}tpy)Ru(tpy\text{-}CONH\text{-}CH_2\text{-}COOH)](PF_6)_2$.[18] With E(vacuum) / eV = -4.44 - E(NHE) = -4.68 - E(SCE) we estimate ZnO-<Ru>$^{+}$-TPA^{+} at +1.45 eV, ZnO(e^-)-<Ru>$^{3+}$-TPA at +1.565 eV and ZnO(e^-)-<Ru>$^{2+}$-TPA^{+} at 0.88 eV.

44. S. V. Kalinin and D. A. Bonnell, *Nano Lett.*, 2004, **4**, 555-560.

3.4 Effect of Band Gap Alignment on the Hole Transport from Semiconducting Block Copolymers to Quantum Dots

Lisa zur Borg,[‡] Donggu Lee,[‡] Jaehoon Lim,[‡] Wan Ki Bae, Myeongjin Park, Seonghoon Lee, Changhee Lee, Kookheon Char and Rudolf Zentel

Abstract:

Semiconducting hole transporting block copolymers were chemically modified to adjust their energy levels to that of CdSe/CdS/CdZnS core shell quantum dots. Hybrids with optimized energy levels were used to build strongly improved quantum dot LEDs (QLED).

Introduction:

Considerable investigation has been devoted to light emitting diodes (LEDs) based on colloidal quantum dots (QDs), because of their unique optical and electrical properties. Specifically, their wide absorption range and narrow spectral bandwidth are in high demand for reproducing pure color spectrum in down-conversion or electroluminescence LEDs. A simple replacement of conventional lumophors with QDs in such devices has demonstrated a higher color-rendering index and broader color gamut.[1-7] Although the conceptual study on QD-based LEDs (QLEDs) has been successfully demonstrated so far,[8-13] multilateral efforts towards higher quantum efficiency, novel device architecture and solution-based accurate printing processes are necessary for the successful realization of QD-based solid state lighting and full-color displays.

Among these efforts, conducting polymers as hole transporting components were found to increase performance[14, 15] and the hybridization of QDs with conducting block copolymers carrying anchor groups is an especially promising approach to improve the morphology at nanoscale. Polymers grafted on QDs significantly improve the stability of the hybrid dispersion by efficient steric stabilization, yielding good solution processibility and thin film formation.[16-19] However, the device performances of conducting polymer@QD hybrid LEDs in previous research have been found to be far below the efficiencies of cutting edge QLEDs (7.3% external quantum efficiency (E.Q.E.) and 200,000 cd/m^2 maximum brightness).[20] The low performances of current

conducting polymer@QD hybrid LEDs are mainly attributed to an imbalanced carrier injection. The large hole injection barrier from the hole transporting layer (HTL) to the valence band of QDs through the highest occupied molecular orbital (HOMO) level of conducting polymers impedes effective and balanced carrier recombination. In order to facilitate the hole injection from the anode to QDs, the energy level difference should be minimized.

In this paper, we present the study of the influence of the band gap alignment of poly(vinyltriphenylamine dimer) (PTPD) derivatives on the hole injection efficiency to red QDs. For this purpose, two block copolymers were synthesized through reversible addition fragmentation chain transfer (RAFT) polymerization, one with electron donating (methoxy) and one with electron withdrawing (trifluormethyl) groups. The effect of the side groups on the band gap alignment, especially on the HOMO level was studied. Cadmium selenide QDs with thick alloyed multi-shells (CdSe/CdS/CdZnS) were hybridized with the polymers through the grafting-to method and characterized. Red QDs have a smaller bandgap and higher HOMO level than green or blue QDs and were therefore the best choice to study the influence of the band gap of the polymers to the hole injection.

Results and Discussion:

As monomers, vinyltriphenylamine dimers (TPD) were chosen. Even though hybrids of QDs and poly(vinyltriphenylamine) (PTPA) based block copolymers with anchor groups were previously reported to improve the morphology at nanoscale, when applied in devices, they showed reduced efficiency at high currents.[18] A significant increase of the device's stability at high currents has been observed when PTPD was used.[21] Despite this positive result, the maximum E.Q.E. has dropped in comparison to the TPA block copolymer based devices, due to the higher hole injection barrier.

Vinyl-TPD monomer *N*,*N'*-Bis(4-methoxyphenyl)-*N*-phenyl-*N'*-4-vinylphenyl-[1,1 'biphenyl]-4,4'-diamine was synthesized according to literature.[22, 23] Vinyl-TPDF monomer *N*,*N*'-2-bis(4-trifluoromethylphenyl)-*N*-phenyl-*N'*-4-vinylphenyl(1,12-biphenyl)-4,4-diamine was synthesized in three steps and is described in detail in the supporting information. The hole transporting polymers were synthesized by RAFT polymerization using dithiobenzoic acid benzyl ester as a chain-transfer agent (Scheme 1). The resulting homopolymers PTPD (**P1**) and PTPDF (**P2**) were characterized by GPC (Figure S 1). They had a narrow polydispersity index (PDI) of 1.10 or less (Table 1) and were prepared with a similar molecular weight for better comparison. The HOMO levels were calculated through the oxidation potential by cyclovoltammetry (CV) in *o*-dichlorobenzene to be -5.2 eV **(P1**) and -5.9 eV (**P2**) (Figure S 1). The polymers show two oxidation peaks which implies that they can be oxidized twice. The resulting LUMO (lowest

unoccupied molecular orbital) levels were calculated by using the HOMO level and determining λ_{onset} via UV-Visible spectroscopy. Interestingly, the chemical modification did not change the LUMO level significantly (**P1**: -2.6 eV and **P2**: -2.7 eV). The electron withdrawing character of the trifluoro methoxy groups and the electron donating character of the methoxy groups determine mostly the HOMO level and thereby the optical bandgap.

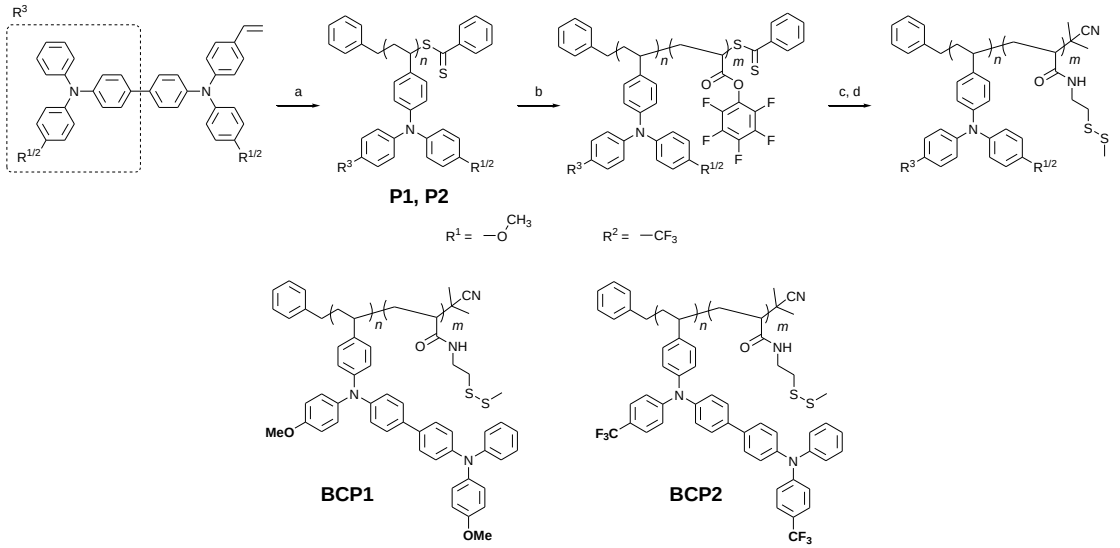

Scheme 1) Synthetic route to **BCP1** and **BCP2**: **a)** Dithiobenzoic acid benzyl ester, AIBN, 80 °C, 48 h; **b)** Pentafluorophenyl acrylate, AIBN, 80 °C, 48 h; **c)** AIBN, 80 °C, 3 h; **d)** Cysteaminmethyl disulfide, NEt_3, 45 °C, 12 h.

The homopolymers were used as macro chain-transfer agents and pentafluorophenyl acrylate active ester was grafted onto them by RAFT polymerization, which yielded the functional block copolymers poly(*N,N'*-2-bis(4-methoxyphenyl)-*N*-phenyl-*N*-4-vinylphenyl(1,12-biphenyl)-4,4-diamine-*b*-(2-methyldisulfanyl)ethylacrylamide, (**BCP1)** and poly(*N,N*'-2-bis(4-trifluorophenyl)-*N*-phenyl-*N*-4-vinylphenyl(1,12-biphenyl)-4,4-diamine-*b*-(2-methyldisulfanyl)ethylacrylamide **(BCP2)**. The second block was kept short; around 5 activated esters in each polymer chain were attached. That was enough to bind the polymers tightly in a multidentate way to the nanoparticles, but short enough to avoid interparticle cross-linking.[24] 2-methyldisulfanyl-ethylamine was synthesized and reacted with the block copolymers in polymer analogue reactions. The disulfide groups are capable of binding to the sufidic surface of the QDs and therefore act as anchor groups.[25]

Table 1. Analytical data of the polymers.

	M_n [g/mol][a]	M_w/M_n[a]	HOMO [eV][b]	LUMO [eV][c]
P1	15,000	1.05	-5.2	-2.6
BCP1	16,300	1.07		
P2	12,600	1.09	-5.9	-2.7
BCP2	13,800	1.07		

[a] GPC, polystyrene standard [b] Cyclovoltammerty in *o*-DCB with tetrabutylammonium fluoride as conducting salt [c] UV/Vis in *o*-DCB

To optimize bandgap alignment between QDs and conducting polymers, red QDs were chosen. Among the three fundamental colors in display applications (i.e., red, green, and blue), the valence band edge of the red QDs is highest and thus most adjacent to the HOMO level of the conducting polymers, suitable for facilitated hole injection from conducting polymers to QDs. In addition to the proper energy level alignment, we also designed the nanostructure of QDs suitable for hybridization. Previously reported QDs are particularly vulnerable to surface degradation due to their thin ZnS or ZnSe shells. Therefore in this study, we introduced thick CdS/CdZnS buffer layer/alloyed shells (~ 2.1 nm) on the red CdSe core (CdSe/CdS/CdZnS structure) through a multiple overcoating process. The as-synthesized QDs showed high photoluminescence quantum yield of up to 80% at deep red emission range (λ_{max} ~ 630 nm, full-width at half-maximum < 30 nm).

Since the electrons have to migrate from the HOMO level of the polymer into the valence band of the QDs, a lower HOMO level is facilitating the charge transport. Hybridization of the QDs with **BCP1** or **BCP2** was performed by the grafting-to approach.[26] The effectiveness of hybrid films of QDs and polymers for QLED application were already proven in previous work.[18,19] The disulfide anchor groups of the conducting polymers could interact with the cationic sites of the QDs and result in the formation of **BCP1@QD** and **BCP2@QD** hybrids. The formation of hybrids was confirmed by a change of solubility, as shown in Figure 1a. The polymers grafted on QDs determine the solubility of the hybrids, so therefore the hybrids are not soluble in hexane (poor solvent for polymers and good solvent for QDs), but in toluene, chloroform or chlorobenzene (good solvent for polymers). As-synthesized hybrids showed a high colloidal stability in toluene as well as a negligible drop in PL QY in solution (less than 1%). In addition to these advantages, the conducting hybrids formed films with highly uniform morphology at nanoscale (Figure 1b), which is particularly essential to maintain the uniform electric field across the device and emit electroluminescence from the entire QD layer. The conducting hybrids prepared here provide i) optimized electrical properties as well as ii) a homogeneous morphology for successful operation of electroluminescence devices.

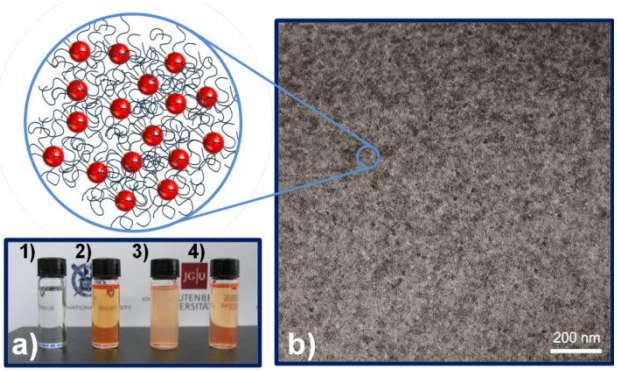

Figure 1. **a)** Picture of the solubility change of polymers, pristine QDs and the hybrids: 1) pure polymer in toluene, 2) hybrid in toluene, 3) hybrid in hexanes, 4) QDs in hexane. **b)** TEM image of the poly(TPDF-*b*-SSMe)@QDs hybrid film with a schematic of the hybridized QDs in the film.

For a better comparison and understanding of the influence of the chemical structure on the device performances, we built QLEDs with inverted structure platform. The inverted structure QLEDs were recently reported to have high device performances, since vacuum evaporated hole injection layer which have superior electrical properties (high hole mobility and low HOMO levels) can be adopted after solution processed QD deposition.[20] This geometry is thus optimal for a study, which focuses on the optimization of hole injection into the QDs. Figure 2 shows a scheme of the energy levels of all materials in the devices and an illustration of the device structure. In the case of **P1**, the holes would need to be lifted up to the HOMO level of the polymer before combining with the electrons inside the QDs. This barrier reduces the efficiency of the device. However, in the case of **P2**, the HOMO level is perfectly adjusted between the hole transport layer (HTL) 4,4',4''-tris(*N*-carbazolyl) triphenylamine (TCTA) and the valence band edge of the QDs. It is a straight forward path for the holes towards the QDs. This well aligned system with a lower hole injection barrier promises high performance devices.

The QLEDs were built with a 45 nm layer of ZnO nanoparticles for electron injection/transporting layer, a 40 nm layer of poly(TPD-*b*-SSMe)@QD (Device 1) and poly(TPDF-*b*-SSMe)@QD (Device 2) as light emitting layer, a 60 nm layer of TCTA as HTL and a 100 nm layer of aluminum as anode. TCTA was selected as optimal hole transport layer due to similar HOMO levels (-5.7 eV) with the anchoring polymers. The electrons are injected through the ITO and the ZnO to the active layer, whereas the holes migrate through the aluminum, cross the HTL and the polymer and recombine with the electrons inside the quantum dots.

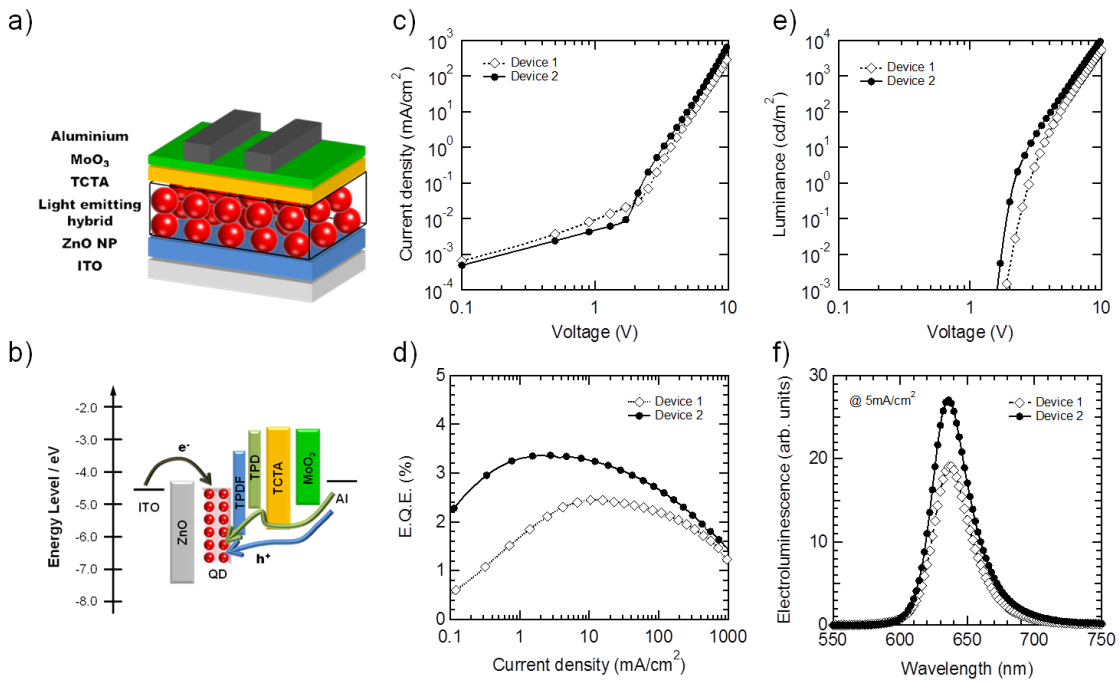

Figure 2. a) Schematic of the device **b)** Energy levels of the materials of the device c) Current density-voltage d) E.Q.E.-current density e) luminance-voltage f) electroluminescence spectra

Figure 2 shows the QLEDs performances with the polymer-QD hybrid active layer. The current density and luminance of Device 2 had a higher value than Device 1 for the overall voltage region, and the turn-on voltage of device 2 was slightly lower than in device 1. These enhancements originated from the smaller hole injection barrier of poly(TPDF-*b*-SSMe) towards the QDs compared to the one from poly(TPD-*b*-SSMe). As a result, maximum E.Q.E. of 3.37% and maximum luminous efficiency (LE_{max}) of 2.71 cd/A of Device 2 were obtained. The values were significantly higher than those of Device 1 ($E.Q.E_{max}$: 2.46%, LE_{max}: 2.00 cd/A). The maximum power efficiency of Device 2 (PE_{max}: 2.77 lm/W) was also increased compared with Device 1 (PE_{max}: 1.26 lm/W). Furthermore, both devices showed a narrow emission with λ_{max} = 637 nm, which derived from the emission of red QDs, and no parasitic emission was observed from organic layers.

Conclusions

In summary, we demonstrated the positive effect of band alignment of the hole transporting polymer on the hole injection into red QDs. Optimal conditions for an efficient hole injection from semiconducting polymers to QDs were found. Thus, highly efficient inverted QLEDs could be built by precisely adjusting the HOMO level of the hole conducting polymer to the valence band edge of red QDs. The HOMO levels were varied by introducing either electron donating methyloxy or electron withdrawing trifluoromethyl side groups. Through the hybridization of

QDs we fabricated uniformly distributed QD hybrid films with a low hole injection barrier. With the help of **BCP2**, the external quantum efficiency and luminance of hybrid QLEDs was enhanced. This approach offers the solution to overcome the poor electrical properties of colloidal QD films, and control the electrical properties of QDs for device applications.

Notes and references

‡ Authors contributed equally

Experimental:

Materials: Unless otherwise indicated, all chemicals and solvents were commercially available and used as received unless otherwise indicated. Pentafluorophenol was obtained from Fluorochem (UK). Anhydrous N,N'-Dimethyl formamide was obtained from Sigma Aldrich and stored over activated molecular sieves (4 Å).2,2'-Azobis(isobutyronitrile) (AIBN) was recrystallized from diethyl ether and stored at -18 °C. Anhydrous THF and dioxane were freshly distilled from sodium. Dithiobenzoic acid benzyl ester was synthesized as previously reported.[27] It was purified by column chromatography with chloroform as eluent. Pentaflourophenyl acrylate (PFPA)[26] and Vinyl-TPD monomer[21] were synthesized as described in the literature. The synthesis of TPDF monomer and CdSe@ZnS QDs are described in the supporting information.

Synthesis:

Synthesis of the block copolymers. As an example, the synthesis of BCP2 is explained. BCP1 was synthesized in the same way. 780 mg P2 (0.06 mmol, 1 eq), 590 mg PFPA (2.5 mmol, 40 eq) and 1 mg AIBN (0.006 mmol, 0.1 eq) were dissolved in 5 mL anhydrous dioxane in a Schlenk tube and equipped with a stirring bar. Oxygen was removed by four freeze-pump-thaw cycles and the flask was immersed into a hot oil bath (80 °C). After stirring for 48 hours, the polymer was precipitated in methanol. The precipitate was collected, redissolved in a few milliliters of anhydrous THF and precipitated in hexanes. This was repeated two more times. The polymer was dried in a 10 mbar vacuum at 40 °C for 12 hours. BCP2 was obtained as yellow powder, 880 mg (42%). GPC: M_n = 13,800 g/mol, M_w = 14,800, PDI: 1.09. ^{19}F NMR ($CDCl_3$, 376 MHz) δ [ppm] = -162.43 (br), -157.09 (br), -153.60 (br), -62.08 (br). FT-IR [cm^{-1}]. 2923, 1785 (-CO-O-), 1604, 1518 (Ar-F), 1493, 1320, 1113, 1068, 823. BCP1: GPC: M_n = 16,300 g/mol, M_w = 17,500, PDI: 1.07. ^{19}F NMR ($CDCl_3$, 376 MHz) δ [ppm] = -162.49 (br), -158.27 (br), -153.35 (br). FT-IR [cm^{-1}]. 2928, 1783 (-CO-O-), 1594, 1522 (Ar-F), 1489, 1238, 1002, 818.
Polymer analog reaction. 500 mg BCP2 (0.04 mmol, 1 eq) were dissolved in 5 mL anhydrous THF in nitrogen atmosphere. 246 mg 2-methyldisulfanyl-ethylamine (2 mmol, 60 eq) and 200 mg

triethylamine (2 mmol, 60 eq) were added. The resulting solution was stirred at 40 °C for 20 hours and then precipitated in methanol. After collecting by centrifugation, the polymer was precipitated three more times in methanol to give 450 mg poly(TPDF-b-SSMe) as a white powder. FT-IR [cm^{-1}]. 2922, 1598 (-CO-NH-), 1495, 1313, 1266, 1164, 1113, 1066, 818, 694. ^{19}F NMR: no signal. Poly(TPD-b-SSMe): FT-IR [cm^{-1}]. 2922, 1604 (-CO-NH-), 1489, 1238, 1036, 820, 694. ^{19}F NMR: no signal.

Preparation of QD-conducting polymer hybrids. QD-poly(TPD-b-SSMe) or QD-poly(TPDF-b-SSMe) hybrid solution was prepared by mixing 0.40 mL of QD dispersion (13 wt% in toluene) with 0.40 mL of conducting polymer solution (5 wt% in toluene). The mixture was immersed in a sonication bath for 20 minutes and then purified by precipitation/redispersion method. The hybrid was precipitated with excess ethanol and redispersed in toluene. After 10 cycles of the purification process the precipitates were redispersed in 1.7 mL of anhydrous toluene (40 mg/mL) and kept in a refrigerator.

Device fabrication and characterization. QD-conducting polymer hybrid devices were fabricated on patterned ITO glass substrates, cleaned with isopropanol, acetone, and methanol in an ultrasonic bath. Firstly, 20 mg/mL of the ZnO solution was spun on a patterned ITO substrate at 2000 rpm for 60 sec and baked in N_2 atmosphere at 90 ^oC for 30 min. The resulting film thickness was 45 nm. Then, 40 nm thick layers of QD-conducting polymer hybrid films were deposited by spin-casting at 3000 rpm for 30 sec. Finally, TCTA (60 nm), MoO_3 (10 nm), and Al (100 nm) were sequentially evaporated with a deposition rate of 0.5–1 Å sec^{-1}, 0.2 Å sec^{-1}, and 3–5 Å sec^{-1} respectively. The current–voltage–luminance characteristics were measured using a Keithley 236 source-measure unit and a Keithley 2000 multimeter coupled with a calibrated Si photodiode. Electroluminescence spectra of the QLEDs were obtained using a Konica-Minolta CS-1000A spectroradiometer.

References:

1. R. Karel Capek, I. Moreels, K. Lambert, D. De Muynck, Q. Zhao, A. Van Tomme, F. Vanhaecke and Z. Hens, *The Journal of Physical Chemistry C*, 2010, **114**, 6371-6376.
2. B. O. Dabbousi, J. Rodriguez-Viejo, F. V. Mikulec, J. R. Heine, H. Mattoussi, R. Ober, K. F. Jensen and M. G. Bawendi, *The Journal of Physical Chemistry B*, 1997, **101**, 9463-9475.
3. M. C. Troparevsky, L. Kronik and J. R. Chelikowsky, *The Journal of Chemical Physics*, 2003, **119**, 2284-2287.
4. D. J. Norris, A. Sacra, C. B. Murray and M. G. Bawendi, *Physical Review Letters*, 1994, **72**, 2612-2615.
5. H. Ma, G.-H. Ma, W.-J. Wang, X.-X. Gao and H.-L. Ma, *Chinese Physics B*, 2008, **17**, 1280.
6. W. K. Bae, K. Char, H. Hur and S. Lee, *Chemistry of Materials*, 2008, **20**, 531-539.
7. J. Lim, S. Jun, E. Jang, H. Baik, H. Kim and J. Cho, *Advanced Materials*, 2007, **19**, 1927-+.
8. M. Sessolo and H. J. Bolink, *Advanced Materials*, 2011, **23**, 1829-1845.
9. M. C. Schlamp, X. Peng and A. P. Alivisatos, *Journal of Applied Physics*, 1997, **82**, 5837-5842.
10. M. Achermann, M. A. Petruska, S. Kos, D. L. Smith, D. D. Koleske and V. I. Klimov, *Nature*, 2004, **429**, 642-646.
11. S. Coe, W. K. Woo, M. Bawendi and V. Bulovic, *Nature*, 2002, **420**, 800-803.

12. S. Dong Ick, Y. Chan Ho, K. Won Tae and K. Tae Whan, *Nanotechnology*, 2009, **20**, 365206.
13. B.-H. Kang, J.-S. Seo, S. Jeong, J. Lee, C.-S. Han, D.-E. Kim, K.-J. Kim, S.-H. Yeom, D.-H. Kwon, H.-R. Kim and S.-W. Kang, *Opt. Express*, 2010, **18**, 18303-18311.
14. V. L. Colvin, M. C. Schlamp and A. P. Alivisatos, *Nature*, 1994, **370**, 354-357.
15. I. H. Campbell and B. K. Crone, *Applied Physics Letters*, 2008, **92**, 043303-043303.
16. D. E. Fogg, L. H. Radzilowski, R. Blanski, R. R. Schrock and E. L. Thomas, *Macromolecules*, 1997, **30**, 417-426.
17. J. Xu, J. Wang, M. Mitchell, P. Mukherjee, M. Jeffries-El, J. W. Petrich and Z. Q. Lin, *Journal of the American Chemical Society*, 2007, **129**, 12828-12833.
18. M. Zorn, W. K. Bae, J. Kwak, H. Lee, C. Lee, R. Zentel and K. Char, *ACS Nano*, 2009, **3**, 1063-1068.
19. J. Kwak, W. K. Bae, M. Zorn, H. Woo, H. Yoon, J. Lim, S. W. Kang, S. Weber, H. J. Butt, R. Zentel, S. Lee, K. Char and C. Lee, *Advanced Materials*, 2009, **21**, 5022-+.
20. J. Kwak, W. K. Bae, D. Lee, I. Park, J. Lim, M. Park, H. Cho, H. Woo, D. Y. Yoon, K. Char, S. Lee and C. Lee, *Nano Letters*, 2012, **12**, 2362-2366.
21. W.-K. Bae, M. Zorn, J. Kwak, H. Woo, J. Lim, D. Lee, S. Lee, R. Zentel, K. Char and C. H. Lee, *submitted*, 2012.
22. M. Zorn, S. A. L. Weber, M. N. Tahir, W. Tremel, H. J. Butt, R. Berger and R. Zentel, *Nano Lett.*, 2010, **10**, 2812-2816.
23. M. Sommer, S. M. Lindner and M. Thelakkat, *Advanced Functional Materials*, 2007, **17**, 1493-1500.
24. S. Meuer, K. Fischer, I. Mey, A. Janshoff, M. Schmidt and R. Zentel, *Macromolecules*, 2008, **41**, 7946-7952.
25. P. S. Billone, L. Maretti, V. Maurel and J. C. Scaiano, *Journal of the American Chemical Society*, 2007, **129**, 14150-14151.
26. L. Zhao and Z. Lin, *Advanced Materials*, 2012, **24**, 4346-4346.
27. H. K. Oh, S. K. Kim, I. H. Cho, H. W. Lee and I. Lee, *Journal of the Chemical Society, Perkin Transactions 2*, 2000, 2306-2310.
28. M. D. Conner, V. Janout, I. Kudelka, P. Dedek, J. Zhu and S. L. Regen, *Langmuir*, 1993, **9**, 2389-2397.

4. Summary

In this dissertation, the synthesis of new block copolymers and the subsequent functionalization of inorganic nanostructures are presented. The hybrid systems were characterized thoroughly, and to some extent, applied in optoelectronic devices. The block copolymers consist of a longer semiconducting and solubility enhancing block, and a shorter anchor group block. Two different polymerization techniques were applied: polymers synthesized via RAFT polymerization were based on vinyltriphenylamine and vinyltriphenylamine dimers, Siegrist polycondensation was used to synthesize conjugated poly(*para*-phenylene vinylene) based block copolymers. In each case, the second block was grafted on using RAFT polymerization. Pentafluorophenyl acrylate active ester was used due to its high reactivity towards amines. The bifunctional anchor groups carried an aliphatic amine on one side and the anchoring functionality, like hydroxides or disulfides, on the other side. They were reacted with the block copolymers in a quantitative polymer analogue reaction.

Vinyltriphenylamine dimer based block copolymers with disulfide anchoring groups were used to functionalize CdSe tetrapods which had different arm lengths. Reference samples without anchor groups were prepared in order to investigate the influence of the disulfide groups on the morphology. The samples were spin-coated for TEM measurements. An effect of polymer loading (stepwise from 90% polymer content down to 50%) and different arm lengths (40 nm, 70 nm and 100 nm) was observed. Samples with short arm lengths and low polymer loading (50%) showed a good distribution and no aggregation of the tetrapods with anchor groups (hybrids) and without (blends). With increasing polymer content, the tetrapods in the blend samples tended to aggregate, however the tetrapods in the hybrid samples were still well dispersed. This effect is more drastic with increasing tetrapod arm length. The film quality at microscale was revealed by fluorescence optical microscopy. Large aggregates were found in the blend samples, whereas the hybrids showed uniform films.

Poly(*para*-phenylene vinylene) with pentyloxy side groups was found to gel in various organic solvents and form thin but long fibers. An active ester block was grafted to, followed by polymer analogue reaction with dopamine hydrochloride. The resulting polymer was attached to TiO_2 nanrods and the gelling behavior of the hybrid was studied. We found that the pure hybrid material did not show a special self-assembly. This was as expected, since the polymer chains are attached to the surface of the nanorods and hence cannot form a network. 10 wt% of pure poly(*para*-phenylene vinylene) was added to the hybrid, and incorporation of the nanorods into the polymer network was found. With increasing polymer content, interesting superstructures were found: like long strands, or micelles with encapsulated nanorods. A light-induced charge

transfer was demonstrated by photoluminescence quenching and by KPFM. We could show that the generated positive charge can travel along the polymer fiber for several hundred nanometers.

Another example of light-induced charge transfer was demonstrated in this work, using a novel donor-chromophore-acceptor nanocomposite. For that, poly(vinyltriphenylamine-*b*-pentafluorophenyl acrylate) was reacted with bifunctional ruthenium bisterpyridyl complexes. It carried an aliphatic amine on one side and a carboxyl group on the opposite side. This bisdirectioanlity was favorable for the attachment of the dye between the electron donating polymer and the electron accepting ZnO nanorods. The hybrids were characterized by TEM, and the nanorods were found to be well dispersed. Photoluminescence measurements were recorded and a complete quenching of the fluorescence of the ruthenium dye was found, which was a hint for a charge separation. KPFM measurements showed a positive charging of the polymer on the surface of the nanorods, which proves the efficient charge generation and separation at the interface of the donor-chromophore-acceptor hybrid.

Finally, the effect of the band gap alignment of the semiconducting polymer on the hole injection into CdSe/CdS/CdZnS core shell QDs is demonstrated. For that, two vinyltriphenylamine dimer based block copolymers with different HOMO levels, but similar LUMO levels were required. We expected to change the band gaps by varying the side groups. A polymer with methoxy side groups was synthesized (**BCP1**). To lower the HOMO level to better match with the QDs, trifluoromethyl groups were introduced (**BCP2**). Characterization with cyclovoltammetry revealed a lower HOMO level. To study the influence of the band gaps on the hole injection, QLEDs were built. For that, CdSe/CdS/CdZnS red QDs were hybridized via the grafting-to approach. This method creates stable films with QDs well dispersed within them. This was proved by the solubility change of the hybridized QDs, which were now soluble in toluene - a good solvent for the polymers. In contrast, pristine QDs precipitated in toluene. TEM images showed that the QDs were well dispersed within the matrix. Inverted structure QLEDs were fabricated, with ITO as a cathode, ZnO nanoparticles as electron conductors, the hybrid as the light emitting layer, TCTA as the hole injection layer and aluminum as an anode. The inverted structure allows the fabrication of highly luminescent and stable devices. Higher performances like external quantum efficiency and lower turn-on voltage were found with **BCP2**. By combining the inverted device structure with the grafting-to approach of semiconducting block copolymers, we showed the importance of a proper energy band alignment on the efficiency of the QLEDs.

In summary, this work presents the design, synthesis and characterization of advanced functional semiconducting polymers and the functionalization of various inorganic nanocrystals, and later, the application of the hybrid materials in optoelectronic devices. The huge impact of the polymer chemistry on the quality and performance of the material is demonstrated.

5. Supporting Information

Contents:

To 3.1: Annealing-Free Enhanced Morphology of Semiconducting Polymer-Inorganic Tetrapod Hybrids

1. Materials

Materials For the synthesis of CdSe tetrapods, cadmium oxide (CdO, 99.95%) was purchased from Alfa Aesar. Selenium (99.99 %, powder), n-trioctylphosphine (TOP, 90%), oleic acid (OA, 90%), 1-octadecene (ODE, 90%) and cetyltrimethylammonium bromide (CTAB, 99+%) were purchased from Sigma Aldrich. All chemicals were used as purchased.

2. Synthesis of tetrapods

Preparation of the injection solution

For the preparation of cadmium oleate ($Cd(OA)_2$) solution, CdO (10 mmol), OA (7.8 mL), ODE (6.2 mL), and TOP (1 mL) were placed in a 100 mL 3-neck round flask coupled with a condenser. The mixture was heated to 280 °C under N_2 flow for 20 min. After the mixture was optically clear, the round flask was cooled down to 50 °C and CTAB (0.14 mmol) was added in a N_2 flow. Separately, Se (12 mmol) and TOP (6 mL) were mixed in a 50 mL 2-neck round flask with a condenser and heated to 200 °C until the mixture became transparent. After it was cooled down to room temperature, the TOPSe (5 mL) solution was added to the $Cd(OA)_2$ solution and the mixture was stirred for 5 min.

CdSe seeds with zincblende crystal structure.

A modified synthetic procedure[1] was employed to prepare CdSe seeds with zincblende crystal structure. Firstly, $Cd(OA)_2$ solution (0.5 mmol mL^{-1}) was prepared by reacting CdO (5 mmol), OA (5 mL), and ODE (5 mL) with the same reaction conditions as described above. Next, Se (1 mmol) and ODE (10 mL) were loaded into a 100 mL 3-neck round flask and heated up to 300 °C in a N_2 flow. When the Se/ODE solution became optically clear, the $Cd(OA)_2$ solution(4 mL, 2 mmol) was rapidly injected into the solution and reacted at 270 °C for 15 min. Finally, ODE (6 mL) was added into the seed solution and cooled down to room temperature.

Synthetic procedure for CdSe tetrapods in terms of CPI approach.

For the 40 nm-long CdSe tetrapods, seed solution (5 ml), OA (2.25 mL), TOP (1.5 mL), 1-ODE (21.25 mL), and CTAB (0.21 mmol) were placed in a 3-neck round flask equipped with a condenser and heated up to 260 °C. When the temperature reached 260 °C, the injection solution (28 mL) was added into the seed solution with an injection rate of 0.5 mL/min. After 40 min reaction, the temperature was raised to 280 °C and the mixture was allowed to react for 16 min. For the 80 nm-long CdSe tetrapods, the seed solution (2.5 mL), OA (2.25 mL), TOP (1.5 mL), 1-

ODE (23.75 mL), and CTAB (0.21 mmol) were placed in a 3-neck round flask, then heated up to 280 °C. The injection solution (30 mL) was then added to the reactor successively: 0.5 mL min^{-1} for 6 min, 0.6 mL min^{-1} for 6.67 min, 0.7 mL min^{-1} for 8.57 min (in this step, the temperature was raised to 280 °C) and 0.8 mL min^{-1} for 8.75 min. In the case of 103 nm-long CdSe tetrapods, the seed solution (1.67 mL), OA (2.25 mL), TOP (1.5 mL), 1-ODE (24.58 mL), and CTAB (0.21 mmol) were loaded in a 3-neck round flask, then heated to 260 °C. The injection solution (40 mL) was added into the seed solution successively: 0.4 mL min^{-1} for 5 min, 0.5 mL min^{-1} for 12 min, 0.6 mL min^{-1} for 6.67 min, 0.7 mL min^{-1} for 5.71 min and 0.8 mL min^{-1} for 30 min (in this step, the temperature was raised to 280 °C). In order to purify the product, chloroform (2 mL) and an excess amount of acetone were added into the resulting solution until it became turbid. The tetrapods were precipitated by centrifugation at 3,000 rpm. After centrifugation, the supernatant was decanted and the precipitate was re-dispersed in an organic solvent such as chloroform, toluene or hexane. The precipitation and re-dispersion were repeated until the samples were sufficiently purified.

[1] L. Liu, Z. Zhuang, T. Xie, Y.-G. Wang, J. Li, Q. Peng, Y. Li, *J. Am. Chem. Soc.* **2009**, *131*, 16423.

To 3.2 Photoinduced Charge Separation of Self-Organized Semiconducting Superstructures Composed of a Functional Polymer-TiO2 Hybrid:

1. Chemicals

Unless otherwise mentioned, all chemical reagents were used as purchased without any further purification. Anhydrous THF was freshly distilled from sodium and dichloromethane from phosphorous pentoxide. DMF was freshly distilled from calcium hydride and not exposed to light until it was used.

2. Synthesis of *N*-[[2,5-bis(pentyloxy)-4-methylphenyl]methylene]

2.1. Synthesis of 2-Methyl-1,4-bis-pentyloxy-benzene.

Methylhydroquinone (2.42 g, 19.7 mmol, 1 eq) was dissolved in anhydrous DMF (30 mL) in a N_2 atmosphere. Potassium carbonate (10.89 g, 79.4 mmol, 4 eq) was dried in a vacuum and added to the solution. The resulting slurry was stirred at 60 °C for 20 minutes. 1-Bromopentane (8.82 g, 58.8 mmol, 3 eq) was added and the mixture was stirred at 80 °C for 12 h. It was then filtrated and washed with chloroform (100 mL) and THF (100 mL). The filtrate was concentrated in vacuum at 45 °C and the dark brown residue was dissolved in hexanes:dichloromethane 3:1 and purified by column chromatography (hexanes:dichloromethane 3:1, silica, $R_f = 0.5$). The product was obtained as colorless, slightly yellow oil (3.57 g, 13.5 mmol, 69%) and kept at -18 °C, where it crystallized in colorless needles.

^{1}H NMR ($CDCl_3$, 300 MHz) δ [ppm] = 0.89-0.94 (m, 6H), 1.32-1.49 (m, 8H), 1.71-1.82 (m, 4H), 2.20 (s, 3H), 3.88 (dt, 4H, J=1.7Hz, J=6.5Hz), 6.62-6.73 (m, 3H). FT-IR [cm^{-1}] 2958 cm^{-1}, 2926 cm^{-1}, 2859 cm^{-1}, 1502 cm^{-1}, 1466 cm^{-1}, 1215 cm^{-1}, 1040 cm^{-1}; 789 cm^{-1}.

2.2. Synthesis of 4-Methyl-2,5-bis-pentyloxy-benzaldehyde by Rieche-Groß-Formylation.

2-Methyl-1,4-bis-pentyloxy-benzene (3.56 g, 13.47 mmol, 1 eq) was dissolved in 10 mL dry dichloromethane in a N_2 atmosphere and cooled to 0 °C. $SnCl_4$ (5.26 g, 20.21 mmol, 1.5 eq), dissolved in a few mL dry dichloromethane, was added slowly. The solution was stirred for 30 minutes before the dichloromethyl methylether (2.32 g, 20.21 mmol, 1.5 eq) was added. While adding, the temperature was kept below 10 °C. It was then stirred for 30 minutes at r.t. and the conversion of the reaction was checked by TLC. After 30 minutes the reaction was finished and quenched by pouring it on 60 g ice. The product was washed with saturated sodium bicarbonate and water and extracted with chloroform. The organic solvent was removed and the brown crude product was recrystallized three times from hexanes (each time 20 mL). For that, it was dissolved at 50 °C and crystallized when cooled to 0 °C. The pure product was obtained as colorless needles (1.55 g, 5.30 mmol, 40%).

^{1}H NMR ($CDCl_3$, 300 MHz) δ [ppm] = 0.88-0.93 (m, 6H), 1.31-1.46 (m, 8H), 1.71-1.84 (m, 4H), 2.25 (s, 3H), 3.92 (t, 2H, J=6.5 Hz), 3.99 (t, 2H, J=6.4 Hz), 6.77 (s, 1H), 7.20 (s, 1H), 10.40 (s, 1H). FT-IR [cm^{-1}] 2958 cm^{-1}, 2927 cm^{-1}, 2860 cm^{-1}, 1679 cm^{-1}, 1611 cm^{-1}, 1499 cm^{-1}, 1461 cm^{-1}, 1412 cm^{-1}, 1208 cm^{-1}; 1033 cm^{-1}.

2.3. Synthesis of N-[[2,5-bis(pentyloxy)-4-methylphenyl]methylene]

4-Methyl-2,5-bis-pentyloxy-benzaldehyde (2.14 g, 7.32 mmol, 1 eq), was dissolved in freshly distilled aniline (4.09 g, 43.93 mmol, 6 eq) and heated to 60 °C. A vacuum of 15 mbar was applied from time to time in order to remove the generated water. After the reaction has finished (no more water is generated, 2 h), a high vacuum was applied until the excess aniline was removed. The pure product was obtained as yellow oil (2.69 g, 7.32 mmol, 100%).
^{1}H NMR ($CDCl_3$, 300 MHz) δ [ppm] = 0.89-0.94 (m, 6H), 1.39-1.50 (m, 8H), 1.75-1.82 (m, 4H), 2.27 (s, 3H), 3.92 (t, 4H, J=5.36 Hz), 6.81 (s, 1H), 7.20 (m, 3H), 7.38 (m, 2H), 7.57 (s, 1H), 8.86 (s, 1H). FT-IR [cm^{-1}] 2958 cm^{-1}, 2926 cm^{-1}, 2872 cm^{-1}, 2859 cm^{-1}, 1620 cm^{-1}, 1598 cm^{-1}, 1588 cm^{-1}, 1414 cm^{-1}, 1202 cm^{-1}; 1034 cm^{-1}, 693 cm^{-1}.

3. Microscope images

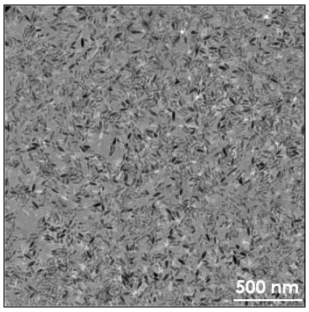

Figure S 1. TEM picture of **P3@TiO_2** (10 mg/mL drop cast from *o*-DCB).

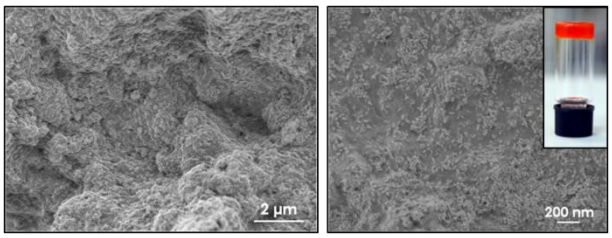

Figure S 2. SEM pictures of **P3@TiO_2** mixed with 50 wt% **P1**, drop cast from *o*-DCB, 30 mg/mL and picture of the gel

4. Spectra

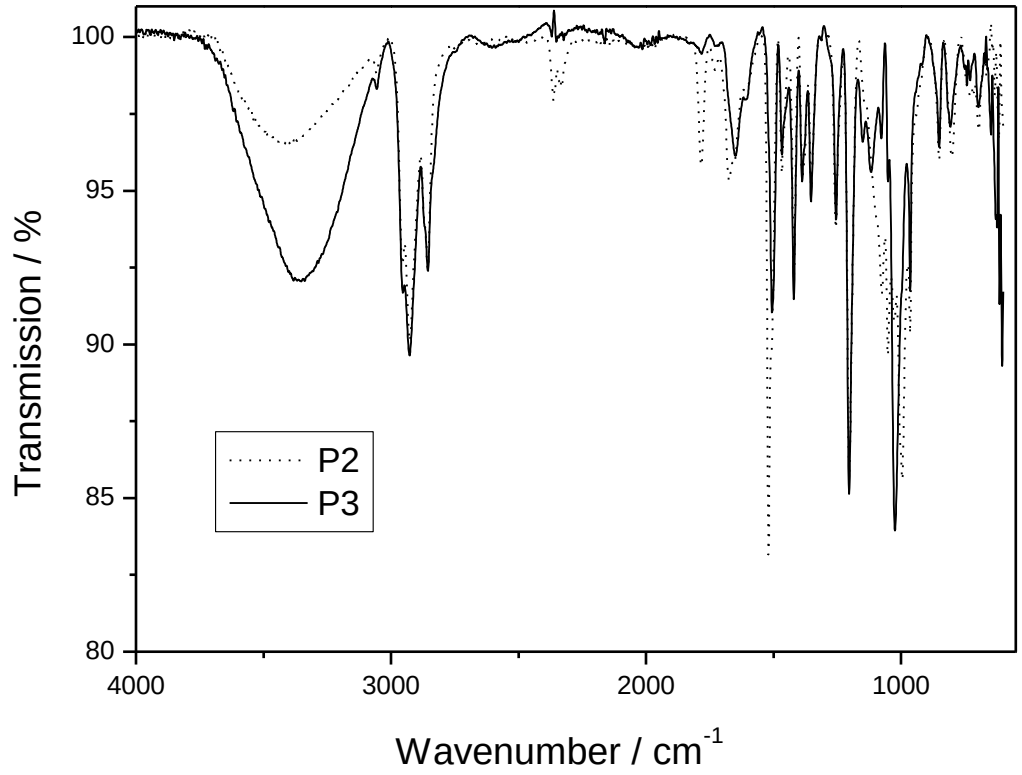

Figure S 3. FT-IR spectrum of the post-polymerization reaction of P2 with dopamine

5. KPFM of P1

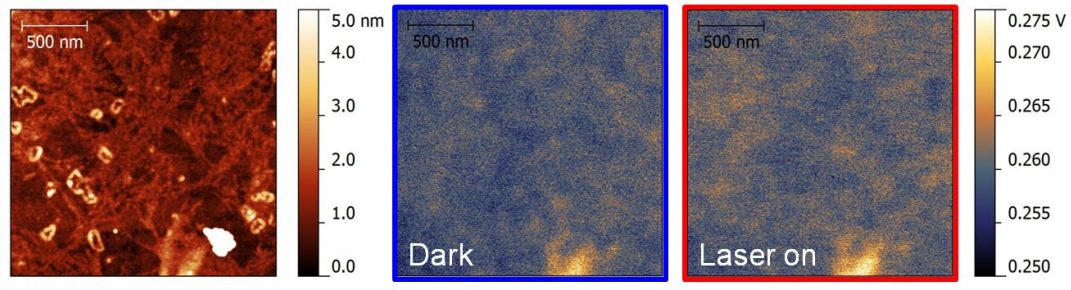

Figure S 4. Kelvin probe force microscopy images of pure **P1**. Left: Topography, middle: KPFM in dark and right: KPFM under illumination (λ=488 nm). No change in the surface potential is observable.

To 3.3: Light-Induced Charge Separation in a Donor-Chromophore-Acceptor Nanocomposite Poly[TPA-Ru(tpy)$_2$]@ZnO

1. FT-IR of [(H_2N-CH_2-CONH-tpy)Ru(tpy-CONH-CH_2-COOH)](PF_6)$_2$ (A)

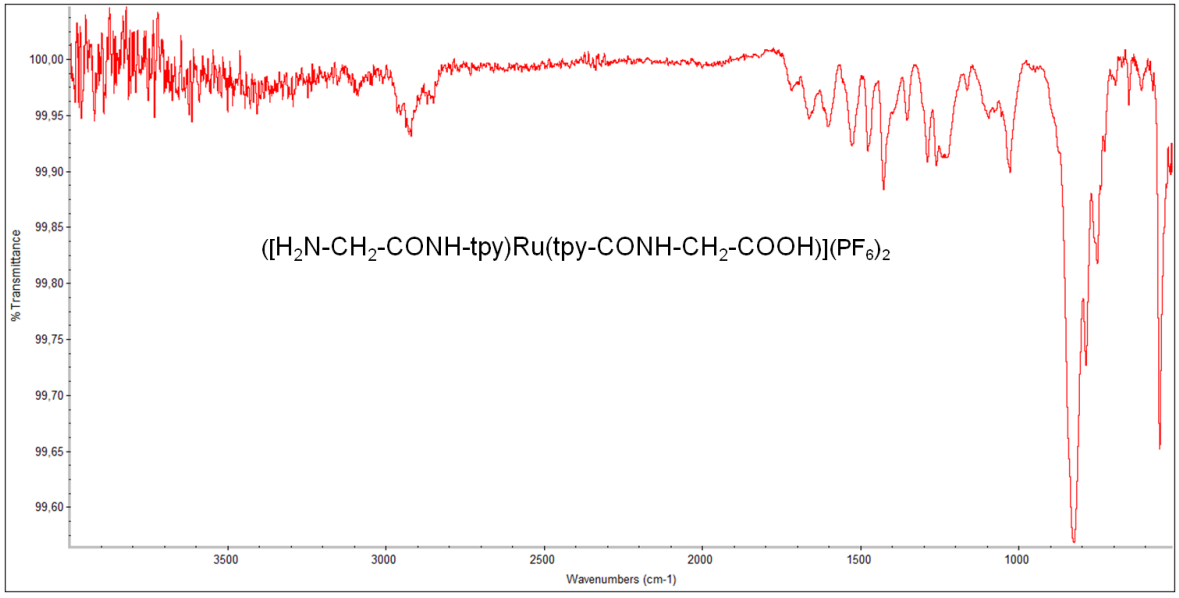

Figure S 1.FT-IR spectrum of **A** (ATR-mode).

2. ^{1}NMR designation of A

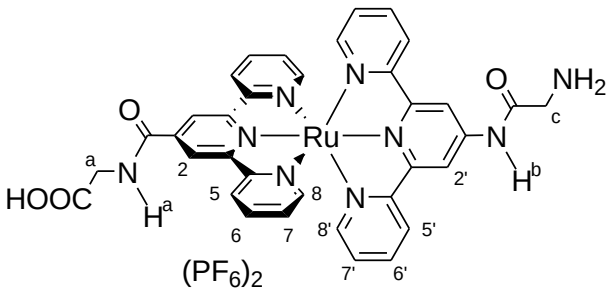

^{1}H NMR: δ_H (600 MHz; CD_3CN; Me_4Si) 9.09 (s, 2H, H^2), 9.05 (s, 2H, $H^{2'}$), 8.59 (s, 1H, NH^b), 8.59 (m, 2H, H^5), 8.41 (m, 2H, $H^{5'}$), 8.16 (m, 1H, NH^a), 7.95 (m, 2H, H^6), 7.93 (m, 2H, $H^{6'}$), 7.44 (m, 2H, H^8), 7.31 (m, 2H, $H^{8'}$), 7.21 (m, 2H, H^7), 7.12 (m, 2H, $H^{7'}$), 4.32-4.30 (m, 2H, CH_2^a), 4.32-4.30 (m, 2H CH_2^b), NH_2 not observed probably due to protonation.

3. ^{19}F NMR of P2 and P3a

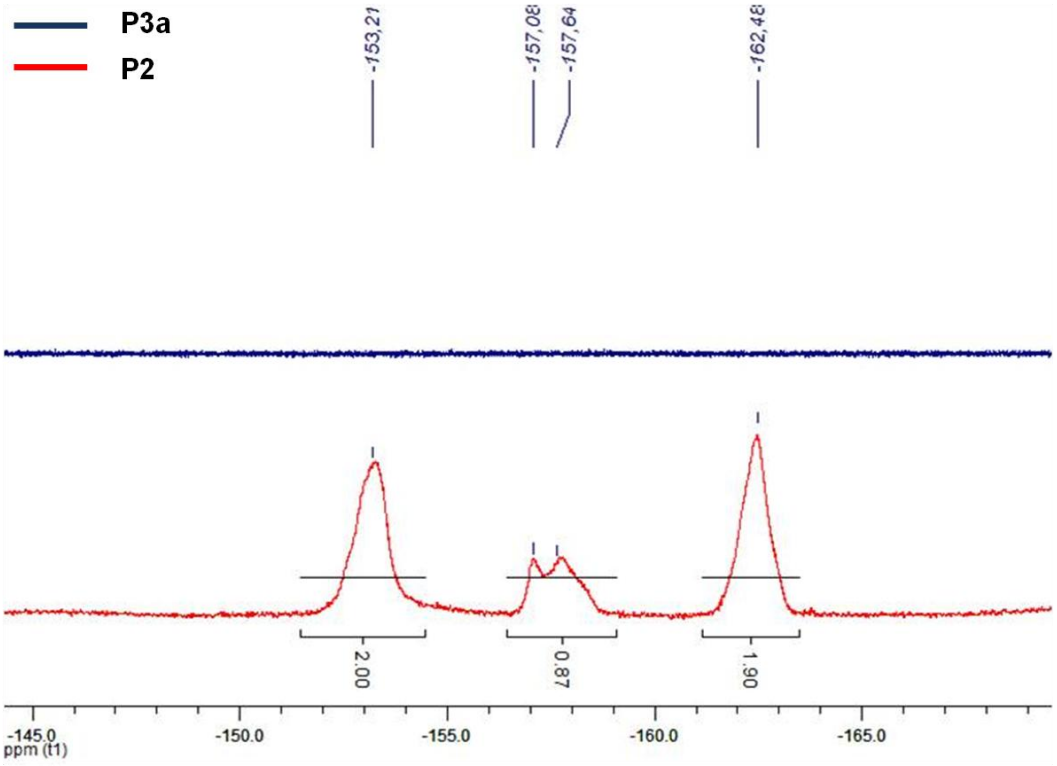

Figure S 2. ^{19}F NMR of **P2** (red) and **P3a** (blue) in $CDCl_3$.

4. FT-IR of A, P2 and P3a

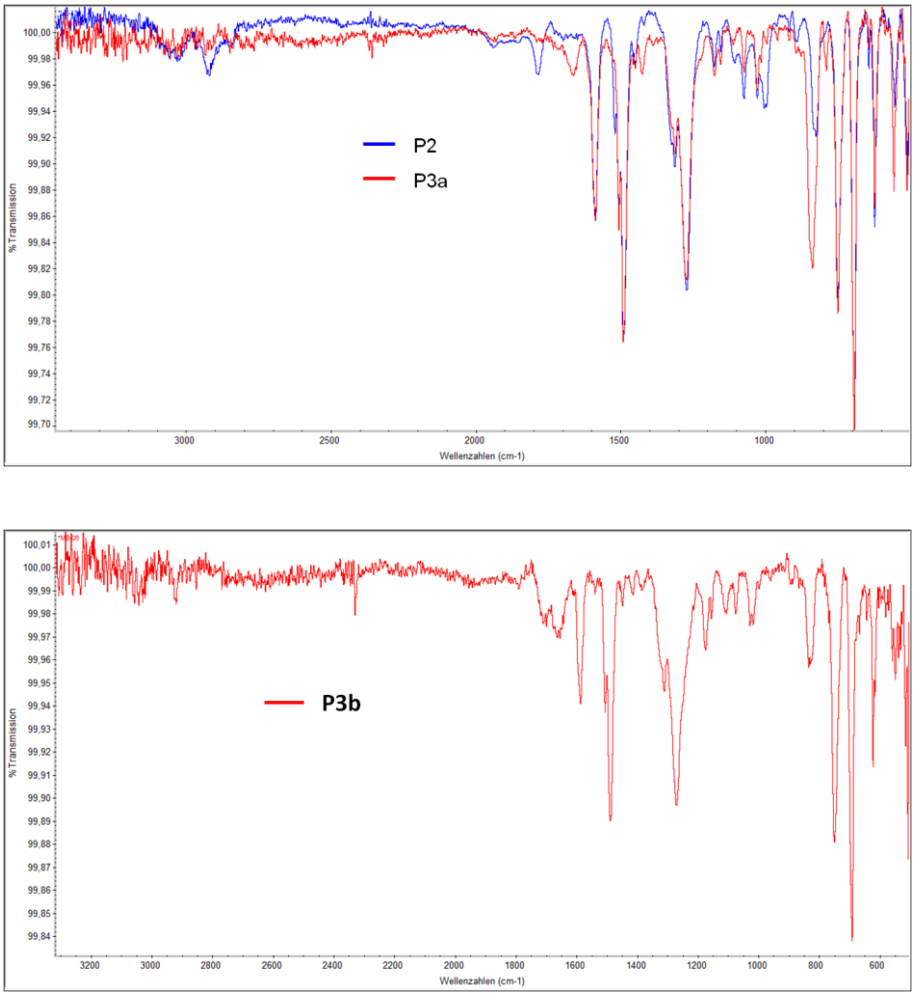

Figure S 3. FT-IR of **P2** and **P3a** (top) and **P3b** (bottom), all in ATR mode.

5. TEM images

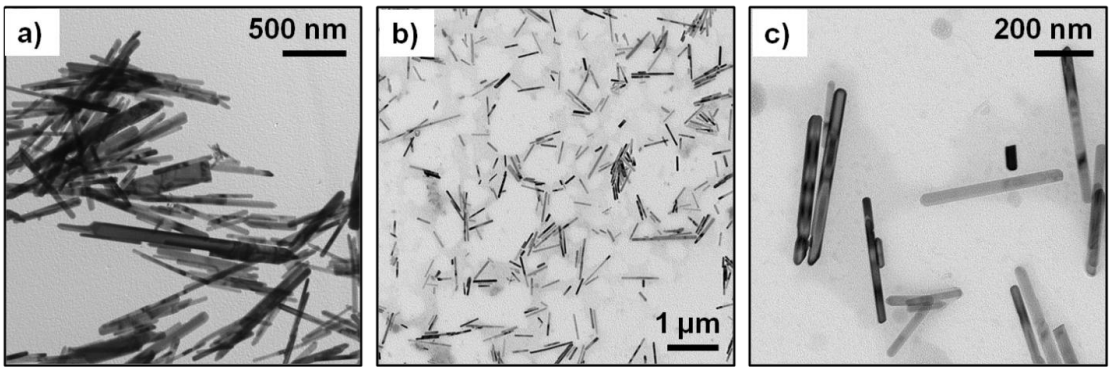

Figure S 4. TEM images of **a)** pristine ZnO. **b)** and **c)** P3a@ZnO, drop cast from THF.

6. Topography image of P3a@ZnO

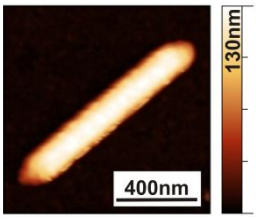

Figure S 5. Topography image of the KPFM measurement on **P3a@ZnO**.

7. UV-Vis spectrum of P3b in THF

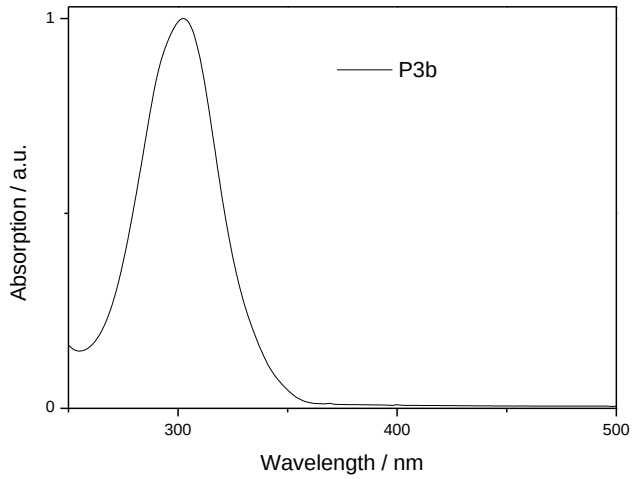

Figure S6. Absorption spectrum of **P3b** in THF.

8. KPFM images of P3b@ZnO

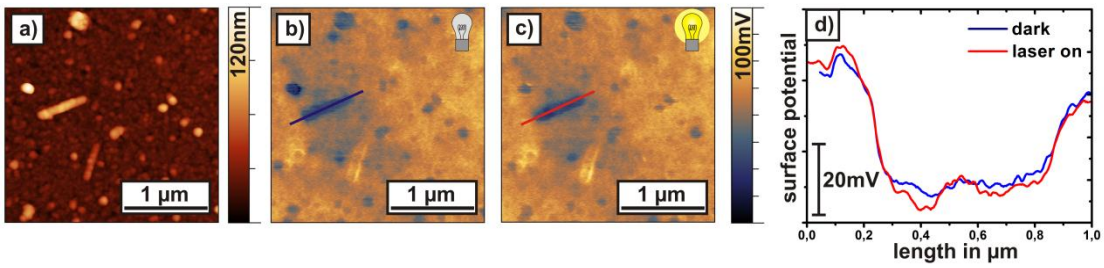

Figure S 6. KPFM measurements performed on **P3b@ZnO**: **a)** Topography **b)** Surface potential map recorded in darkness. **c)** Surface potential map recorded under laser illumination of a wavelength of 488 nm. **d)** Line profile of the surface potential across the particle indicated by the line in the respective surface potential map. No photo-response can be observed for this D-A system.

To 3.4: Effect of Band Gap Alignment on the Hole Transport from Semiconducting Block Copolymers to Quantum Dots

1. Chemicals and Instrumentation

Chemicals.

Unless mentioned otherwise, all chemicals were used as purchased. Methanol was dried over Mg and distilled afterwards. Toluene was distilled from calcium hydride. DMF was freshly distilled from calcium hydride and not exposed to light. THF was freshly distilled from sodium. CdO (99.9 %), zinc oxide (ZnO, ≥99.0%), oleic acid (OA, 90%), myristic acid (My, 99%), 1-octadecene (1-ODE, 90%), n-trioctylphosphine (TOP, 90%), 1-dodecanethiol (DDT, 97%), zinc acetate dehydrate ($Zn(Ac)_2 \cdot 2H_2O$, > 98%), were purchased from Sigma-Aldrich. Potassium hydroxide (KOH, GR reagent) was obtained from Duksan Phrmaceutical Co. Ltd.

Instrumentation.

All ^{1}H and ^{13}C NMR spectra were recorded on a Bruker 300 MHz FT NMR spectrometer. All ^{19}F NMR spectra were recorded on a Bruker 400 MHz FT NMR spectrometer. Chemical shifts (δ) are given in parts per million relative to TMS. Samples were prepared in deuterated solvents and their signals referenced to residual nondeuterated solvent signals. The polymers' molecular weight was determined by gel permeation chromatography (GPC) in tetrahydrofuran (THF) as solvent and with the following parts: pump PU 1580, auto sampler AS1555, UV detector UV 1575 (detection at 254 nm), RI detector RI 1530 from JASCO. Columns were used from MZ-Analysentechnik: MZ-Gel SDplus 10.2 Å and MZ-Gel SDplus 10.6 Å. Calibration was done using polystyrene standards purchased from Polymer Standard Services. IR spectra were recorded on Perkin-Elmer 100 FTIR spectrometer using an ATR unit. UV-Vis spectra were recorded using a Jasco V-630 spectrophotometer (1 cm x 1 cm quartz cell). Emission spectra were recorded on a Varian Cary Eclipse. TEM pictures were taken on a Philips EM-420: 120kV with CCD-Camera. Cyclovoltammetric measurements were taken with a PGSTAT30 from Autolab (Metrohm) in o-dichlorobenzene with tetrabutyl ammonium tetrafluoroboride as conductive salt. Ag/AgCl with saturated LiCl in ethanol was used as reference electrode, graphit as counter electrode and platin as working electrode. The scan rate was 0.01 V/s and the step potential 0.00244 V.

2. Synthesis of 2-methyldisulfanyl-ethylamine

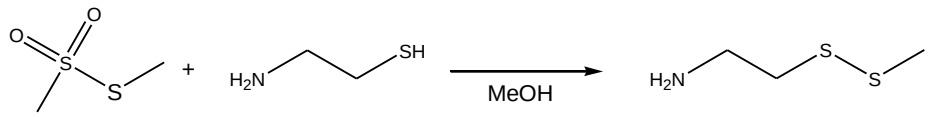

Scheme S 1. Synthesis of 2-methyldisulfanyl-ethylamine

2-Methyldisulfanyl-ethylamine was synthesized in a slightly different way than according to literature.[28] 5.00 g cysteamine hydrochloride (44.0 mmol, 1 eq) were dissolved in 30 mL of dry methanol in a nitrogen atmosphere and cooled to 0 °C while stirring. 4.63 g methyl methanethiosulfonate (36.7 mmol, 1.2 eq) was dissolved in 20 mL of dry methanol was added dropwise. The solution was stirred for 16 h at room temperature. The solvent was removed in vacuum and the residual oil was dissolved in 5 mL of dry dichloromethane. It was then washed three times with 5 N sodium bicarbonate and one time with water. After drying with magnesium sulfate and evaporating the solvent, 2.56 g (20.8 mmol, 47%) of the product were obtained as slightly yellow oil.

^{1}H NMR: ($CDCl_3$, 300 MHz) δ [ppm] = 1.30 (s, 2 H, -NH_2), 2.34 (s, 3 H, -CH_3), 2.71 (t, 2 H, -S-CH_2- J^1 = 6.3 Hz, J^2 = 6.07 Hz), 2.95 (t, 2 H, H_2N-CH_2-, J^1 = 6.2 Hz, J^2 = 6.1 Hz).

2.1. Synthesis of N,N'-Bis(4-trifluoromethyl phenyl)-N,N'-bisphenyl-1,1'-bisphenyl-4,4'-diamine (TPDF) via Buchwald-Hartwig coupling

2.18 g tris(dibenzylideneaceton)dipalladium(0) (2.38 mmol, 0.04 eq) and 3.10 g 1,1‘-bis-(diphenylphosphino)ferrocene (5.60 mmol, 0.08 eq) were dissolved in 50 mL of anhydrous toluene in a nitrogen atmosphere. Oxygen was removed with two freeze-pump-thaw cycles. 29.43 g 4-bromobenzotrifluorid (130.78 mmol, 2.2 eq), 20 g N,N’-diphenylbenzidine (59.44 mmol, 1 eq) and 17.14 g sodium tert-butoxid (178.32 mmol, 3 eq) were dispersed in 250 mL of dry toluene. The mixture was degassed with one freeze-thaw-pump cycle. The catalyst solution was added via a canula and the resulting mixture was degassed again The flask was immersed in a hot oil bath (90 °C) and stirred over night. 250 mL of methanol were added to quench the reaction and the crude product was extracted with water/diethyl ether. After evaporation of the solvent, the product was purified via column chromatography (silica gel, hexanes:ethyl acetate 10:1, R_f = 0.5). 24.63 g (39.4 mmol, 66%) TPDF were obtained as a light yellow powder.

^{1}H NMR ($CDCl_3$, 300 MHz) δ [ppm] = 7.09-7.17 (m, 14 H), 7.29-7.34 (m, 4 H), 7.41-7.50 (m, 8 H).

^{13}C NMR (CDCl3, 75 MHz) δ [ppm] = 121.42, 122.7, 122.89, 123.33, 124.43, 125.38, 125.62, 126.36, 127.79, 129.69, 135.96, 146.00, 146.73, 150.75.

FD-MS [m/z] calcd. for $C_{38}H_{26}F_6N_2$ 624.20; found 623.37 (100.00%), 624.36 (48.05%), 625.35 (8.57%), 626.34 (1.25%).

2.2. Synthesis of N,N'-2-bis(4-trifluoromethyl phenyl)-N-phenyl-N'-4-formylphenyl(1,12-biphenyl)-4,4-diamine (aldehyde-TPDF)

24.63 g TPDF (39.4 mmol, 1 eq) were dissolved in 110 mL of anhydrous DMF in a nitrogen atmosphere in a Schlenk tube and cooled down to 0 °C in an ice bath. 15.10 g phosphoroxychlorid (98.5 mmol, 2.5 eq) were added dropwise over 20 minutes. The solution was stirred for 20 more minutes at 0 °C and then immersed into a warm oil bath (50 °C). The oil bath was then heated up to 80 °C and the reaction was stirred over night. It was then poured into a 1.2 N sodium acetate solution (1000 mL) and stirred for 30 minutes. The crude product was collected by filtration, washed with water and dried at high vacuum. It was then purified by column chromatography (silica gel, hexanes:dichloromethane 1:1, $R_f = 0.4$). The starting material (9.00 g, 14.4 mmol, 37%) could be recovered as well for repeating the reaction ($R_f = 0.7$). 10.00 g aldehyde-TPDF (15.3 mmol, 39%) were obtained as yellow powder.

^{1}H NMR ($CDCl_3$, 300 MHz) δ [ppm] = 7.09-7.34 (m, 15 H), 7.42-7.57 (m, 8 H), 7.75 (d, 2 H, J = 8.8 Hz), 9.86 (s, 1H, -CHO).

^{13}C NMR ($CDCl_3$, 75 MHz) δ [ppm] = 121.59, 122.32, 122.65, 123.01, 123.44, 124.34, 124.53, 125.23, 125.67, 126.35, 126.77, 127.91, 128.22, 129.72, 130.70, 131.40, 135.43, 137.74, 144.77, 146.36, 146.66, 149.46, 150.68, 152.36, 190.48.

FD MS [m/z] calcd. for $C_{39}H_{26}F_6N_2O$ 652.19; found 651.25 (100.00%), 652.25 (45.64%), 653.25 (8.31%).

2.3. Synthesis of N,N'-2-bis(4-trifluoromethyl phenyl)-N-phenyl-N'-4-vinylphenyl(1,12-biphenyl)-4,4-diamine (vinyl-TPDF)

23.38 g Methyltriphosphonium bromide (62.1 mmol, 3 eq) and 7.34 g potassium tert-butoxide (62.1 mmol, 3 eq) were dissolved in 400 mL anhydrous THF in a nitrogen atmosphere, cooled to 0 °C and allowed to react for 90 minutes. 13.15 g Aldehyde-TPDF (20.7 mmol, 1 eq) were dissolved in 87 mL anhydrous THF in a nitrogen atmosphere and added quickly dropwise to the yellow suspension. The reaction mixture was stirred for 16 hours at room temperature. It was then cooled to 0 °C again and 220 mL 10% HCl were added carefully. The product was extracted with chloroform/saturated sodium hyrogencarbonate and finally washed with water. The combined organic phases were dried with magnesium sulfate and the solvent was removed under reduced pressure. By column chromatography (silica gel, hexanes:dichloromethane 1:1, $R_f = 0.8$), 11.51 g vinyl-TPDF (17.7 mmol, 85%) were obtained as a white powder.

^{1}H NMR ($CDCl_3$, 300 MHz) δ [ppm] = 5.21 (d, 1 H, Htrans, J = 11.7 Hz), 5.68 (d, 1 H, Hcis, J = 18.4 Hz), 6.68 (dd, 1 H, 4J = 17.6 Hz H*trans*, 10.9 Hz H*cis*), 7.08-7.17 (m, 12 H), 7.28-7.36 (m, 4 H), 7.41-7.50 (m, 7 H).

^{13}C NMR ($CDCl_3$, 75 MHz) δ [ppm] = 113.26, 121.42, 122.90, 123.15, 123.34, 123.58, 124.43, 125.20, 125.36, 125.45, 125.61, 126.37, 127.45, 127.79, 129.69, 133.63, 136.00, 145.80, 146.03, 146.26, 146.73, 150.52, 150.75.

FD-MS [m/z] calcd. for $C_{40}H_{28}F_6N_2$ 650.22; found 649.34 (100.00%), 650.32 (37.58%), 651.34 (8.35%).

Anal. calcd. for $C_{38}H_{26}F_6N_2$ [%] C 73.84, H 4.34, N 4.31; found C 73.75, H 4.45, N 4.04.

3. RAFT polymerizations

4.00 g Vinyl-TPDF (6.2 mmol, 120 eq), 12.5 mg dithiobenzoic acid benzyl ester (0.05 mmol, 1 eq) and 0.8 mg 2,2'-azobis(2-methylpropionitrile) (AIBN) (0.005 mmol, 0.1 eq) were dissolved in 7 mL of anhydrous dioxane in a Schlenk tube and equipped with a stirring bar. Oxygen was removed with four freeze-pump-thaw cycles and the flask was immersed into a hot oil bath (80 °C). After stirring for 48 hours, the polymer was precipitated in methanol. The precipitate was collected, redissolved in a few milliliters of anhydrous THF and precipitated in methanol again. This was repeated two more times. The polymer was dried in a 10 mbar vacuum at 40 °C for 12 hours. P2 was obtained as yellow powder, 1.68 g (42%).

GPC: M_n = 12,600 g/mol, M_w = 13,900, PDI: 1.10. ^{1}H NMR ($CDCl_3$, 300 MHz) δ [ppm] = 1.72-2.31 (br, 3H), 6.62 (br, 2H), 6.94 (br, 11H), 7.16 (br, 6H), 7.29 (br, 3H). ^{19}F NMR ($CDCl_3$, 376 MHz)δ [ppm] = -62.08 (br).

RAFT-polymerization of **P1**. The polymerization was carried out under the same conditions as for vinyl-TPDF. P1: GPC: M_n = 15,000 g/mol, M_w = 15,800, PDI: 1.05.

4. Cyclovoltammetry

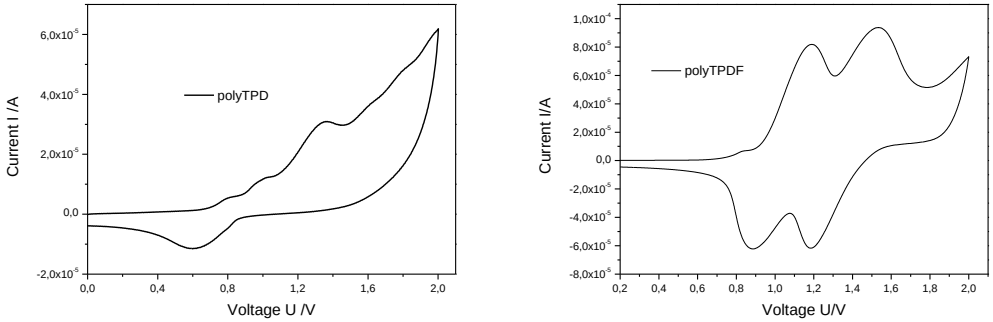

Figure S 1. Cyclovoltammetry of polyTPD (left) and polyTPDF (right) in *o*-dichlorobenzene.

5. GPC

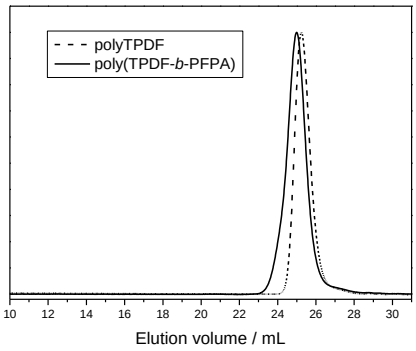

Figure S 2. GPC trace of PTPDF and poly (TPDF-*b*-PFPA)

6. Synthesis of CdSe/CdS/CdZnS/CdZnS red QDs

Prior to the synthesis of QDs, zinc oleate ($Zn(OA)_2$), cadmium oleate ($Cd(OA)_2$), TOPSe, and TOPS were prepared as shell-forming precursors. For the $Cd(OA)_2$, 5 mmol of CdO, 5 mL of OA, and 5 mL of 1-ODE were loaded in a 50 mL 3-neck flask with a condenser and heated to 280 oC under N_2 flow. In a case of the $Zn(OA)_2$, 10 mmol of ZnO, 10 mL of OA, and 10 mL of 1-ODE were placed in 50 mL 3-neck flask with a condenser and heated to 300 °C under N_2 flow. In both cases, the color of the mixtures gradually changed from turbid brown (Cd solution) or cloudy (Zn solution) to optically-clear, which means that the cadmium oleate or zinc oleate has formed. At the end of reaction, the solutions were cooled down and kept at 50 oC for $Cd(OA)_2$ and 100 oC for $Zn(OA)_2$. In the meantime, for the TOPSe and TOPS, 1 mmol of elemental selenium was dissolved in 0.5 mL of TOP (TOPSe) and 8 mmol of elemental sulfur was dissolved in 4 mL of TOP (TOPS), in a N_2 atmosphere.

Red-emitting CdSe/CdS/CdZnS QDs were prepared by a one-pot multi-step procedure. For the CdSe core, 1 mmol of CdO, 3 mmol of My and 15 mL of 1-ODE were placed in 100 mL 3-neck flask and heated to 270 oC under N_2 flow. Once the mixture became optically clear, 0.25 mL of TOPSe was rapidly injected into the flask. After 3 min of reaction, 1.5 mmol of DDT and 2 mL of $Zn(OA)_2$ were added dropwise to the flask and the reaction temperature was increased to 300 °C. Over 30 min of reaction, the first CdS shell was overgrown on the core and $Zn(OA)_2$ monolayer was absorbed on the surface of CdS shell, which helps the subsequent growth of a CdZnS shell. At the end of reaction, 4 mL of $Zn(OA)_2$ and 1.5 mL of TOPS were added to the flask and 2 mL of $Cd(OA)_2$ was injected dropwise into the flask for 1 min. Throughout the following reaction for 9 min, a CdZnS shell was grown on previous CdSe/CdS QDs. Finally, an additional CdZnS shell was introduced by adding 6 mL of $Zn(OA)_2$, 2 mL of TOPS, and dropping 3 mL of $Cd(OA)_2$ for

1 min. After 5 min of reaction, the flask was quickly quenched to room temperature. The as-synthesized QDs were purified by precipitating with ethanol and re-dispersing in toluene repeatedly (5 times). The final products were dispersed in toluene and kept in the refrigerator.

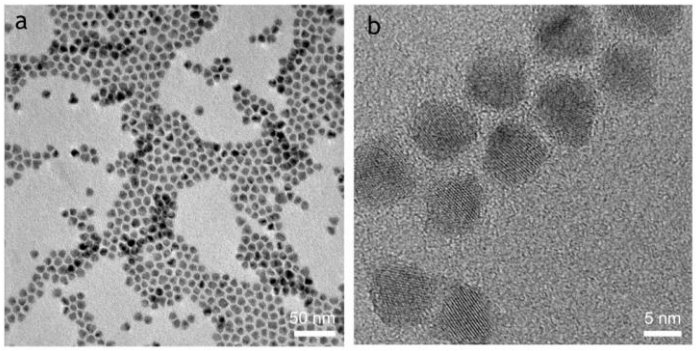

Figure S 3. (a) A low magnification and **(b)** a high-resolution transmission electron microscopy images of red QDs (average diameter: 8.2 nm).

7. Synthesis of ZnO nanoparticles

ZnO nanoparticles were synthesized modifying the method reported by Pacholski et al.[1] Firstly, 3 g of $Zn(ac)_2 \cdot 2H_2O$ and 120 mL of methanol were placed in 3-neck round bottom flask and heated to 60 °C. At that temperature, 60 mL KOH solution containing 1.51 g of KOH was added dropwise into the $Zn(ac)_2 \cdot 2H_2O$ solution with strong agitation. The reaction mixture was kept at 60 °C for 2 hr 15 min. At the end of reaction, the product appeared as a milky solution. After precipitating the product by centrifugation at 4000 rpm, the product was washed with methanol twice. Finally, the product was centrifuged again and redispersed in 5 mL of butanol.

[1] Pacholski, C., Kornowski, A. & Weller, H. Angew. Chem., Int. Ed. 2008, 41, 1188-1191.

8. UV-Visible and photoluminescence measurements

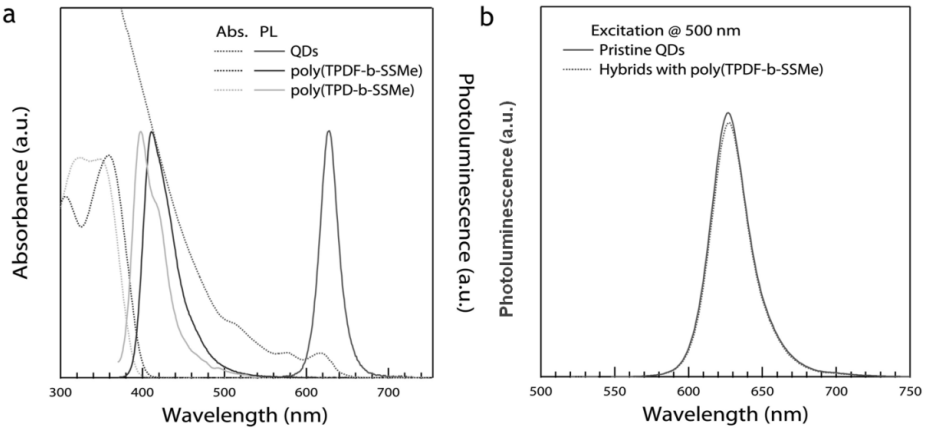

Figure S 4. (a) Absorption (dotted lines, left) and PL spectra (solid lines, right) of red QDs , poly(TPDF-*b*-SSMe), and poly(TPD-*b*-SSMe). **(b)** Photoluminescence spectra of pristine red QDs (solid line) and poly(TPDF-*b*-SSMe)-red QD hybrids (dotted line).

This insignificant reduction of emission infers that the non-radiative energy transfer (i.e., Förster and Dexter energy transfer) or exciton dissociation (by type-II bandgap alignment) are inhibited. It is attributed to the thick inorganic shell of QDs. The thick shell provides a space between the QD cores and the conducting polymers, which prevents their electrical contact as well as reducing the energy transfer efficiency.

9. Thickness dependence of the E.Q.E.

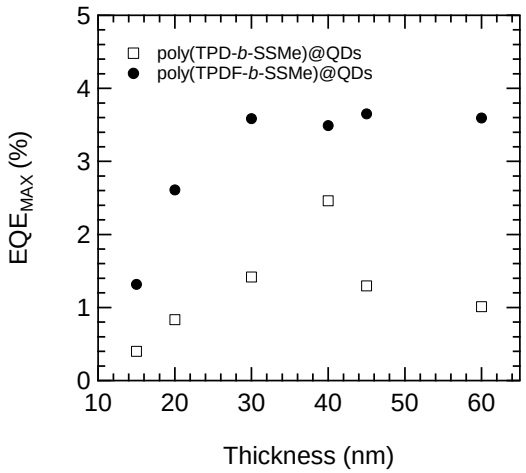

Figure S 5. Maximum E.Q.E. with various thickness of hybrid light emitting layer.

We also investigated the thickness dependence of the hybrid light emitting layers. The E.Q.E_{max} of Device 2 had a saturated tendency over 40 nm. This tendency might be explained by the enhanced

carrier transport properties of the poly(TPDF-*b*-SSMe)@QD films due to the small hole injection barrier. In contrast, Device 1 had a drastic efficiency drop at higher thicknesses. This result shows that the E.Q.E. of Device 2 is not dependent on the thickness of the active layer, but device 1 needs thorough optimization.

10. Notes:

We found that the ratio between the QDs and the polymer is very important for the efficiency of the LEDs. If the polymer content is too high, parasitic emission is observed, and if the content is too low, the film forming properties and charge transport become poor. We found the best results at a ratio of QDs to polymer of 3:1. For similar reasons, the concentration of the hybrid dispersion plays a big role. A concentration of 40 mg/mL was found to give the best results.

List of Publications

F. Jochum, **L. zur Borg**, P. J. Roth, P. Theato, Thermo- and Light-Responsive Polymers Containing Photoswitchable Azobenzene End Groups, *Macromolecules* **2009**, *42*, 7854

O. Yurchenko, D. Freytag, **L. zur Borg**, R. Zentel, J. Heinze, S. Ludwigs, Electrochemically Induced Reversible and Irreversible Coupling of Triarylamines, *Journal of Physical Chemistry B* **2012**, *116*, 30

J. Lim, W.K. Bae, K.U. Park, **L. zur Borg**, R. Zentel, S. Lee, K. Char, Scalable and Controlled Synthesis of CdSe Tetrapods with High Morphological Uniformity via the Continuous Precursor Injection Approach Using Halide Ligands, *Chem. Mater*. **2012**, *accepted*

L. zur Borg, A. Domanski, A. Breivogel, M. Bürger, R. Berger, K. Heinze, R. Zentel, Light-Induced Charge Separation in a Donor-Chromophore-Acceptor Nanocomposite Poly[TPA-Ru(tpy)$_2$]@ZnO, *J. Mater. Chem C*, **2013**, DOI: 10.1039/C2TC00535B

L. zur Borg, A. Domanski, R. Berger, R. Zentel, Photoinduced Charge Separation of Self-Organized Semiconducting Superstructures Composed of a Functional Polymer-TiO_2 Hybrid, *submitted*

L. zur Borg, D. Lee, J. Lim, W.K. Bae, M. Park, S. Lee, C. Lee, K. Char, R. Zentel, Effect of Band Gap Alignment on the Hole Transport from Semiconducting Block Copolymers to Quantum Dots, *submitted*

L. zur Borg, J. Lim, D. Lee, C. Lee, R. Zentel, K. Char, Annealing-Free Enhanced Morphology of Semiconducting Polymer-Inorganic Tetrapod Hybrids, *in preparation*

L. zur Borg, C. Schüll, H. Frey, R. Zentel, Self-Assembling Behavior of Semiconducting Linear-Hyperbranched Block Copolymers, *in preparation*

Acknowledgments

At first, I wish to thank [redacted], for giving me the opportunity to write my dissertation in his group and for the helpful advices and discussions.

Sincere thanks to [redacted] for the chance to work in his group for six months. He welcomed me warmly and I appreciate this very much.

Furthermore, I wish to thank [redacted] for giving me the opportunity to test my materials in real applications.

A big thank you to [redacted] for her scientific advice and her good collaboration.

Also, I thank the DFG for financial support (International Research Training Group "Self-Organized Materials for Optoelectronics" IRTG 1404).

I thank [redacted] sincerely for the measurements of my samples and many scientific discussions, but also for the good time in the IRTG.

A special thanks to [redacted], who supported me professionally and personally throughout my time in Korea. Furthermore, I thank him for the translation of the abstract in Korean.

I also thank [redacted] for the creative testing of my materials in LEDs and solar cells and for the good collaboration.

Many thanks to [redacted] for the preparation of the dye and the friendly time in Korea.

I also thank all co-authors of the publications for their help and discussions.

Thanks [redacted], [redacted], [redacted], [redacted] and [redacted] for their support with the syntheses.

Grateful thanks to [redacted] and [redacted] for their help.

Many thanks to the former and current members of IRTG, [redacted] and [redacted] who helped me so much when I had questions and problems.

Furthermore, I thank all students who have been to Korea with me. Thanks to you it was a great time which I remember with pleasure. In this context, special thanks to [redacted], [redacted], [redacted] and [redacted]

Thanks to [redacted] for the scientific support and the good time in Korea.

I thank [redacted] for the great time at work.

Many thanks to [redacted] for the exciting and great time being roommates, the support during the studies, for the good friendship as well as the nice journeys we made together.

Special thanks to [redacted] for the nice time at university, in which she was always there for me professionally and personally. I am also very grateful for the good friendship that we built up in the last years.

I thank [redacted] and [redacted] for the good friendship since the beginning of our studies. It was great that we faced everything together. You were always there for me.

[redacted] I am entirely myself with you. Thank you for the love and understanding that you always give to me.

The last thanks go to [redacted]. It is great that you made this possible for me and you always believed in me. This means a lot to me.

All these people contributed to this work and I am sincerely grateful. I wish them all the best for their future!

Danksagung

An erster Stelle danke ich [redacted], mir die Möglichkeit gegeben zu haben an seinem Lehrstuhl meine Doktorarbeit schreiben zu können und für die hilfreichen wissenschaftlichen Ratschläge und Diskussionen.

Sehr herzlich bedanke ich mich bei [redacted] für die Chance, sechs Monate in seiner Gruppe zu arbeiten. Ich wurde sehr freundlich aufgenommen und weiß das sehr zu schätzen.

Weiterhin bedanke ich mich bei [redacted] für die Möglichkeit, meine synthetisierten Materialien in echten Anwendungen zu erproben und somit auch zu verbessern.

Ein großer Dank geht an [redacted] für wissenschaftlichen Anregungen und die gute Kooperation.

Ausserdem danke ich dem DFG für die finanzielle Unterstützung (International Research Training Group "Self-Organized Materials for Optoelectronics" IRTG 1404).

[redacted] danke ich sehr herzlich für die Vermessung meiner Proben und die vielen wissenschaftlichen Diskussionen, aber auch für die schöne im IRTG.

Ein ganz besonderer Dank geht an [redacted], der mir in Korea immer wissenschaftlich und privat zur Seite gestanden hat. Zudem danke ich ihm für die Übersetzung der Zusammenfassung auf Koreanisch.

Mein Dank geht auch an [redacted] für das kreative Testen meiner Materialien in LEDs und Solarzellen und die gute Kooperation.

[redacted] danke ich sehr für die Bereitstellung seines Farbstoffes und die freundschaftliche Zeit in Korea.

Zudem danke ich allen Koautoren der Veröffentlichungen für ihre Hilfe und Diskussionen.

Ich danke [redacted], [redacted], [redacted], [redacted] und [redacted] für ihre Unterstützung bei den Synthesen.

Ein ganz lieber Dank auch an [redacted] und [redacted] für ihre Hilfe.

Mein Dank geht auch an [redacted], [redacted] und der [redacted], die mir bei Fragen und Problemen geholfen haben.

Außerdem bedanke ich mich bei allen Studenten, die mit mir in Korea waren. Dank euch war es eine tolle Zeit, an die ich gerne zurückdenke. Besonders danken möchte ich in diesem Kontext [redacted], [redacted], [redacted] und [redacted].

[redacted], danke für die wissenschaftliche Unterstützung und die schöne Zeit in Korea.

[redacted] danke ich für die super Zeit im Arbeitskreis.

Bei [redacted] bedanke ich mich für die aufregende und tolle Zeit in der WG, die Unterstützung während des Studiums, für die gute Freundschaft sowie die schönen Reisen, die wir zusammen gemacht haben.

Bei [redacted] bedanke ich mich von Herzen für eine schöne Zeit in der Uni, in der sie mir privat und wissenschaftlich immer zur Seite gestanden hat. Zudem bedanke ich mich für die sehr gute Freundschaft, die wir in den letzten Jahren aufgebaut haben.

[redacted] und [redacted] danke ich für die sehr gute Freundschaft seit Beginn des Studiums. Es war einfach super dass wir alles zusammen durchstehen konnten. Ihr wart wirklich immer für mich da, sei es für die Uni oder im Privaten.

[redacted] bei dir bin ich ganz ich selbst. Danke für die Liebe und das Verständnis, das du mir immer gibst.

[redacted] gilt der letzte Dank. Es ist toll dass ihr mir dies ermöglicht habt, und immer an mich geglaubt habt. Das bedeutet mir sehr sehr viel.

Alle diese Menschen haben einen Beitrag zu dieser Arbeit geleistet und ich danke ihnen von Herzen. Ich wünsche Allen alles Gute für ihre Zukunft!